AN ABSTRACT OF THE THESIS OF

ALI REZA SEPASKHAH (Name) for the DOCTOR OF PHILOSOPHY (Degree)

in SOIL SCIENCE (Major) presented on September 14, 1973 (Date)

Title: EXPERIMENTAL ANALYSIS OF SUBSURFACE HEATING AND IRRIGATION ON THE TEMPERATURE AND WATER CONTENT OF SOILS

Abstract approved: Larry Boersma

Multiple use of waste heat from power plants may become an important consideration in the development, siting, and certification of these plants. A multiple use system of components that can beneficially utilize waste heat may include home heating and cooling, greenhouses, animal enclosures, open basins for single cell protein production and fish farming, and open field soil warming.

A subsurface irrigation-soil warming system utilizing waste heat was analyzed in this study. Thermal power plant condenser cooling water pumped through buried porous pipes was considered as a heat and water source for soil heating and subsurface irrigation. Energy is transferred from the heat source to the surrounding soil, warming it above its natural temperature. In addition, water seeping from the porous pipe prevents drying around the heat source and

supplies the plant roots throughout the soil profile while avoiding the large evaporation losses at the soil surface associated with surface irrigation methods.

Experiments were conducted in the laboratory to study this system. Soil was packed in containers 48 cm deep, 40 cm wide, and 4 cm thick. A heat source consisting of a copper covered electrical resistance wire was placed against one side of the box at a depth of 32 cm. A water source consisting of a porous tube was placed 2 cm above the heat source. The contained soil slab thus represented a subsurface soil warming and irrigation system with heat and water sources at depths of 32 and 30 cm respectively and a 77 cm spacing.

A series of experiments was conducted with heat source temperatures of 29, 36, and 44 C, and surface heat load cycles with maxima of 0, 13, 52, and 117 watts. These experiments were repeated for Quincy, Cloquato, and Chehalis soils. The box filled with soil was saturated with water and then drained. Experiments were initiated by energizing the heat source. Temperature distributions throughout the soil profile and rates of energy dissipation were measured. Water application rates required to maintain a constant soil water content were obtained. In each experiment, water was applied at such a rate that the water content at a point near the heat source, monitored with a gamma ray attenuation system, remained constant.

Apparent thermal conductivities of Quincy, Cloquato, and Chehalis soils as a function of water content were measured at 25 and 45 C by the heat probe method. The soil apparent thermal conductivity was also computed from a theoretical model based on its mineral composition, porosity, water content, and the thermal conductivity of the individual components. This model takes into account the vapor flow contribution to the apparent thermal conductivity in wet soils. Its magnitude depends on the available air-filled pore space, total porosity, and the free energy of the retained water. Predicted and experimental values of thermal conductivities showed good agreement.

Soil temperature distributions were calculated using theoretical models presented in the literature. Predicted and measured isotherms showed good agreement.

Energy dissipation rates as a function of soil thermal conductivity, temperature differences between heat source and soil surface, and depth and spacing of heat source were obtained. They were in agreement with those calculated from theoretical considerations. The total land area required to dissipate the waste energy from a 1000 MWe power plant operating with 34 percent efficiency was calculated for each of the three soils used in the experiments. It was found that 2841, 3714, and 4390 hectare would be required for Quincy, Cloquato, and Chehalis soils respectively. Quincy soil would require

the smallest land area for this purpose because of its higher thermal conductivity. Economical and technical considerations for the installation of subsurface heating and irrigation systems require flat land close to the electrical power plant. Large areas of flat land are not always present.

Subsurface irrigation replenished water lost by surface evaporation. Water use rates were obtained as a function of temperature differences between heat source and soil surface, soil type, and a range of surface heat loads.

The water application rates ranged from 1.50 mm/day for Chehalis soil with a heat source temperature of 29 C in combination with the lowest surface heat load to 6.0 mm/day for Quincy soil with a heat source temperature of 44 C in combination with the highest surface heat load. These rates were adequate to prevent drying around the heat sources and supply the water needs of an actively growing crop. The effective use of this system depends on the development of suitable tubing to conduct and discharge water which could be used without clogging of the pores through which water seeps into the ground.

The proposed soil warming and irrigation system does not appear to be an attractive alternative power plant cooling system. The system holds promise however as an economically attractive management system for the production of high value crops.

Experimental Analysis of Subsurface Heating and Irrigation on the Temperature and Water Content of Soils

by

Ali Reza Sepaskhah

A THESIS

submitted to

Oregon State University

in partial fulfillment of
the requirements for the
degree of

Doctor of Philosophy

June 1974

APPROVED:

Redacted for privacy

Professor of Soil Science
in charge of major

Redacted for privacy

Head of Department of Soil Science

Redacted for privacy

Dean of Graduate School

Date thesis is presented September 1973

Typed by Clover Redfern for Ali Reza Sepaskhah

ACKNOWLEDGMENTS

The author wishes to express his gratitude and deep appreciation to Dr. Larry Boersma for his valuable guidance, advice, encouragement, constructive criticism during the course of this study, and for the many hours of critical editing of this dissertation.

Appreciation is also expressed to Dr. C.H. Ullery, Department of Soil Science, Dr. O.A. Boedtker, Physics Department, Dr. R.H. Brooks, Department of Agricultural Engineering, and Dr. R.E. Berry, Department of Entomology, for their willingness to take time to serve on the author's graduate committee. Their advice was very helpful and is greatly valued.

Words of appreciation are expressed to Dr. L.R. Davis, Department of Mechanical Engineering for his constructive criticism and editing of this thesis.

Technical assistance of Mr. Gary Jarman is gratefully acknowledged.

Financial support from the Office of Water Resrouces Research, United State Department of the Interior, and the Oregon Agricultural Experiment Station is gratefully acknowledged.

The author expresses gratitude to his parents, whose encouragement made his ambition for advanced study possible. He wishes to dedicate this thesis to them.

TABLE OF CONTENTS

LIST OF FIGURES

LIST OF TABLES

LIST OF SYMBOLS

a, b, c = particles axes in 3 dimensions, cm.

A = regression line intercept with coordinate in Figure 29, $cal/cm^2 min$.

A_0 = surface temperature amplitude, C.

B, B' = slopes of regression lines, $cal/cm^2 min\ C$.

C = heat capacity, $cal/cm^3 C$.

C_a = heat capacity of air, $cal/cm^3 C$.

C_s = heat capacity of soil particles, $cal/cm^3 C$.

C_w = heat capacity of water, $cal/cm^3 C$.

d = pore diameter, cm.

D = damping depth, cm.

D_0 = diffusion coefficient of water vapor in air, cm^2/sec.

E = total evaporation during a specified period, cm.

F = rate of energy loss from heat source, $cal/cm^2 min$.

g_a = depolarization factor in the a axis, dimensionless.

g_b = depolarization factor in the b axis, dimensionless.

g_c = depolarization factor in the c axis, dimensionless.

G = "shape factor," cm^{-1}.

h = distance from soil surface to the heat source, cm.

I = electrical current, amperes.

k = ratio of the average gradient in the dispersed materials and the corresponding quantity in the medium, dimensionless.

k_a = ratio of the average temperature gradient in the air pockets and the corresponding quantity in the medium, dimensionless.

k_{s0} = ratio of the average temperature gradient in the solid material and the corresponding quantity in the medium, dimensionless.

L = latent heat of vaporization, cal/g.

m = number of types of granules, dimensionless.

M = molecular weight of water, g/mole.

n = integers, 1, 2, . . . , dimensionless.

N = number of heat sources on either side of the center heat source, dimensionless.

p = vapor pressure, mm Hg.

p_0 = saturation vapor pressure, mm Hg.

P = total pressure of the soil atmosphere, mm Hg.

q = heat flow rate per unit length of the heat source, cal/cm sec.

Q = heat input in the heat probe, cal/sec.

r = radius of the heat source, cm.

R = gas constant of water vapor, cal/g K.

s = lateral distance between heat sources, cm.

t = time, sec.

t_1 = time at which the maximum temperature at a depth y occurs.

T = temperature, Kelvin (K).

T_2-T_1 = increase in temperature (C) during the time period from t_1 to t_2, sec.

T_{ay} = average temperature at any depth, C.

T_s = temperature of the heat source, C.

T_{su} = soil surface temperature, C.

$T_{(x,y)}$ = temperature of the medium at any point in a vertical plane in the system, C.

$T_{(y,t)}$ = temperature at any depth and time, C.

V = voltage of AC power supply, volts.

x = horizontal distance from the heat source, cm.

x_a = volume fraction occupied by air, dimensionless.

x_{s0} = volume fraction occupied by the solid materials, dimensionless.

x_w = volume fraction occupied by water, dimensionless.

y = vertical distance from the soil surface, cm.

z = thickness of soil column, cm.

z_c = container wall thickness, cm.

a = proportionality constant of equal axes to non equal axis of spheroid particles.

ν = frequency, sec^{-1}.

ω = angular frequency, sec^{-1}.

ϕ_0 = phase constant, radian.

λ = thermal conductivity of the soil, cal/cm sec C.

λ_a = thermal conductivity of dry air, cal/cm sec C.

$\lambda_{eff.}$ = effective thermal conductivity of air, cal/cm sec C.

λ_{s0} = thermal conductivity of the solid materials, cal/cm sec C.

λ_v = thermal conductivity due to vapor movement, cal/cm sec C.

λ_v^s = thermal conductivity due to vapor movement in pores saturated with water vapor, cal/cm sec C.

λ_w = thermal conductivity of water, cal/cm sec C.

λ_0 = thermal conductivity of dispersing medium, cal/cm sec C.

λ_1 = thermal conductivity of the dispersed materials, cal/cm sec C.

ϵ = soil porosity, cm^3/cm^3.

θ = soil water content, cm^3/cm^3.

θ_e = water content at which the continuous medium is changed cm^3/cm^3.

Ω = electrical resistance, ohms/cm.

σ = surface tension of water, dyne/cm.

ρ = density of water, g/cm^3.

ρ_c = bulk density of container, g/cm^3.

ρ_s = bulk density of the soil, g/cm^3.

τ = fraction of time that the heat source was energized, dimensionless.

Λ = transmitted radiation intensities.

Λ_0 = incident radiation intensities.

μ = mass absorption coefficient, cm^2/g.

μ_c = mass absorption coefficient of container materials, cm^2/g.

μ_s = mass absorption coefficient of soil, cm^2/g.

μ_w = mass absorption coefficient of water, cm^2/g.

ΔH = heat flux into a layer to thickness Δy, $cal/cm^2 min$.

Δt = time interval, min.

ΔT = change in temperature, C.

Δy = thickness of a layer of soil, cm.

$\Delta \theta$ = fractional change in soil water content, cm^3/cm^3.

$\frac{dp_0}{dT}$ = slope of saturation vapor pressure versus temperature, mm Hg/C.

EXPERIMENTAL ANALYSIS OF SUBSURFACE HEATING AND IRRIGATION ON THE TEMPERATURE AND WATER CONTENT OF SOILS

INTRODUCTION

Statement of the Problem

Soil temperature and air temperature are important climatic factors affecting plant growth. The optimum soil temperature varies with plant species and variety. The optimum root temperature for species indigenous to warm climates is above that for temperate species (Neilsen and Humphries, 1966). It is known that within certain temperature ranges, biological activity doubles with each temperature increase of 10 C. But temperatures too low or too high are lethal to plants (Salisbury and Ross, 1969). In general, air temperature controls reproductive growth while vegetative growth is controlled by root temperature. High rates of production depend on early germination, emergence, and vigorous vegetative growth. In geographical regions where soil temperatures are not favorable for seed germination and early vigorous growth, high yields are not possible without increasing the soil temperature to an optimum level. Unfavorable soil temperatures at planting time often produce a poor stand and consequently a reduced yield. Retarded growth of young seedlings not only reduces yield but also adversely affects the quality

of the crop produced (Richards et al., 1952). Favorable soil temperatures may make it possible to produce two or more crops per year or achieve earlier crop maturity which may have marketing advantages (Boersma, 1970).

Control of temperature in agricultural activities is limited primarily to greenhouse horticulture. Several approaches to increasing the soil temperature in the open field have been taken. Clarkson (1960) mulched soil with black polyethylene plastic. He observed that temperatures were 20-25 F higher at the surface of the mulch and 2 inches above the mulch than at corresponding locations on non-mulched fields. Petroleum mulch was used by Kowsar et al. (1969) to increase soil temperature. The higher temperature in mulched soil was attributed to a blackbody effect of the petroleum mulch and the higher thermal conductivity of the soil resulting from the conservation of soil water below the petroleum skin. Ridging may increase soil temperature by 3 C (Shaw and Buchele, 1957). Orientation of rows can affect soil temperature. Larson and Willis (1957) showed that with north-south rows more radiation is absorbed by the soil than with east-west rows. All these methods depend on available energy and may not increase the soil temperature to an optimum level under unfavorable circumstances.

Other methods of increasing the soil temperature have been discussed by Bunting and Cartwright (1957). They suggested that

heating the soil by means of electrically energized heating cables would always be too expensive, but that it might be possible to use waste heat from power stations for this purpose. Boersma (1970) pointed out that surface irrigation is not a feasible method for imparting the energy in condenser cooling water to the soil. The large quantities of water that would be needed would keep the soil flooded most of the time. Boersma (1970) and Boersma and Rykbost (1973) proposed an integrated system for multiple use of the waste heat from power plants. They suggested, that as a part of an integrated complex warm water be circulated through an underground system of pipes thus heating the soil.

Underground heat sources impose a temperature field on the natural soil temperature distribution. The resulting temperature distribution depends on the source temperature, air temperature, and depth and spacing of the heat sources. Power plants with cooling towers are normally designed so that the temperature of the effluent is between 26.5 and 47.5 C (Yarosh et al., 1972). The temperature of the cooling water, the natural soil temperature regime, and the type of crop to be grown, are important factors to be considered in the design of a subsurface soil warming system.

Energy dissipation in the soil depends on the temperature gradient, thermal conductivity, and depth and spacing of the heat sources. Heat source temperature, soil surface temperature, and

depth of heat source are parameters that influence the magnitude of the temperature gradient. Soil thermal conductivity is a critical parameter in controlling the rate of energy dissipation from soil warming systems. The apparent thermal conductivity of the soil is a function of the physical properties of the soil. Important among these are soil texture, soil temperature, and soil water content. The total land surface area required to dissipate a given amount of energy, therefore, depends on the air temperature, heat source temperature, soil type, soil water content, and depth and spacing of the heat sources.

Potential Problems and Opportunities

Moisture migration due to temperature gradients occurs in the soil. This mechanism can produce a dry region around the proposed heat sources. Arman et al. (1964), Milne and Mochlinski (1964), and Boersma and Rykbost (1973) reported that this drying can occur at low as well as high temperatures of the heat sources and with any type of soil. Soil surrounding a heating cable is dried to a stage at which the capillary film of water between soil particles is broken. Rewetting the soil is usually very slow (Milne and Mochlinski, 1964). Rykbost (1973) found that the soil water content decreased in the 60-90 cm layer with heat sources at the 90 cm depth. A small but very dry core developed around the heat sources during the summer.

A continuous supply of water near the heat source would prevent the observed drying of the soil. Enough water should be supplied to maintain a constant and high level of water content. This system would make use of the thermal gradients as a driving force to distribute the water through the soil profile.

Subsurface irrigation even without heating the soil has given good results in terms of increased yields and decreased water requirements in comparison with other methods of water application (Hanson and Williams, 1968; Hanson et al., 1970). In principle, if water is introduced slowly into or near the root zone of a plant, it will spread by capillary action in the soil and thus become available for utilization by the plant. If the location of the water application point and the rate of application is properly chosen, it should be possible to supply the demand of the plant without any significant seepage losses and with the region of moist soil maintained below the soil surface to minimize evaporation. The amount of water saved would be a function of the type of crop, soil type, ambient conditions, and efficiency of the comparative methods. Hanson and Williams (1968) and Hanson et al. (1970) estimated potential water savings to exceed 25 percent over furrow irrigation for cotton in New Mexico. Zetzsche (1964) and Newman (1965) reported comparable 1963 cotton yields on 42 percent less irrigation water in Texas using subsurface irrigation. Furthermore, more nearly optimum soil water levels could be achieved with

subsurface irrigation than with conventional methods of irrigation.

Scope of the Study

Experiments were conducted in the laboratory to study the effect of heat source temperature on the temperature distribution around line heat sources in three different soils. Sinusoidal soil surface heat loads were applied to study the effect of different climatic conditions on the temperature distributions. Effects of heat source temperature, soil surface temperature, and soil texture on rate of heat dissipation were studied. Water was applied near the heat source to determine the rate of water application required to maintain a constant soil water content at different heat source temperatures. Water content distributions and rates of water application were measured.

Field conditions were simulated by packing soils in containers with inside dimensions of 48 x 40 x 4 cm. Thermal insulation was provided on all sides, except the soil surface. A heat source was placed at a depth of 32 cm and 1.5 cm from one side of the box. The soil slab and heat source thus represented a system of parallel line heat sources with a spacing of 77 cm placed at a depth of 32 cm with a lower boundary at 48 cm. Dimensions of the system were dictated by available laboratory equipment. The heat source consisted of a copper tube (O.D. = 0.7 cm) with a resistance heater imbedded in it. Its temperature was controlled thermostatically during each experiment.

A porous tube (O.D. = 0.9 cm) with pore sizes ranging from 60 to 70 microns was placed immediately above the heat source. Water was released from the tube to the surrounding soil. Water was supplied with a Mariotte bottle connected to the porous tube.

The experiments were conducted to develop a physical basis for predicting temperature distributions in soil profiles heated with parallel line heat sources. For this purpose results of laboratory experiments were to be compared with analytical solutions reported in the literature. A second major objective of the study was the evaluation of the proposed soil warming system for different soil types. Three soils ranging from loamy sand to silt loam were therefore included in the experiments. The third major objective of the study was to evaluate the feasibility of using subsurface irrigation in combination with subsurface soil warming. It was considered to be of great interest to determine the effect of soil warming on the rate of water distribution in the soil from a subsurface irrigation system.

THERMAL CONDUCTIVITY OF SOILS

Introduction

Heat flow through soils is controlled by the apparent soil thermal conductivity and existing temperature gradients. Soil thermal conductivity is of interest to disciplines concerned with temperature distributions in the soil and adjacent air, the energy balance at the soil surface, and the soil warming system discussed in this dissertation. It is an essential factor in determining the flow of heat away from industrial installations in the ground such as underground high voltage cables, steam lines, and cross-country oil pipe lines.

The thermal conductivity of soils is a function of the properties of the solid materials but also depends on soil texture, pore space, and water content. Heat flow in soils occurs by conduction through the solid particles, through the water present as continuous films on the particles or as liquid rings around the contact points between particles, and through the air in the soil pore spaces. The thermal conductivity of water is about 20 times greater than that of air, but much smaller than that of the solid soil particles. The thermal conductivity of the solid soil particles varies according to structure and chemical composition of the soil minerals. Heat flow in moist soils occurs also as a result of vapor transfer. Water vapor molecules diffuse from warm to cold regions under the influence of vapor pressure gradients caused

by the temperature differences. Liquid phase water movement may occur as a result of surface tension differences between warm and cold regions. Surface tension decreases with increasing temperature resulting in water potential gradients between two points with different temperatures.

The influence of the composition of the soil on its thermal properties is such that thermal conductivity of the dry material increases in the sequence clay-loam-sand. This was confirmed by Smith and Byers (1938) who measured the thermal conductivities of soils with various textural characteristics. Nakshabandi and Kohnke (1965) made similar observations. Differences in thermal conductivities are also caused by differences in soil aggregation. Sandy soils are poorly aggregated and therefore have less pore space and better contact between particles than well-aggregated clay or loam soils. Soil texture has only a small effect on the thermal conductivity as long as the material is dry, has a single grain structure, and the bulk density is constant.

Thermal conductivity increases with increasing soil water content and decreasing air filled pore space. The thickness of water films on the soil particles increases with increasing soil-water content. The presence of thicker water films at the points of contact between particles increases the thermal contact between them. Smith (1939) found that the increase per unit of water added was larger in

coarse-textured soils than in soils with a fine texture. This can be explained on the basis of the lower conductivity of the clay particles and the reduced water vapor diffusion in the fine textured soil.

Nakshabandi and Kohnke (1965) measured the thermal conductivity of soils with different textures. They also observed the increase in thermal conductivity with water content. The increase per unit water added was greater in coarse-textured soils than in fine-textured soils. The relationship between thermal conductivity and soil water potential was similar for soils with different textures. This is due to the fact that the arrangement of water molecules in the soil is determined by the water potential. The thickness and geometry of water shells around the particles determines the conductivity of the soil-air-water system.

Not much information is available on the effect of temperature on the apparent thermal conductivity of soils. Research has been done to determine the temperature effect on the apparent thermal conductivity of building materials. Luikov (1966) reported that the apparent thermal conductivity for dry concrete is independent of temperature in the range of 12-70 C, but for wet concrete it increases with an increase in temperature. The higher the water content of the concrete, the greater the increase in the apparent thermal conductivity in relation to temperature. The apparent thermal conductivity of sand increases with temperature according to Yankelev (1954). His

measurements showed apparent thermal conductivity values of 0.61, 0.78, and 0.81 mcal/cm sec C at 50, 75, and 140 C, respectively.

Theoretical Basis for the Soil Thermal Conductivity Calculation

Attempts have been made to predict the thermal conductivity of soils by considering the several mechanisms of heat transfer (Gemant, 1950; de Vries, 1952; Webb, 1956; Woodside, 1958). Soil particles are usually considered spherical and dispersed in a continuous medium of air and/or water. Gemant (1950) assumed the water to occupy wedge-shaped rings at the contact points between the spheres, the volume of these rings varying with the water content. Webb (1956) criticized the neglect of the air-phase conductivity by Gemant (1950) and included it in his model. Both authors assumed the heat flow, at all points in the material, to be parallel to the direction of a mean temperature gradient. Incorrect results may follow from this assumption since it does not hold true for porous media such as soils. Gemant (1950) reported good agreement between experimental and calculated data for water contents of 5 and 25 percent. Below a water content of 5 percent, the experimental values were higher than the calculated values. The measured thermal conductivity of dry soil was three times higher than the predicted thermal conductivity according to Webb's (1956) calculations. This discrepancy was attributed to the

assumptions that the particles are ideally packed spheres and that there is a point contact between the particles. Woodside (1958) developed a model which could be used to predict the thermal conductivity of snow or porous material consisting of solid and gas phases with porosities higher than 47.7 percent. The model does not meet the assumed conditions at porosities less than 47.7 percent. His equation is not applicable to moist porous materials which consist of solid, liquid, and gases in a complex system.

De Vries Model

An equation derived originally by Maxwell and Lord Rayleigh for the calculation of the electrical conductivity of porous materials was used by de Vries (1952) to calculate soil thermal conductivity. He developed a model that can be used to predict the thermal conductivity of a system made up of non-spherical solid particles.

Heat transfer in soils is complicated by the presence of water in the pores. Water evaporates in warm regions and condenses onto colder surfaces some distance away. This heat transfer mechanism modifies the thermal conductivity of the medium. It may be accounted for by using an effective thermal conductivity for the air which includes a term representing the contribution of water vapor diffusion (de Vries, 1952; Woodside, 1958) as follows:

$$\lambda_{effective} = \lambda_a + \lambda_v , \qquad (1)$$

where λ_a is the thermal conductivity of dry air (cal/cm sec C), and λ_v is the thermal conductivity due to vapor movement (cal/cm sec C).

Vapor diffusion is initiated by vapor pressure differences due to temperature differences. Its magnitude depends on the temperature differences and the vapor diffusion coefficient which is temperature dependent. Models have been proposed by Krischer and Rohnalter (1940) to calculate the thermal conductivity due to vapor movement, λ_v^s, in pores saturated with water vapor. Effects of temperature and temperature differences on vapor diffusion were accounted for in these models. De Vries (1963) using the Krischer and Rohnalter (1940) model to calculate the vapor transfer component of the apparent thermal conductivity found good agreement between measured and calculated apparent thermal conductivity of sandy soil at different temperatures. The temperature effect was most pronounced at low water content, where the vapor movement contribution to the apparent thermal conductivity is highest.

When water is considered to be the continuous phase and several types of granules of different shape and/or with different conductivities are present, the thermal conductivities is given by:

$$\lambda = \frac{x_w\lambda_w + \sum_{i=1}^{m} k_{s0}x_{s0}\lambda_{s0} + k_a x_a \lambda_a}{x_w + \sum_{i=1}^{m} k_{s0}x_{s0} + k_a x_a}, \qquad (2)$$

where x_w, x_a, x_{s0}, are the volume fractions occupied by water, air, and the solid material, respectively; $\lambda_w, \lambda_a, \lambda_{s0}$ are the thermal conductivities in cal/cm sec C of water, air and solid material, respectively; k is the ratio of the average temperature gradient in the granules and the corresponding quantity in the medium, and m is the number of type of granules.

The value of k depends on the ratio of thermal conductivities, size and shape of the granules, and their relative positions. When soil granules are assumed to be spheroids, the k value is given by:

$$k_{s0} = \frac{2}{3}\frac{1}{1+(\frac{\lambda_{s0}}{\lambda_w}-1)g_a} + \frac{1}{3}\frac{1}{1+(\frac{\lambda_{s0}}{\lambda_w}-1)g_c}, \qquad (3)$$

and

$$k_a = \frac{2}{3}\frac{1}{1+(\frac{\lambda_a}{\lambda_w}-1)g_a} + \frac{1}{3}\frac{1}{1+(\frac{\lambda_a}{\lambda_w}-1)g_c}, \qquad (4)$$

which are special cases of the more general form:

$$k = \frac{1}{3} \sum_{a,b,c} \left[1+\left(\frac{\lambda_1}{\lambda_0} - 1\right)g_a\right]^{-1} , \qquad (5)$$

where $a, b,$ and c are the axes of the randomly oriented ellipsoidal granules, g_a, g_b, and g_c are the depolarization factors in the direction of the a, b, and c axes, and λ_1 and λ_0 are the thermal conductivities of particles and medium, respectively. The factors g_a, g_b, and g_c satisfy the relation

$$g_a + g_b + g_c = 1 . \qquad (6)$$

For the spheroids with axes $a = b = \alpha c$ the value of $g_a = g_b$ can be read from Figure 1 for α values varying from 0.1 to 100, while g_c follows from (6). In general, it is assumed that the values of g_a and g_c for air and water pockets vary linearly with x_a and x_w. In unsaturated samples with water as the continuous medium

$$g_a = 0.333 - \frac{x_a}{\epsilon}(0.333-0.035) \qquad (7)$$

for $0 \leq x_a \leq (\epsilon-\theta_e)$, where ϵ is the porosity (cm^3/cm^3), θ_e is the water content (cm^3/cm^3) at which the continuous medium is changed from water to air, and x_a is the volume fraction of air. When air is considered to be the continuous medium, g_a is given by:

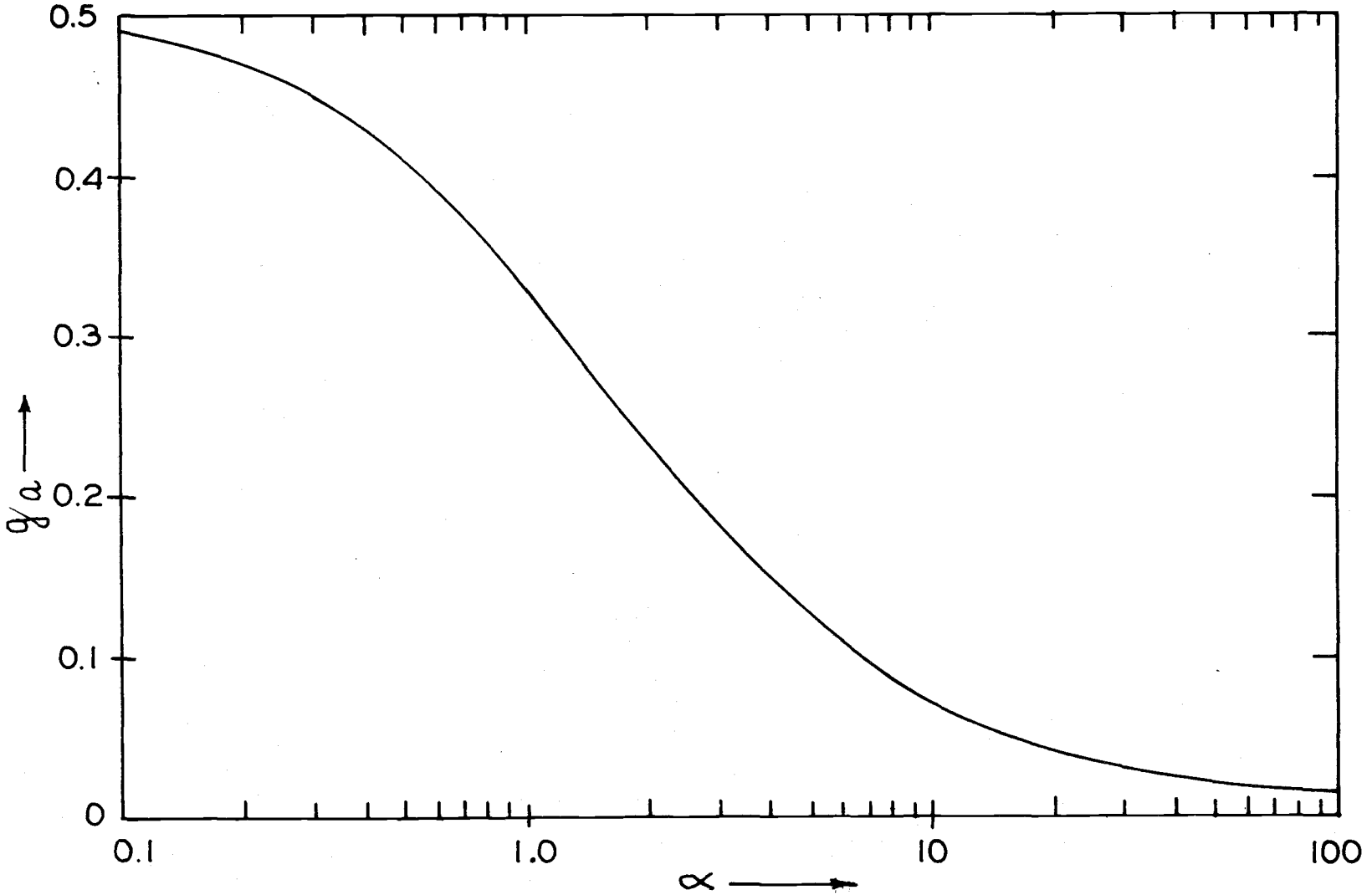

Figure 1. Values of g_a as a function of α for ellipsoids of revolution with axes $a = b = \alpha c$. After de Vries (1963).

$$g_a = 0.013 + \frac{x_w}{\theta_e}(0.098-0.013) \qquad (8)$$

for $0 \leq x_w \leq \theta_e$, where x_w is the volume fraction of soil water. The value of θ_e was between soil field capacity and the water content at the wilting point (de Vries, 1963). Appropriate values of θ_e for different soils are obtained by trial and error. The value of θ_e depends on the soil texture and soil temperature.

When air is considered to be the continuous medium, equations identical to Equations (2), (3), and (4) are used except that the positions of the subscripts "a" and "w" are interchanged and k_a becomes k_w. For water contents below θ_e the effective conductivity of air varies as a result of decreasing relative humidity. It is usually assumed that λ_v decreases linearly with the soil water fraction x_w, from λ_v^s at $x_w = \theta_e$ to zero at $x_w = 0$, so that the effective conductivity of air in air-filled pores becomes:

$$\lambda_a + \lambda_v = \lambda_a + \frac{x_w}{\theta_e}(\lambda_v^s - \lambda_a) \qquad (9)$$

where λ_v^s is the thermal conductivity due to vapor movement in water vapor saturated air. An expression was given by Krischer and Rohnalter (1940) to calculate λ_v^s as follows:

$$\lambda_v^s = \frac{LD_0P}{RT(P-p_0)} \frac{dp_0}{dT} \quad (10)$$

where λ_v^s is the thermal conductivity due to the movement of water vapor in saturated air (cal/cm sec C), L is latent heat of vaporization (cal/g), R is gas constant (0.11 cal/g K) for water vapor, D_0 is diffusion coefficient of water vapor in air (cm^2/sec), P is total pressure of the atmosphere in the soil (mm Hg), p_0 is the saturation vapor pressure (mm Hg), and dp_0/dT is the slope of saturation vapor pressure versus temperature curve (mm Hg/C). The values of λ_v^s as a function of temperature are needed to estimate the apparent thermal conductivity of soil at different temperatures. These values can be calculated by Equation (10).

Experimental Procedures

Values of the apparent thermal conductivity of the soil are needed to predict temperature distributions and energy dissipation rates for the proposed soil warming systems. The apparent thermal conductivity varies with soil water content, texture, and temperature. Experiments were conducted in the laboratory to measure the apparent thermal conductivity as a function of soil water content at 25 C and 45 C for Quincy, Cloquato, and Chehalis soils.

The particle size distributions and other specifications of the

soils used in the experiments are shown in Table 1. Measurements were made at water contents ranging from oven dry to saturation and at 25 C and 45 C.

Table 1. Physical properties of the soils used.

Soil	Particle Size			Porosity	Water Content -1500 -- Joules/kg --	Water Content -30 -- Joules/kg --	Bulk Density
	Sand	Silt	Clay				
	------ % ------			-------- cm^3/cm^3 --------			g/cm^3
Quincy loamy sand	90	6	4	0.475	0.070	0.185	1.69
Cloquato loam	43	37	20	0.600	0.140	0.350	1.18
Chehalis silt loam	9	64	27	0.600	0.180	0.395	1.16

The samples were prepared by adding the amount of water required to bring a prepacked, air dry, sample to the desired water content. The air dry soil was packed in a glass jar that was tapped once on the top of the laboratory bench with each scoop of sample poured into it. The number of scoops per jar was the same for each sample. Predetermined quantities of water were applied to the samples such that no water was ponded on the soil surface. This method of water application prevented trapping of air in the samples. Samples with low water content were prepared by pouring air dry soil on a plastic sheet and spreading it evenly in a thin layer. Required amounts of water were then sprinkled onto the soil. It was shaken in a

plastic bag to distribute the water uniformly and packed into the jars. These were capped with a lid with a hole in the center to later receive the conductivity probe.. The lid and the lid hole were masked by tape to prevent water loss by evaporation. The containers were kept in a constant temperature cabinet for 5-7 days to insure uniform distribution of water and temperature throughout the samples before the measurements were made.

A transient method was used to measure the apparent soil thermal conductivity (Schleirmacher, 1888; Hopper and Lepper, 1950). This method is based on the equation for cylindrical heat flow which can be derived from the basic heat conduction equation combined with the continuity equation using a Fourier solution to the differential equation. The final results can be written as:

$$T_2 - T_1 = \frac{q}{4\pi\lambda} \ln \frac{t_2}{t_1} \qquad (11)$$

where $T_2 - T_1$ is the increase in temperature (C) near the heat source during the time period from t_1 to t_2 in seconds, q is the total amount of heat input (cal/cm sec) and λ is the apparent soil thermal conductivity (cal/cm sec C). Equation (11) states that the rate of temperature rise of a cylindrical probe, embedded in an semi-infinite medium and heated at a constant rate, is proportional to the logarithm of time ratio and inversely proportional to the

apparent thermal conductivity of the surrounding medium. The samples contained in glass jars with a large diameter compared to that of the probe, represent a semi-infinite medium. Details of this method are described by Cochran, Boersma and Youngberg (1967).

The line heat source consisted of a needle with a built-in heating filament and thermistor. The needle was inserted vertically from the top into the soil sample. The temperature increase of the thermal conductivity probe resulting from a constant rate of heat input was recorded with a Heath strip chart recorder. The recorder was adjusted to read 1 C for its full span to facilitate reading of the probe temperature to the third decimal place. The temperature increase as a function of time was recorded for a period of 4-8 minutes. A chart trace is shown in Figure 2. Plotting the increase of temperature (C) versus the logarithm of tims (seconds) results in a straight line (Figure 3). The slope of this line is $q/4\pi\lambda$ from which λ can be calculated provided the rate of heat input q is known. The heater in the needle was energized by a six-volt DC battery. The current was measured by a galvanometer. Then q was calculated from the equation:

$$q = \frac{I^2 \Omega}{4.185} \tag{12}$$

where I is the current (amperes), Ω is the resistance (ohms/cm), and the factor 4.185 is the conversion factor from Joules to calories.

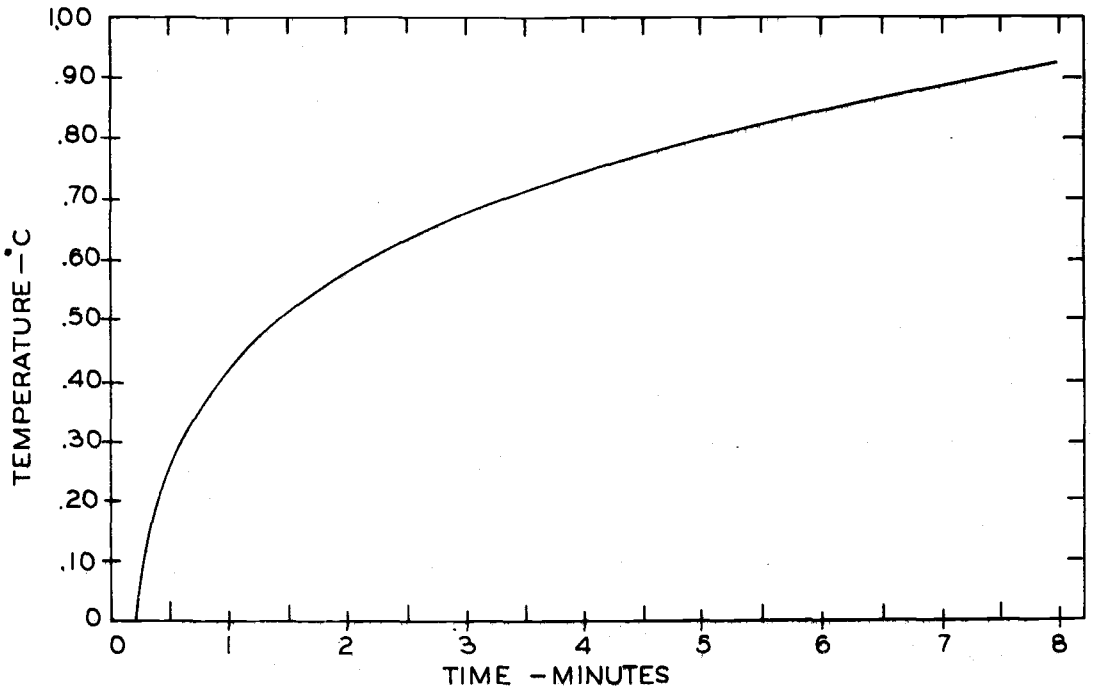

Figure 2. Temperature rise of the thermal conductivity probe inserted in a sample as a function of time.

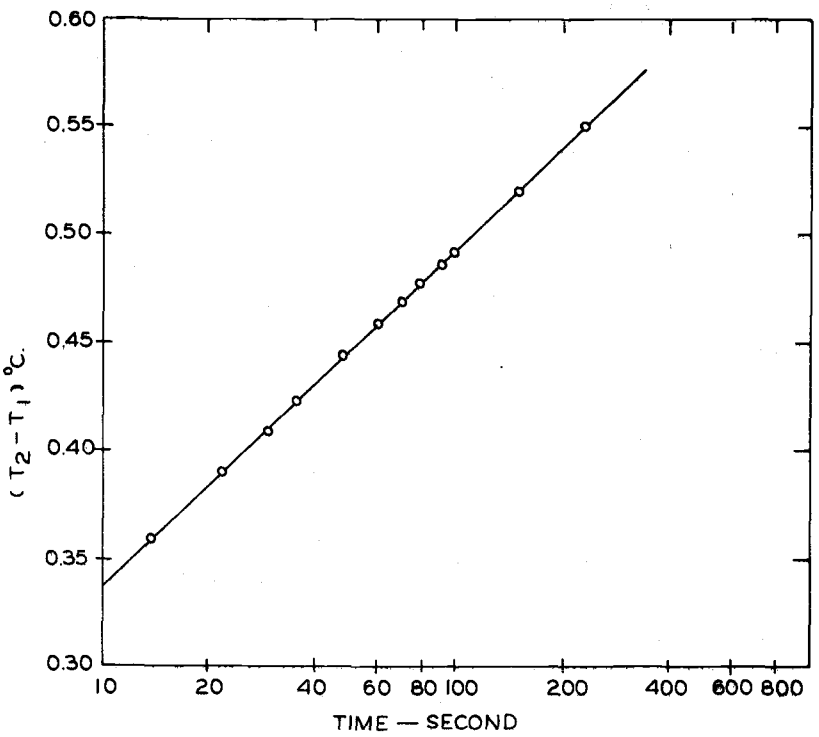

Figure 3. Graph of (T_2-T_1) as a function of logarithm of time.

The water content of each sample was determined gravimetrically immediately after the apparent thermal conductivity measurements were completed.

Results

Apparent thermal conductivities as a function of water content are shown in Figures 4, 6, and 6. Measurements were made at 25 C and 45 C.

Equations (3) and (4) along with (7) and (8) were used to calculate the apparent thermal conductivities. The thermal conductivity of air in water vapor filled pores was obtained from Equation (1) and (10) at water contents above θ_e. Values of θ_e were found by trial and error. The thermal conductivity of air used in the calculations at water contents less than θ_e was computed with Equation (9). A complete list of the parameters and their values used in the computation is shown in Table 2. The thermal conductivities of the soil constituents were adopted from de Vries (1963).

The values of the effective water content, θ_e, were chosen at the points where the apparent thermal conductivity declines sharply as soil-water content decreased. At this water content calculations with the soil air as well as with the soil water as the continuous medium were made. Average values of the computed apparent thermal conductivities for each condition were used at this critical water content.

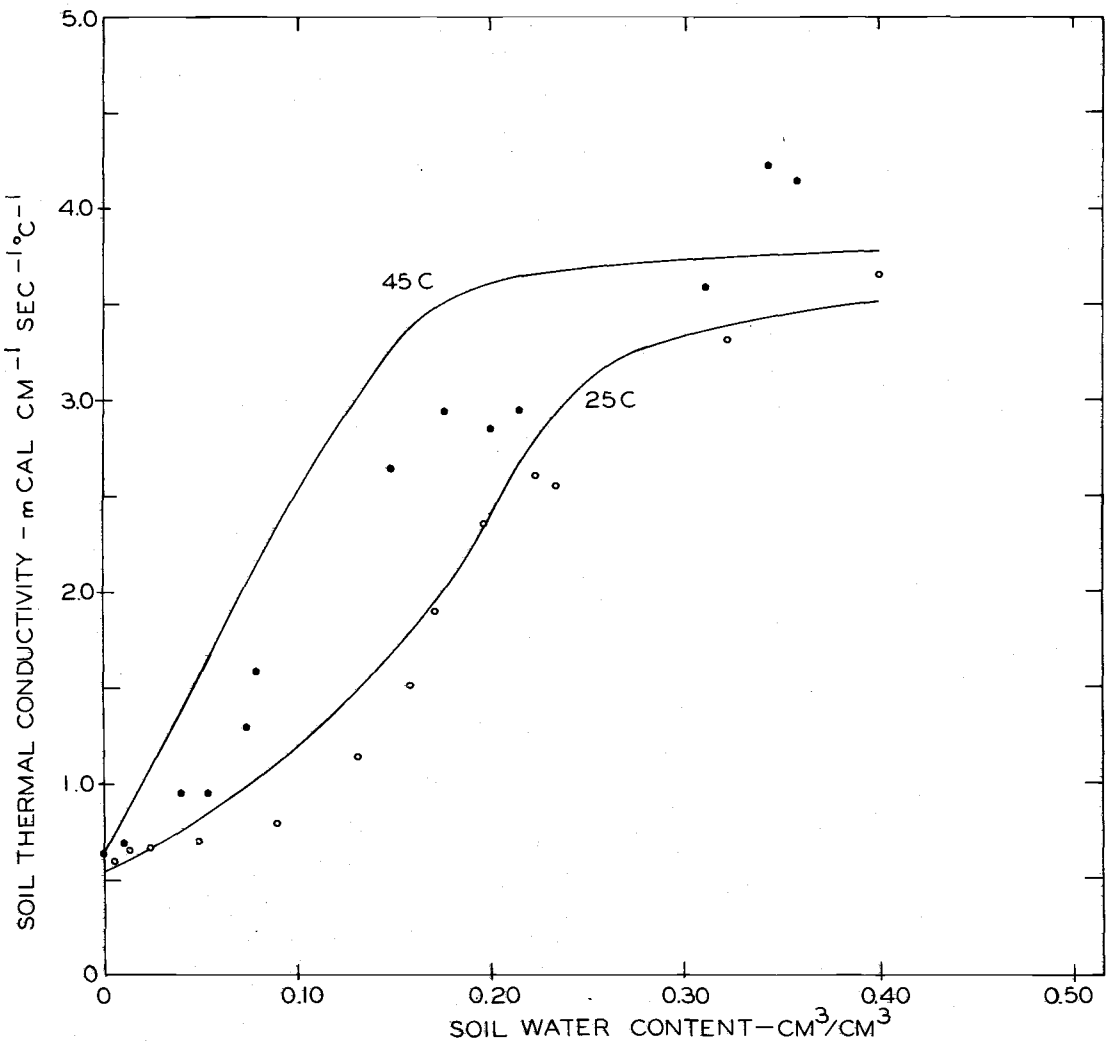

Figure 4. Apparent thermal conductivity of the Quincy soil as a function of water content measured at 25 C (open circles) and 45 C (closed circles). The solid lines are based on calculations according to the de Vries (1963) model.

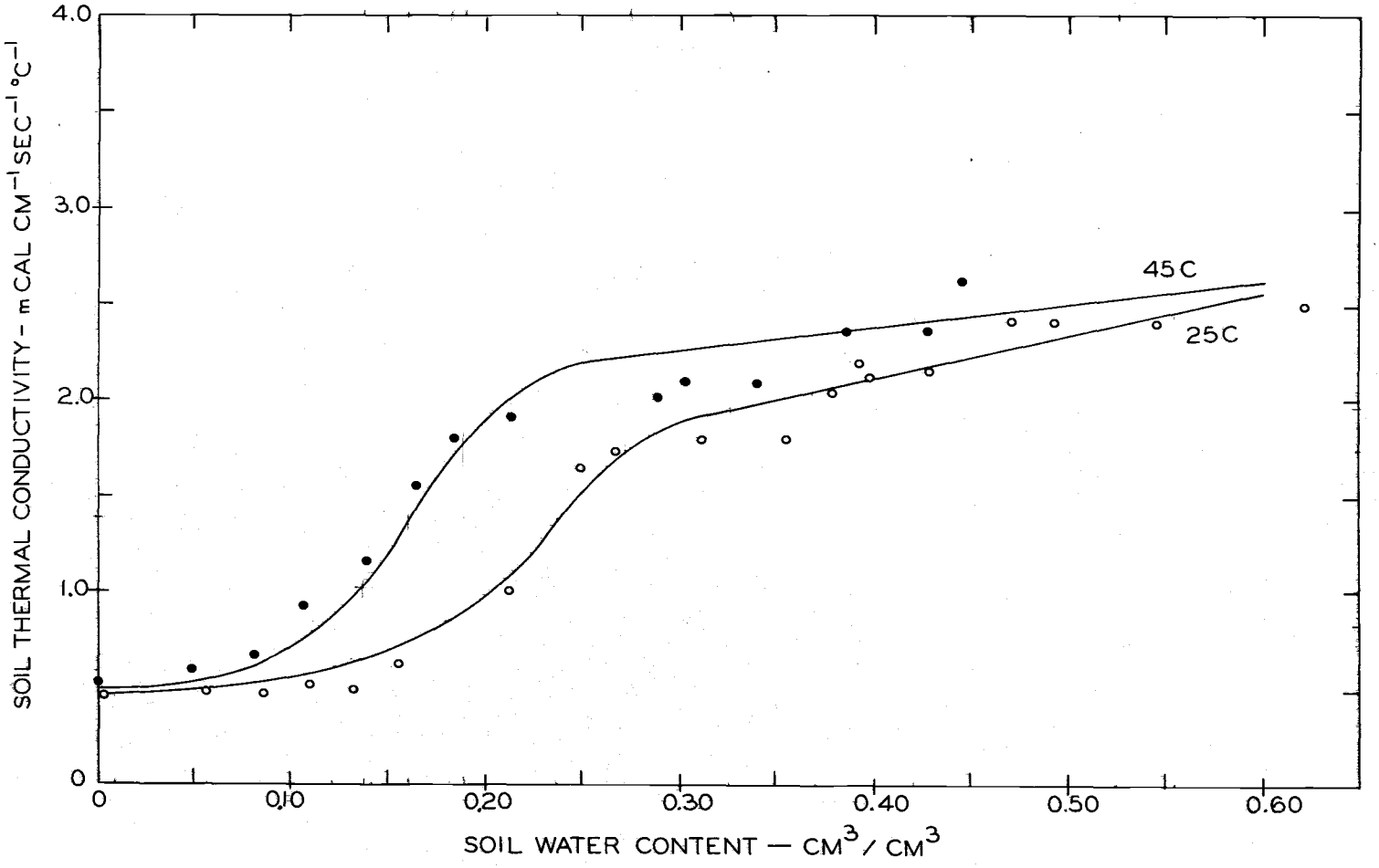

Figure 5. Apparent thermal conductivity of the Cloquato soil as a function of water content measured at 25 C (open circles) and 45 C (closed circles). The solid lines are based on calculations according to the de Vries (1963) model.

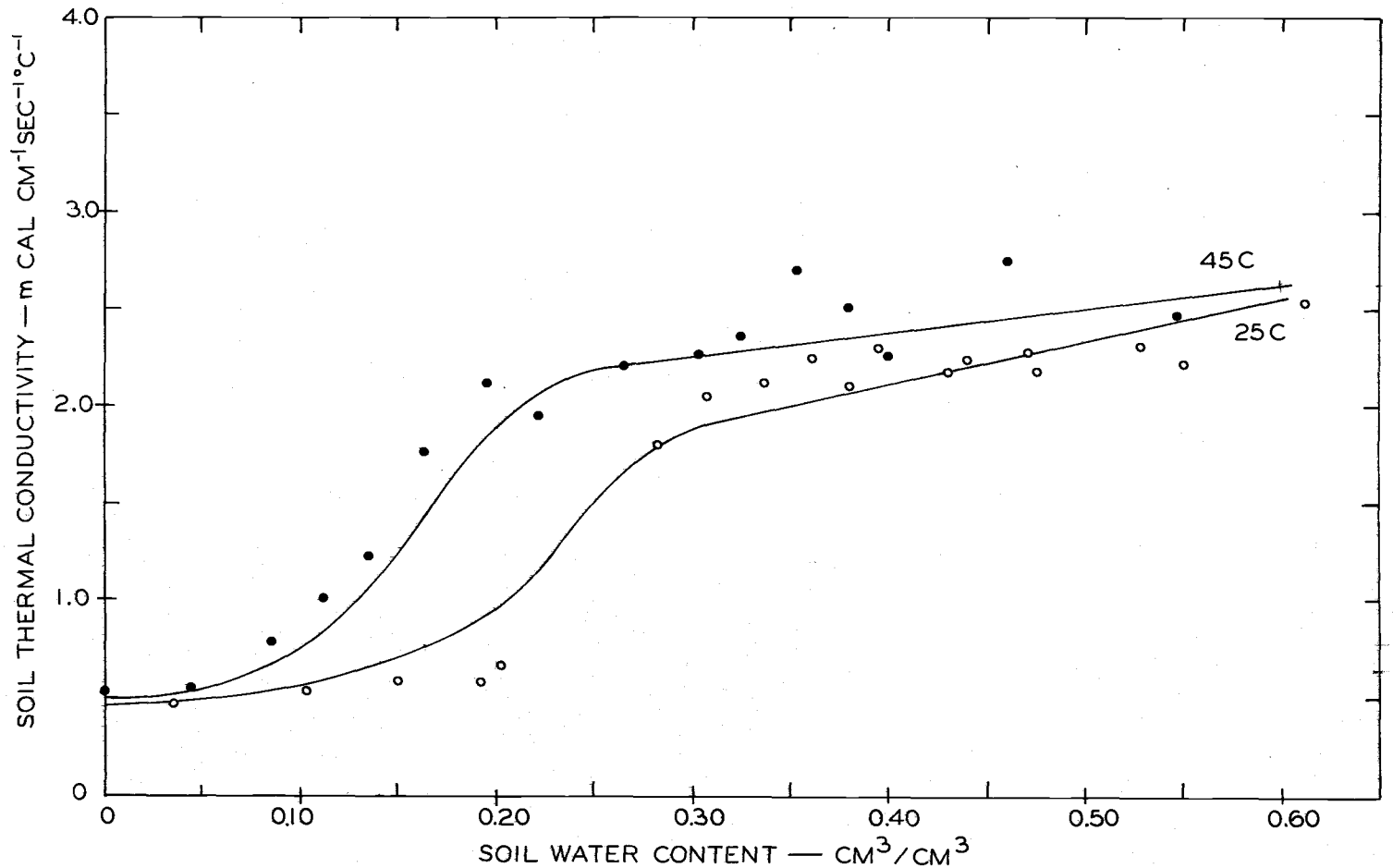

Figure 6. Apparent thermal conductivity of the Chehalis soil as a function of water content measured at 25 C (open circles) and 45 C (closed circles). The solid lines are based on calculations according to the de Vries (1963) model.

Table 2. List of parameters and their values used in the calculation of the apparent soil thermal conductivities.

Material	Effective Water Content, θ_e		Thermal Conductivity of Soil Constituents	
	25 C	45 C	25 C	45 C
	-- cm^3/cm^3 --		---mcal/cm sec C---	
Quincy	0.25	0.20	8.0	8.0
Cloquato	0.25	0.19	5.25	5.25
Chehalis	0.25	0.19	5.25	5.25
Water	--	--	1.43	1.53
Air	--	--	0.0615	0.0650

Results of the calculations and measurements are shown in Tables 3, 4, and 5. Ratios of experimental and computed apparent thermal conductivities are also given.

The computed apparent thermal conductivities of the air dry soil were much lower than the measured values. De Vries (1963) stated that when value of λ_s/λ_a is of order of 100, the λ values derived from Equation (2) for dry conditions are lower than actual values. He proposed a correction factor of 1.25 for dry sandy soils. The values of λ_s/λ_a in dry Quincy, Cloquato and Chehalis soils were on the order of 100 in the present experiments. Hence, computed values at zero water content were multiplied by correction factors of 1.75, 1.75, and 1.25 for Chehalis, Cloquato, and Quincy soils, respectively, to match with the measured apparent thermal conductivities.

Table 3. Experimental (λ_e) and computed (λ_c) values of apparent thermal conductivity for Quincy loamy sand at 25 and 45 C.

25 C				45 C			
	Apparent Thermal Conductivity, λ		$\frac{\lambda_e}{\lambda_c}$		Apparent Thermal Conductivity, λ		$\frac{\lambda_e}{\lambda_c}$
X_w	(λ_e)	(λ_c)		X_w	(λ_e)	(λ_c)	
cm^3/cm^3	- mcal/cm sec C -			cm^3/cm^3	- mcal/cm sec C -		
0.004	0.60	0.55	1.09	0.000	0.63	0.65	0.97
0.014	0.64	0.60	1.07	0.010	0.66	0.82	0.81
0.024	0.66	0.66	1.00	0.039	0.93	1.33	0.70
0.049	0.68	0.82	0.83	0.053	0.94	1.58	0.60
0.090	0.79	1.10	0.72	0.073	1.28	1.92	0.67
0.132	1.14	1.45	0.79	0.078	1.59	2.17	0.73
0.159	1.51	1.78	0.85	0.148	2.63	3.23	0.81
0.172	1.90	1.97	0.97	0.176	2.94	3.66	0.80
0.196	2.35	2.36	1.00	0.200	2.85	3.67	0.78
0.223	2.60	2.95	0.88	0.213	2.94	3.68	0.80
0.233	2.54	2.98	0.85	0.311	3.58	3.73	0.96
0.322	3.30	3.27	1.01	0.342	4.22	3.75	1.13
0.400	4.14	3.52	1.18	0.354	4.14	3.75	1.10

Table 4. Experimental (λ_e) and computed (λ_c) values of apparent thermal conductivity for Cloquato loam at 25 and 45 C.

25 C				45 C			
	Apparent Thermal Conductivity, λ		$\frac{\lambda_e}{\lambda_c}$		Apparent Thermal Conductivity, λ		$\frac{\lambda_e}{\lambda_c}$
X_w	(λ_e)	(λ_c)		X_w	(λ_e)	(λ_c)	
cm^3/cm^3	-mcal/cm sec C-			cm^3/cm^3	-mcal/cm sec C-		
0.006	0.47	0.47	1.00	0.000	0.55	0.50	1.10
0.054	0.47	0.49	0.96	0.050	0.61	0.52	1.17
0.086	0.48	0.53	0.91	0.082	0.67	0.62	1.08
0.110	0.52	0.57	0.91	0.112	0.95	0.76	1.25
0.132	0.49	0.63	0.78	0.140	1.17	1.06	1.10
0.157	0.63	0.73	0.86	0.166	1.58	1.41	1.12
0.214	1.03	1.10	0.94	0.186	1.81	1.73	1.05
0.249	1.65	1.70	0.97	0.213	1.89	2.00	0.95
0.267	1.77	1.83	0.97	0.290	2.02	2.25	0.90
0.312	1.80	1.92	0.94	0.306	2.09	2.28	0.92
0.357	1.81	2.02	0.90	0.341	2.09	2.32	0.90
0.378	2.05	2.08	0.99	0.385	2.37	2.37	1.00
0.392	2.20	2.10	1.05	0.428	2.37	2.43	0.98
0.397	2.17	2.11	1.03	0.444	2.62	2.44	1.07
0.428	2.16	2.18	0.99				
0.471	2.41	2.27	1.06				
0.493	2.42	2.33	1.04				
0.544	2.39	2.44	0.98				

Table 5. Experimental (λ_e) and computed (λ_c) values of apparent thermal conductivity for Chehalis silt loam at 25 and 45 C.

25 C				45 C			
	Apparent Thermal Conductivity, λ		$\frac{\lambda_e}{\lambda_c}$		Apparent Thermal Conductivity, λ		$\frac{\lambda_e}{\lambda_c}$
X_w	(λ_e)	(λ_c)		X_w	(λ_e)	(λ_c)	
cm^3/cm^3	-mcal/cm sec C-			cm^3/cm^3	-mcal/cm sec C-		
0.035	0.48	0.47	1.02	0.000	0.53	0.50	1.06
0.104	0.54	0.57	0.95	0.045	0.52	0.53	0.98
0.150	0.58	0.70	0.83	0.087	0.80	0.68	1.18
0.193	0.60	0.91	0.66	0.111	1.01	0.84	1.20
0.203	0.67	0.98	0.68	0.136	1.22	1.05	1.16
0.282	1.78	1.85	0.96	0.164	1.77	1.45	1.22
0.308	2.07	1.91	1.08	0.194	2.10	1.85	1.14
0.340	2.14	1.99	1.08	0.219	1.96	2.05	0.96
0.360	2.26	2.03	1.11	0.265	2.19	2.22	0.99
0.379	2.13	2.08	1.02	0.302	2.26	2.26	1.00
0.394	2.32	2.10	1.11	0.325	2.37	2.29	1.04
0.428	2.20	2.18	1.01	0.353	2.70	2.32	1.16
0.440	2.26	2.21	1.02	0.380	2.52	2.35	1.07
0.469	2.31	2.27	1.02	0.401	2.24	2.38	0.94
0.474	2.20	2.28	0.97	0.459	2.75	2.45	1.12
0.529	2.33	2.40	0.97	0.555	2.44	2.58	0.95
0.550	2.24	2.45	0.91				

The computed results are in good agreement with experimental values for Cloquato and Chehalis soils. The computed values are systematically slightly higher at 25 C and slightly lower at 45 C at low water contents for both these soils. This may be due to incorrectly having assumed a linear relationship between the effective thermal conductivity of the air and the soil water content at water contents below θ_e.

Experimental values for the Quincy soil (Table 2) at low water contents are systematically lower than the computed results. The quantity of water required to wet the soil samples to the desired level at low water content was very small. It was difficult to mix the required amount of water with the dry soil to obtain a uniform water content in the samples. Non-uniform water distribution at low water content could result in experimental values of apparent thermal conductivities lower than the values corresponding to the average water content.

Theoretical estimates of the apparent thermal conductivity of a soil can be obtained if the mineral composition, porosity, and water content and the thermal conductivities of each of these components are known. The accuracy of the thermal conductivities obtained by this procedure (de Vries, 1963) is sufficient for many practical applications. At water contents higher than 0.2 to 0.3 cm^3/cm^3, the predicted apparent thermal conductivities differed from the measured

values by about 10 percent for Cloquato and Chehalis soils (Tables 3 and 4). The deviations were greater than 10 percent for Quincy at almost all water contents (Table 2), and at low water contents for Cloquato and Chehalis soils. Variation of the apparent thermal conductivity in a given soil at a given depth due to the nonhomogeneity of the soil and due to irregular changes in the water content may be expected to be of the order of 5 to 10 percent (de Vries, 1963).

Discussion

Thermal Conductivity as a Function of Particle Size

The coarse textured Quincy soil has a higher thermal conductivity than the fine textured Cloquato or Chehalis soils in the air dry state. This difference may be attributed to the lower thermal conductivity of the granular material in fine-textured soils. De Vries (1963) reported thermal conductivities of 21, 11, and 7 mcal/cm sec C for quartz, granite, and clay minerals, respectively. Nakshabandi and Kohnke (1965) also showed the apparent thermal conductivity of air dry soil to increase with particle size. Nagpal and Boersma (1974) comparing the thermal conductivities of glass bead media of different sizes could not show the effect of grain size on the apparent thermal conductivity of the medium. Glass beads possess the same thermal conductivity regardless of bead size. These results suggest that the

small differences in the thermal conductivities of the air-dry materials used in the experiments are due to differences in the thermal conductivities of the particle materials and not to the size of the particles.

Thermal Conductivity as a Function of Soil Water Content

Apparent thermal conductivities of the three materials remained unchanged as the water content increased from zero to certain specific values (Figures 4, 5, and 6). The amount of water in the soils at which the apparent thermal conductivities started to increase is shown in Figure 7 as a function of clay content at 25 and 45 C. The indicated behavior can be explained by soil-water interactions. At low water content molecules of water form only thin films on the soil particles. As more water is added the thickness of the water films increases and wedges are formed at the contact points between particles. At very low water content the water films on the surfaces are only a few molecules thick and water does not fill interstices between them (Wadsworth, 1944). The films are uniform and do not improve the thermal contact between soil particles, so that heat flow is not appreciably enhanced. The amount of water required to produce films of a given thickness depends on the specific surface area of the particles which is a function of particle size, shape, and clay content. Clay particles are small but have a high specific external and internal

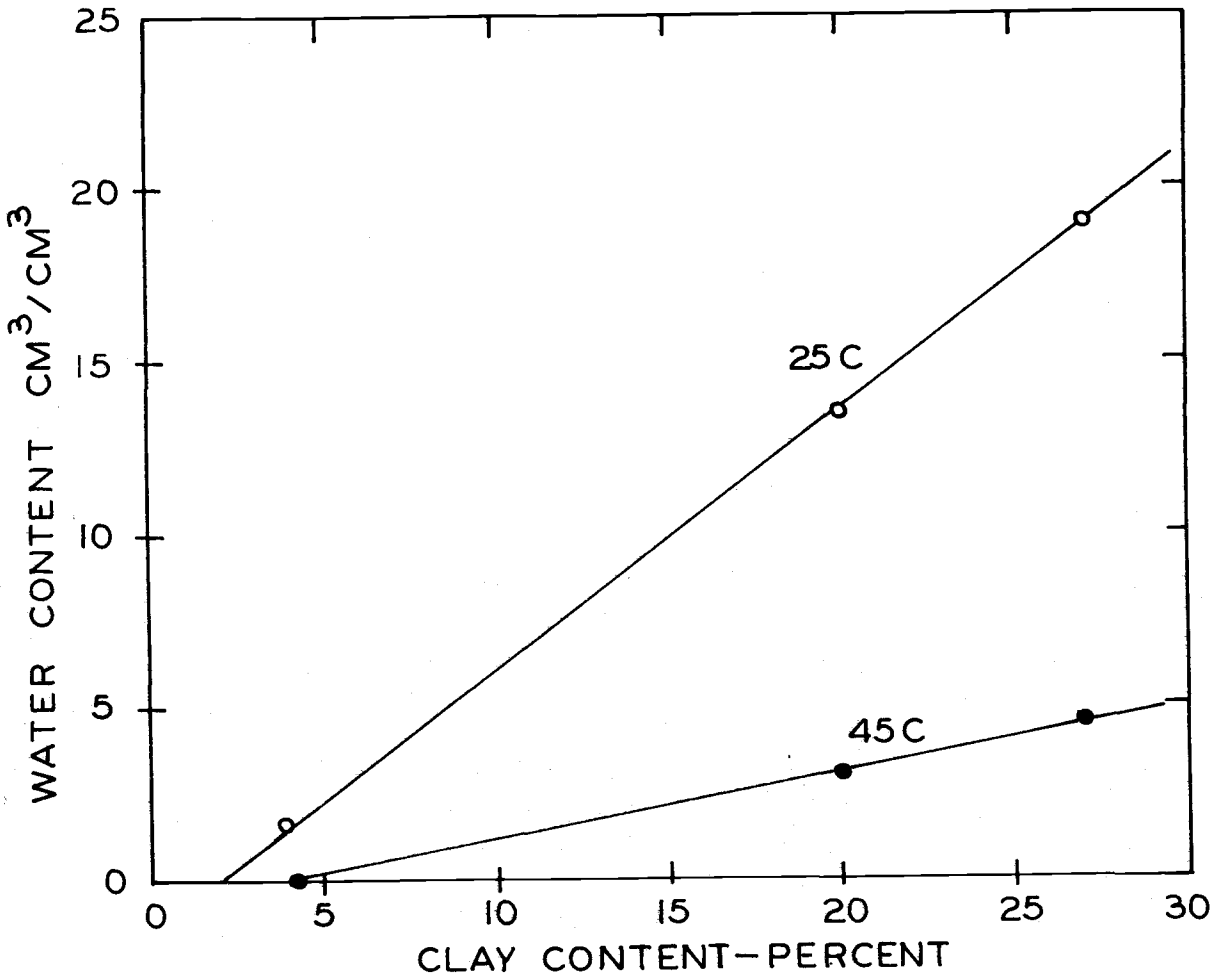

Figure 7. Maximum water content range below which the apparent thermal conductivity of the soils is constant, plotted as a function of the clay content, measured at 25 C (open circles) and 45 C (closed circles).

surface area. Clay soils need to absorb more water than sandy soils to produce the wedges which contribute to increased heat flow.

The water absorbed by the clay particles is tightly bound but can be driven off at higher temperatures. Examination of Figures 4, 5, and 6 shows that the water content at which the bound water can be driven off and contribute to heat flow decreases as a function of temperature (Figure 7).

The apparent thermal conductivities of the three soils increases with water content except at very low water content. The increase in the apparent thermal conductivity per unit of water added is greater in the coarse-textured soil than in the fine-textured soils at both temperatures. Similar observations were made by Smith (1939) and Nakshabandi and Kohnke (1965). The rate of increase of the apparent thermal conductivity with soil water content is highest at low water contents. Here the increase is due to the addition of water in the wedges at the particle contact points. The surface through which heat is conducted increases rapidly with the first increments of water added. With further additions of water, soil pores gradually are filled and the rate of increase of the apparent thermal conductivity becomes smaller.

Apparent thermal conductivity differences between the three soils are more pronounced at the higher water contents. This again shows the influence of the thermal conductivities of the particles

themselves. The sandy soil had a higher apparent thermal conductivity at water contents near saturation. Similar results were obtained by Chudnovskii (1962). He measured the apparent thermal conductivities of quartz sand and of limestone with the same grain size distributions as a function of water content. The difference between the apparent thermal conductivities of the two materials was small at the dry condition, but at a water content of 20 percent, the ratio of apparent thermal conductivities of quartz sand and limestone was 1.5.

Thermal Conductivity as a Function of Soil Water Potential

When the apparent thermal conductivity is plotted as a function of soil water potential, dissimilarities due to textural differences appear (Figure 8). These differences are greatest between coarse-textured (Quincy) and fine-textured (Cloquato and Chehalis) soils at high water potentials. No textural differences at soil water potentials lower than about -400 Joules/kg were found at 25 C. Results shown in Figure 8 are best understood by considering the soil water characteristic curves for the three soils (Figure 9). These graphs show that most of the soil water in Quincy loamy sand is withdrawn over a very narrow potential range, corresponding to the range over which its apparent thermal conductivity decreases (Figure 8). The soil water characteristic curves for Cloquato and Chehalis show that the

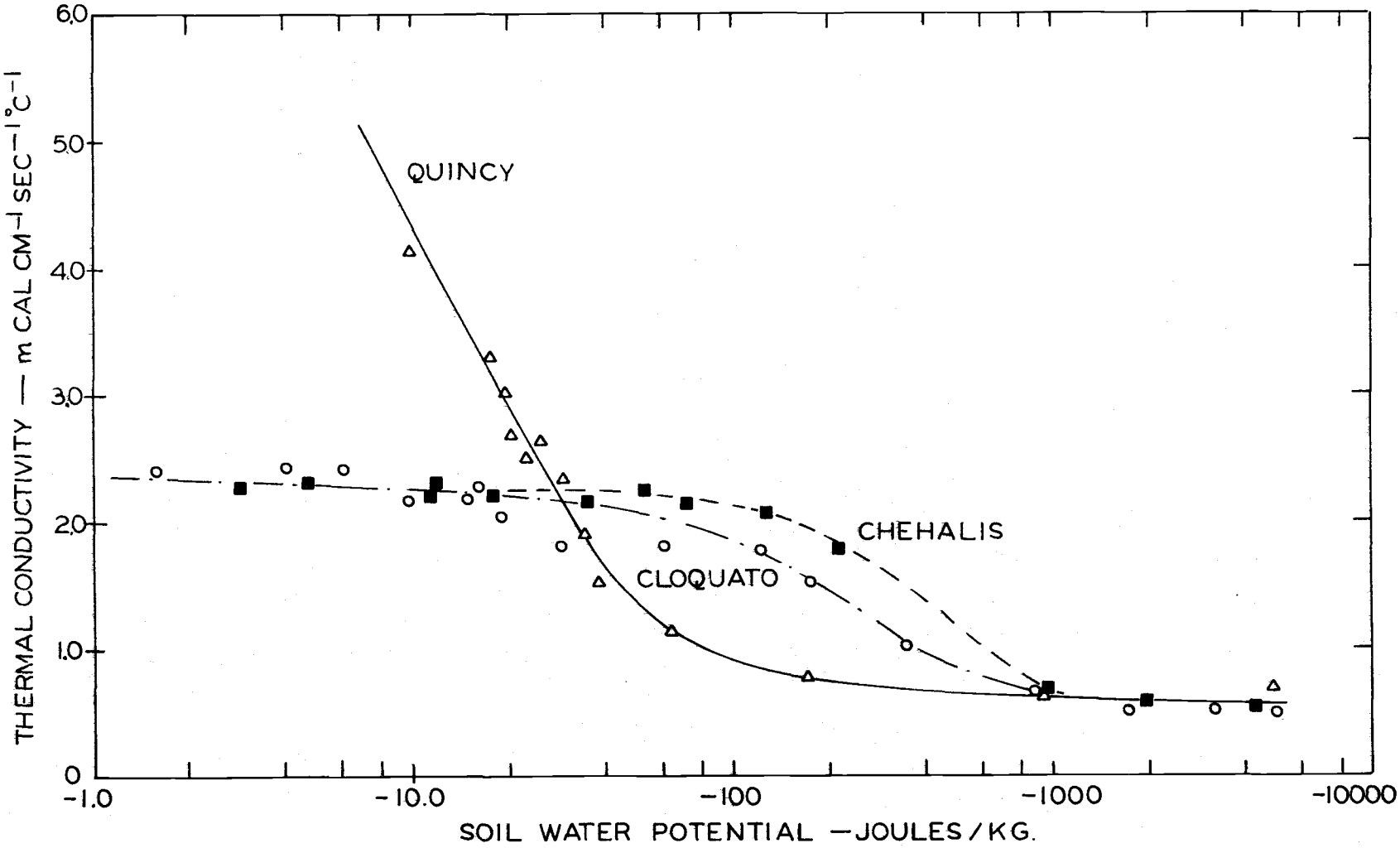

Figure 8. The apparent thermal conductivities of the Quincy, Cloquato, and Chehalis soils as a function of soil water potential at 25 C.

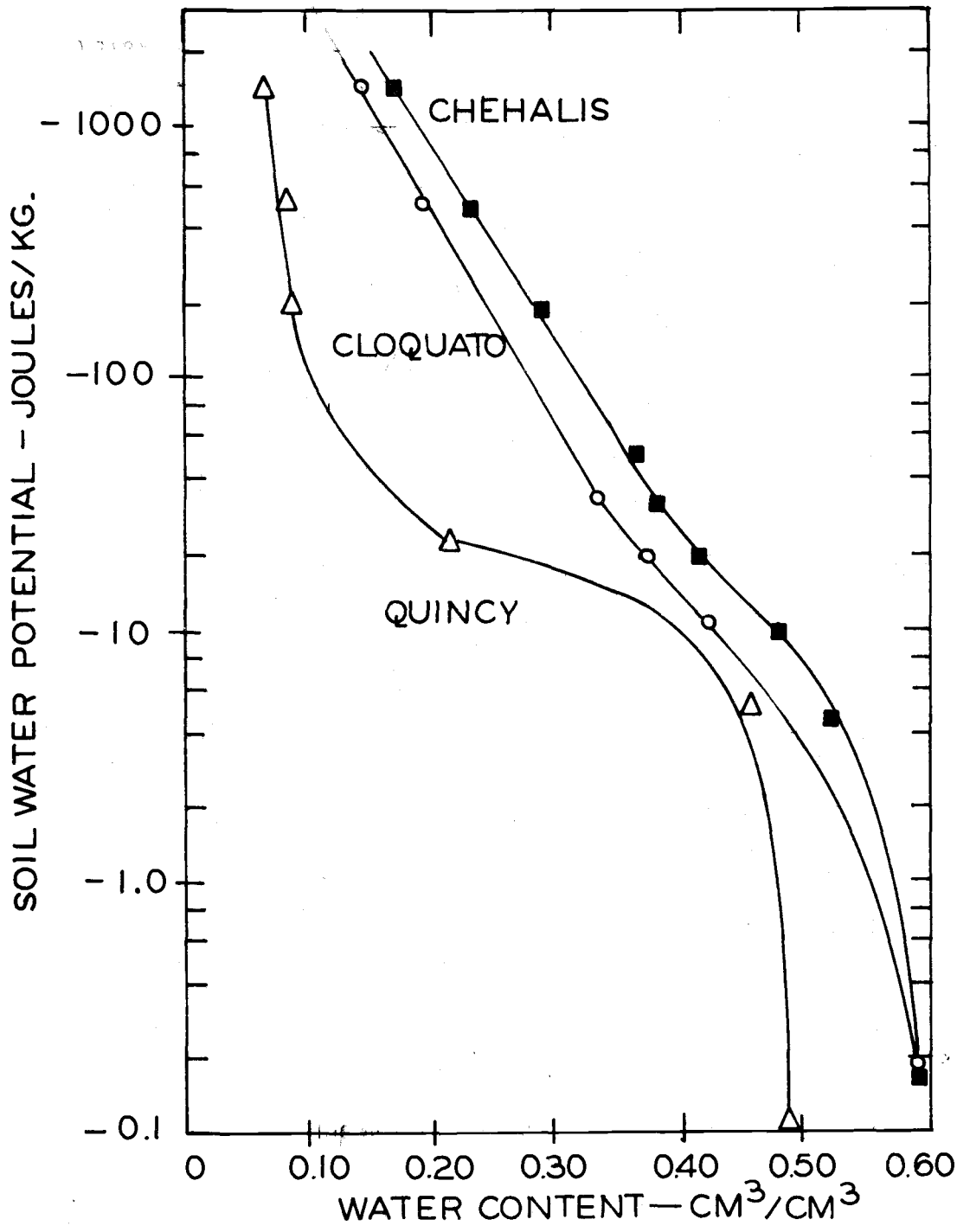

Figure 9. Soil water characteristic curves for the three soils used in the experiments. The data points shown were obtained with the pressure plate and the pressure membrane techniques. Packed cores were used for the measurements at potentials higher than -600 Joules/kg and bulk samples were used for the measurements at lower potentials.

gradual decrease of the thermal conductivities for these two soils corresponds with the gradual decrease of soil water content as the water potential decreases. Nagpal and Boersma (1974) reported pronounced textural differences in the relationship thermal conductivity-water potential for glass beads at water potentials higher than about -70 Joules/kg. The results shown in Figure 9 are in agreement with these findings.

Thermal Conductivity as a Function of Porosity

The apparent thermal conductivity of a porous medium is determined by the thermal conductivities of its constituent fractions (solid, water, and air). Porous materials with similar particles and similar total porosities should have unique thermal conductivities at various volumetric water contents. Skaggs and Smith (1967) calculated the thermal conductivity of a soil as a function of pore space and water content. Their results showed an increasing resistance to heat flow at identical water contents with increasing pore space. The effect of total pore space on the apparent thermal conductivity was most pronounced at the highest soil water contents.

Cloquato loam and Chehalis silt loam have a porosity of 60 percent and the thermal conductivities of the particles are identical. Total porosity of the Quincy loamy sand is 46.5 percent and the thermal conductivity of its particles is higher. Similarities between

the apparent thermal conductivities of the Cloquato and Chehalis soils as a function of soil water content and their difference from Quincy soil was therefore expected and in agreement with literature reports. Nakshabandi and Kohnke (1965) observed textural differences in the apparent thermal conductivity versus soil water content relationship for fine sand, silt loam, and clay with porosities of 40, 48, and 58 percent, respectively. These differences were attributed to differences in air-filled pore space at identical water contents. At higher water contents where good contact between particles increases the apparent thermal conductivity, the thermal conductivity of the particles themselves becomes important. The higher apparent thermal conductivity of the sand at identical water contents is in part due to the higher thermal conductivity of the sand particles.

Thermal Conductivity as a Function of Temperature

Apparent thermal conductivities did not change much by the increase in temperature from 25 C to 45 C at the very low water contents. The slight increase of the apparent thermal conductivities of dry soils with temperature can be attributed to increased thermal conductivity of the air at higher temperatures.

The apparent thermal conductivities of the soils increased appreciably as a function of temperature as soil water content increased. The configuration of the water films on the soil particles

remains the same at a given water content at 25 and 45 C and it should not change the conduction between particles. But a substantial increase in the apparent thermal conductivity occurred as a result of the temperature increase. The higher apparent thermal conductivity at the higher temperature is due to enhanced vapor transfer through the air-filled pores. The increases in the apparent thermal conductivities as a result of the temperature increase from 25 to 45 C are smaller at the high water contents. This is so because air filled pore space available for vapor diffusion is less.

Effective thermal conductivity of an air-filled pore is due to heat conductance, λ_a and convective vapor movement, λ_v so that

$$\lambda_{eff.} = \lambda_a + \lambda_v ,$$

where λ_a changes slightly with temperature, increasing from 0.0615 to 0.0650 mcal/cm sec C as the temperature increases from 25 to 45 C. However, λ_v varies greatly with temperature. Krischer and Rohnalter (1940) derived Equation (10) to calculate λ_v^s for conditions where the air in the pores is saturated with water vapor. Equation (10) shows that λ_v^s varies with dp_0/dT. Saturated vapor pressure is an exponential function of temperature, so that the value of dp_0/dT varies with temperature. The ratio of dp_0/dT at 45 C and 25 C is $r = 2.6$.

Ratios of the apparent thermal conductivities of the three soils at 45 C and 25 C are shown in Figure 10 as a function of the pore volume fraction available for vapor diffusion. The maximum values of the ratios are 2.15, 2.73, and 2.96, respectively. Comparison of these values with the ratio of dp_0/dT at 45 and 25 C, which is equal to 2.61, suggests that increased vapor diffusion was the prime mechanism causing the increase of apparent thermal conductivity with temperature at low soil water content. The ratio of $\lambda_{45}/\lambda_{25}$ approaches one at air-filled porosities higher than 0.95 and lower than 0.45. It never becomes equal to one because of the higher thermal conductivities of air and water at higher temperatures. The contribution of vapor diffusion to apparent thermal conductivity increases as soil water content decreases or the air-filled pore volume increases.

The ratios of $\lambda_{45}/\lambda_{25}$ are lowest for the Quincy sand. This is so because the apparent thermal conductivity of the sand particles is higher than that of the clay particles. The relative contribution of vapor transfer is therefore smaller.

The contribution of water vapor diffusion to the apparent thermal conductivity depends on the vapor pressure gradient and the diffusion coefficient. These parameters both increase with temperature. The vapor diffusion coefficient also increases with increasing air-filled porosity. Therefore, the temperature effect on the apparent

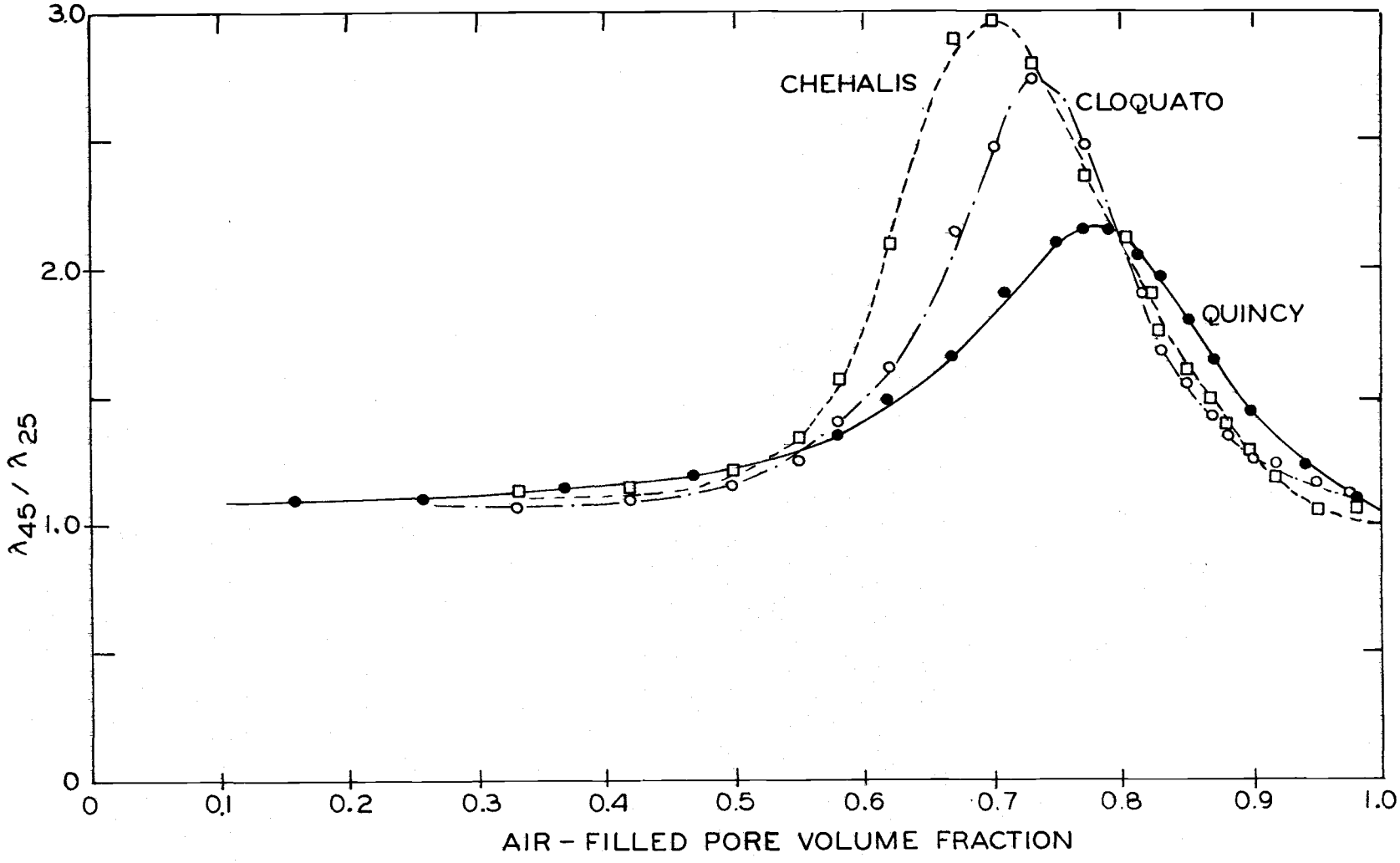

Figure 10. Ratios of the apparent thermal conductivities at 45 and 25 C ($\lambda_{45}/\lambda_{25}$) for the three soils as a function of the air-filled pore volume reported as a percentage of the total pore volume.

thermal conductivity is greatest in soil with the highest air-filled porosity. At extremely low water content the ratio $\lambda_{45}/\lambda_{25}$ decreases (Figure 10). This decrease occurs because the air-filled pores are not saturated with water vapor at these low water contents. Philip and de Vries (1957) have shown that when the soil air is not saturated with water vapor the value of λ_v is proportional to the relative humidity, p/p_0, thus:

$$\lambda_v = \frac{p}{p_0} \lambda_v^s \tag{13}$$

and

$$\frac{p}{p_0} = \exp\left(\frac{4M\sigma}{\rho dRT} \right) \tag{14}$$

where p is the water vapor pressure (mm Hg), M is the molecular weight of water (gram/mole), σ is the surface tension of water (dyne/cm), ρ is the density of water (gram/cm^3), d is the pore diameter (cm), R is the gas constant (8.314×10^7 erg/mole K), and T is the Kelvin temperature. At extremely low water content only small pores are filled with water. According to Equations (13) and (14), σ_v decreases and so does its contribution to the apparent thermal conductivity.

The maximum ratio of apparent thermal conductivities at 45 and 25 C occurred at the air-filled porosities of 0.78, 0.73, and 0.70 in Quincy, Cloquato and Chehalis soils respectively (Figure 10). These

values correspond to water contents of 0.11, 0.15, and 0.18 cm^3/cm^3.

At high water contents the pore volume available for vapor diffusion is very small and discontinuous. The ratios approach one near saturation. Temperature was found to have only a small effect on the apparent thermal conductivities at water contents higher than 0.20, 0.25, and 0.30 cm^3/cm^3 in Quincy, Cloquato and Chehalis soils, respectively.

Conclusions

The apparent thermal conductivities of soils change with water content. The changes are greatest at water content levels between field capacity and wilting point. The apparent thermal conductivity does not vary with water content at extremely low levels. Water increases the thermal contact between soil particles and enhances heat flow in the soil by increasing soil apparent thermal conductivity. At low water contents, water molecules form layers on the surfaces of clay particles and do not contribute to heat flow. The water content at which the water begins to have an effect on the apparent thermal conductivity was proportional to the clay content.

In unsaturated soil, air-filled pores are available for vapor diffusion resulting from vapor density gradients. Vapor flow contributed to the apparent thermal conductivity. Its effect is greatest at low water contents where enough water is available to produce

saturated conditions and enough pore space is present for vapor flow to occur.

The apparent thermal conductivity increased with temperature. This increase, due to an increase in the thermal conductivity of water, is negligible. Temperature has a significant effect on the apparent thermal conductivity by increasing the vapor pressure gradients in air-filled pores. In the range of water contents where vapor flow contributes significantly to the apparent thermal conductivity, the maximum $\lambda_{45}/\lambda_{25}$ values were 2.15, 2.73, and 2.96 for Quincy, Cloquato, and Chehalis soils, respectively. The value of the vapor pressure ratio at 45 and 25 C is 2.6 which is close to the maximum ratios obtained for the three soils. Vapor diffusion did not contribute significantly to the apparent thermal conductivity at water contents above field capacity where the air-filled pore volume available for vapor flow is small and probably discontinuous.

A plot of the apparent thermal conductivity versus soil water potential showed differences between soils with different textures except at water potentials lower than -300 to -400 Joules/kg.

The de Vries (1963) model can be used satisfactorily to calculate apparent thermal conductivities of soils using the thermal conductivities of the solid particles, porosity, and water content.

A temperature increase from 25 to 45 C increased the apparent thermal conductivity almost three times at low water content. This suggests that appreciable error may result from the use of a constant value for the thermal conductivity in heat flow problems in soils.

EXPERIMENTAL PROCEDURES FOR THE ANALYSIS OF SUBSURFACE SOIL WARMING AND IRRIGATION SYSTEMS

Soil columns were used in laboratory studies to simulate the open field soil warming system. Soils were contained in boxes 48 cm deep, 40 cm long, and 4 cm wide on the inside (Figure 11). The box was made of 0.5 cm thick acrylic plastic. Dimensions of the container were dictated by available materials and laboratory equipment. A heat source 0.7 cm in diameter consisting of a copper covered electrical resistance heating wire was placed 32 cm deep and 1.5 cm from the inside of the right hand wall of the box. This configuration simulated an open field soil warming system with heat sources 32 cm deep, 77 cm apart. Small holes were drilled through the wall of the box for the insertion of thermistors for temperature measurements.

Physical properties of the soils used are shown in Table 1. Air dried soil materials were packed in the containers and saturated with water from below until free water appeared at the soil surface. At this time the soil column was disconnected from the water source and excess water was allowed to drain. Surface evaporation was prevented during the drainage period. The containers were then covered with styrofoam on all sides except at the soil surface and thermistors were inserted at the pre-determined points. All preparations and experiments were conducted in a constant temperature room

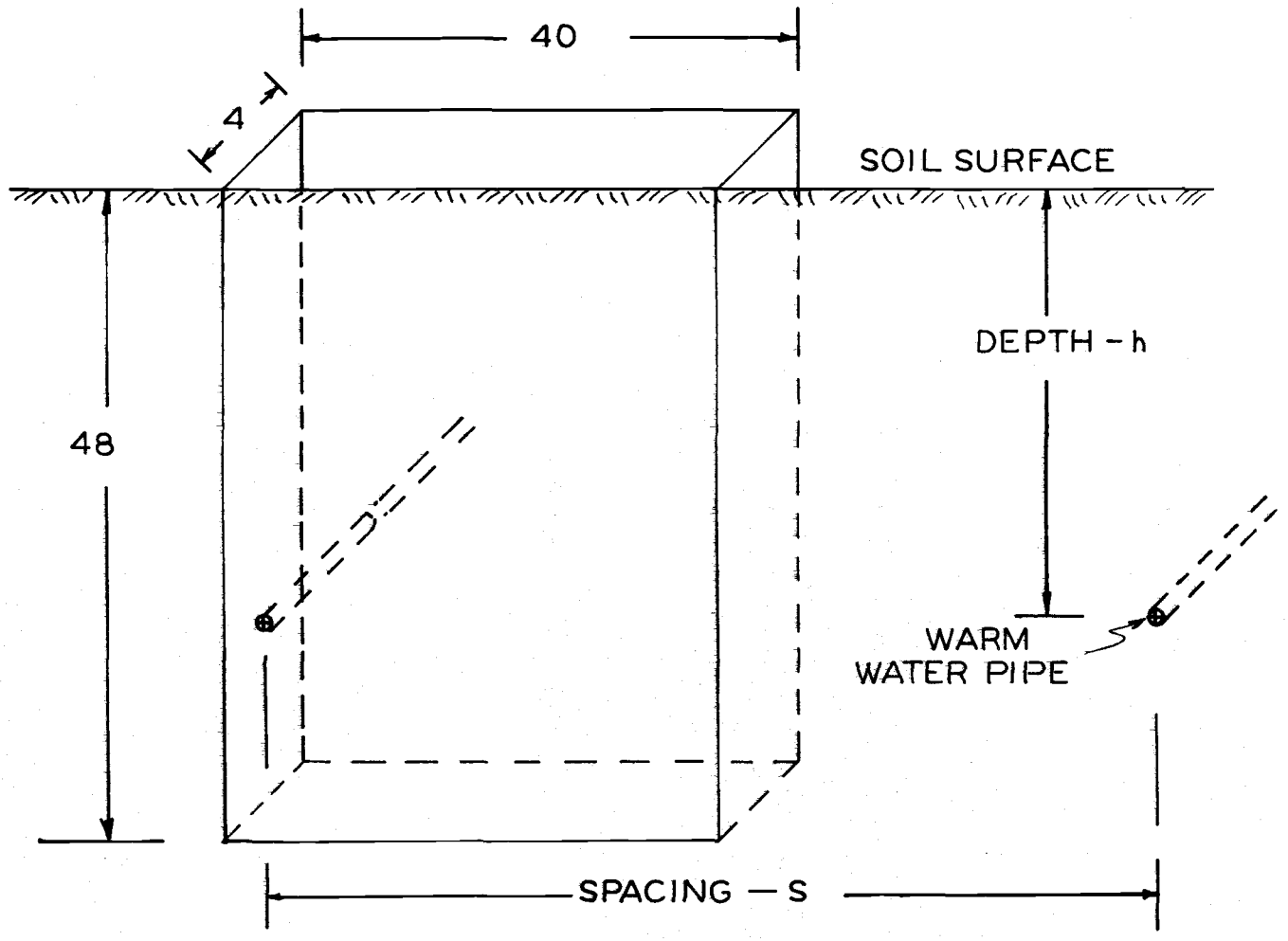

Figure 11. Geometry of the experimental soil slab used for the laboratory experiments. The heat source representing the warm water pipe was at a depth of 32 cm. The water source (not shown) was immediately above the heat source.

maintained at 22 ± 1 C.

Heating the Sample

The heat source consisted of a resistance heating element made of number 22 helically wound nichrome wire with a total resistance of 5.31 ohms. The wire coil was covered with heat shrinkable P.V.C. tubing and inserted in copper tubing with an O.D. of 0.5 cm, 13.4 cm long. The heat source was energized by an AC power supply of 3.43 volts at heat source temperatures of 29, and 36 C, and at 4.10 volts at the heat source temperature of 44 C. The temperature of the heat source was controlled by a Barber Colman CP5152 Temperature Controller. Periods during which the heat source was energized were recorded with a Rustrak event recorder. Rate of heat input at the heat source was calculated from the duration of heating periods using the equation

$$Q = \frac{V^2 \tau}{4.18 \Omega} \tag{15}$$

where V is the voltage of the AC power supply (volts), Ω is the resistance of the heating element (ohms), τ is the fraction of time that the heater was energized, and Q is the heat input (cal/sec). The heat source temperature was adjustable. Experiments were conducted at heat source temperatures of 29, 36, and 44 C for each soil sample.

A series of experiments was conducted with the soil surface temperature constant at the temperature of the room. Further experiments were conducted with diurnal temperature variations at the soil surface. These were obtained with a resistance heating element positioned 10 cm above the soil surface. The heat flux from this source was regulated with a sinusoidal power controller. The resistance heating element consisted of number 22 helically wound nichrome wire with a total resistance of 48 ohms. The wire coils were stretched slightly to fit three parallel rows 45 cm long with 2.5 cm between centers and were supported by porcelain insulators at each end. Additional resistance wire was used for series connections between the rows to avoid an abrupt cool end effect. A U-shaped polished stainless steel reflector and auxiliary aluminum foil end pieces directed the heat energy downwards. An aluminum frame held the heater assembly 10 cm above the soil surface.

Power for the heating element was derived from a Hewlett-Packard 6443B 300 watt DC power supply with a capacity of 2.5 amperes at 120 volts. The instrument was modified for remote voltage programming by use of a variable external voltage.

A controller was constructed to provide an approximate sinusoidal power input to the sample. The time base was selected so that the positive half cycle (0-180 degrees) was 12 hours long. No power was applied to the sample during the negative half cycle.

During this time conductive and radiative cooling continued. Heat output from the heater as a function of time is shown in Figure 12. Maximum heat input occurred six hours (90 degrees) after initiating the heating cycle. The basic sinusoidal voltage was derived from a continuous rotation sine function potentiometer driven by a synchronous motor. An appropriate resistance-voltage network was calculated to transform the sinusoidal resistance function into a shaped voltage to program the power supply for a sinusoidal output. The peak rate of energy output was adjustable. Experiments were conducted at maximum voltages of 25, 50, and 75 volts into the 48 ohm heater, producing maximum energy output rates of 13, 52, and 117 watts, respectively (Table 6).

Table 6. List of experiments conducted in the laboratory study of the soil warming system.

Experiment No.		Heat Source Temperature	Subsurface Irrigation	Peak Rate of Irradiation
		°C		Watt
1	Quincy	29	yes	0
2	Quincy	29	yes	13
3	Quincy	29	yes	52
4	Quincy	29	yes	117
5	Cloquato	36	yes	0
6	Cloquato	36	yes	13
7	Cloquato	36	yes	52
8	Cloquato	36	yes	117
9	Chehalis	44	yes	0
10	Chehalis	44	yes	13
11	Chehalis	44	yes	52
12	Chehalis	44	yes	117
13	Quincy	29	no	117

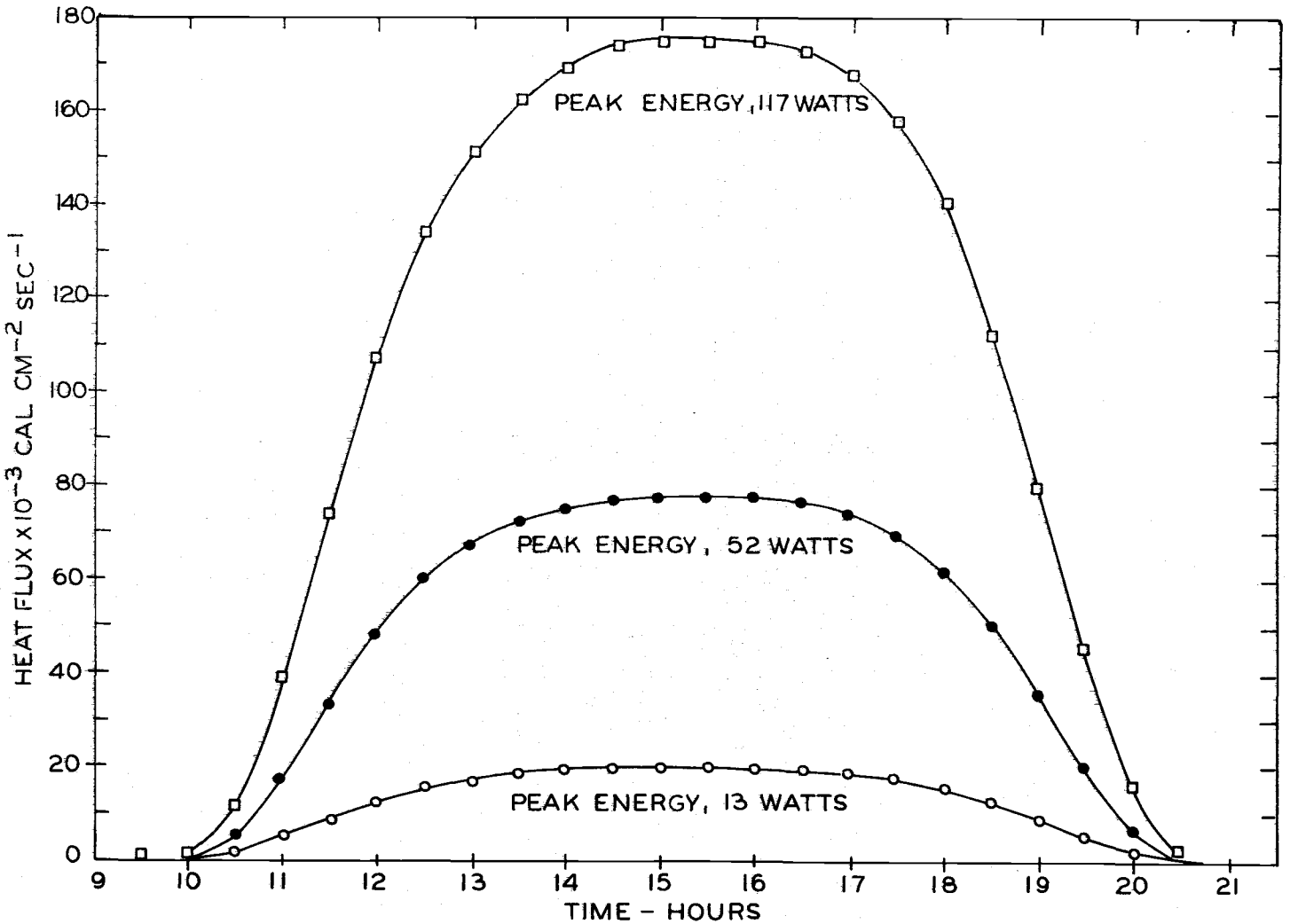

Figure 12. Heat output of the soil surface heater as a function of time. Three rates of energy output were used.

Temperature Measurements

The temperature sensors (thermistors) were inserted into holes drilled through the side of the soil container. Temperature measurements were made at depths of 1, 3, 6, 12, 24, 28, 32, 34, 38, and 46 cm, with vertical rows placed at distances of 1, 4, 8, 16, and 36 cm from the side of the box (Figure 13). The thermistors penetrated about 2 cm into the sample. Fenwall GB 41P8 glass probe thermistors were used. Each thermistor was calibrated individually, against a Hewlett-Packard 2801A quartz thermometer, in terms of its resistance as a function of temperature. Thermistor resistance values at several temperatures were obtained and plotted (Figure 14).

A single channel strip chart recorder was employed to record the resistance of each thermistor. The chart readings were calibrated in terms of resistance with a resistance box. A plot of the chart reading as a function of resistance is shown in Figure 15. Thermistors with similar calibration specifications were classified in separate groups. For each group of thermistors, a relation was drawn between chart reading and temperature. A table was prepared showing the temperature corresponding to a given chart reading.

After the soil column was put in place, experiments were commenced by energizing the heat source. Temperature readings were obtained at two-hour intervals. The temperature measuring

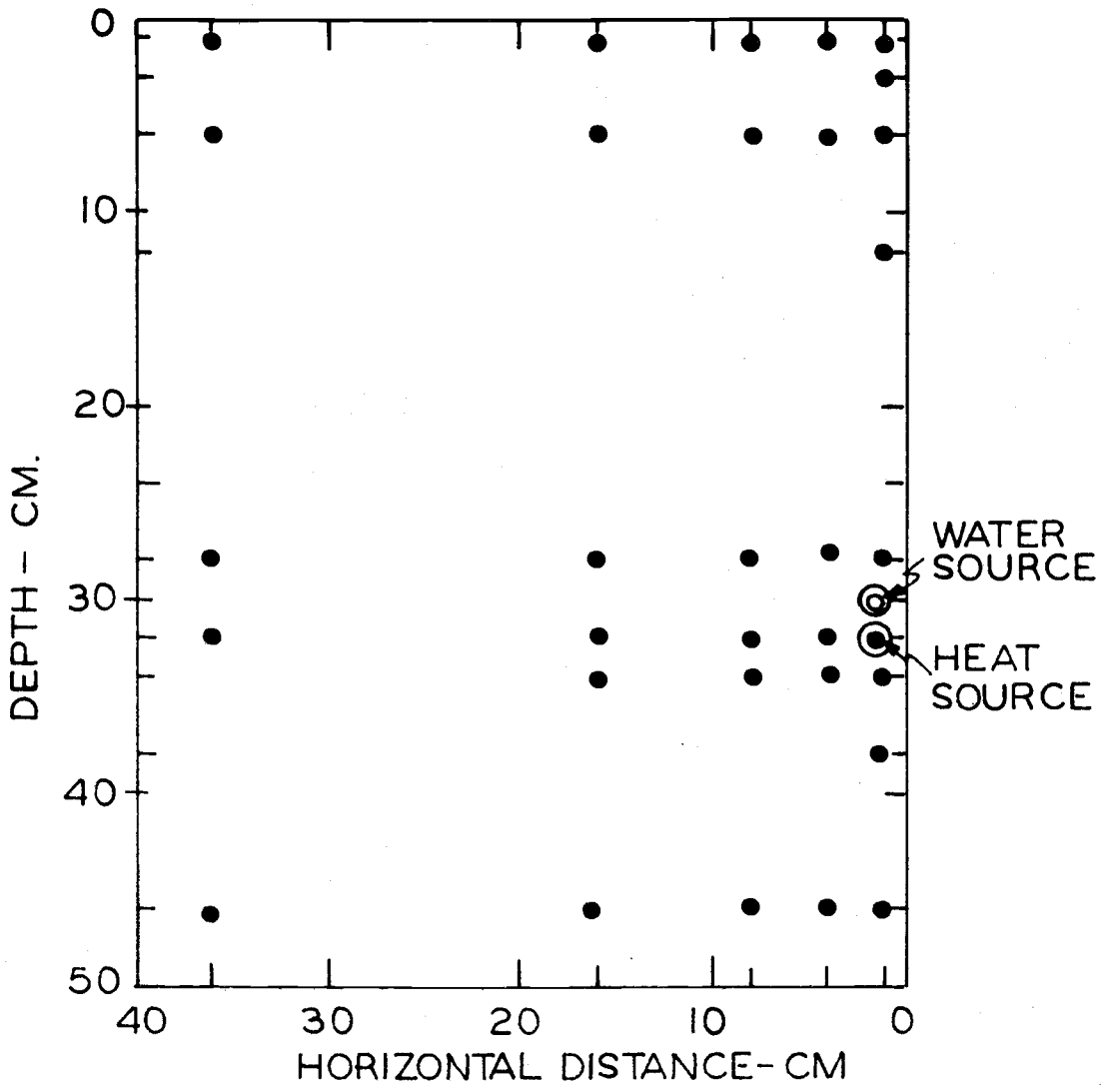

Figure 13. Thermistor placement.

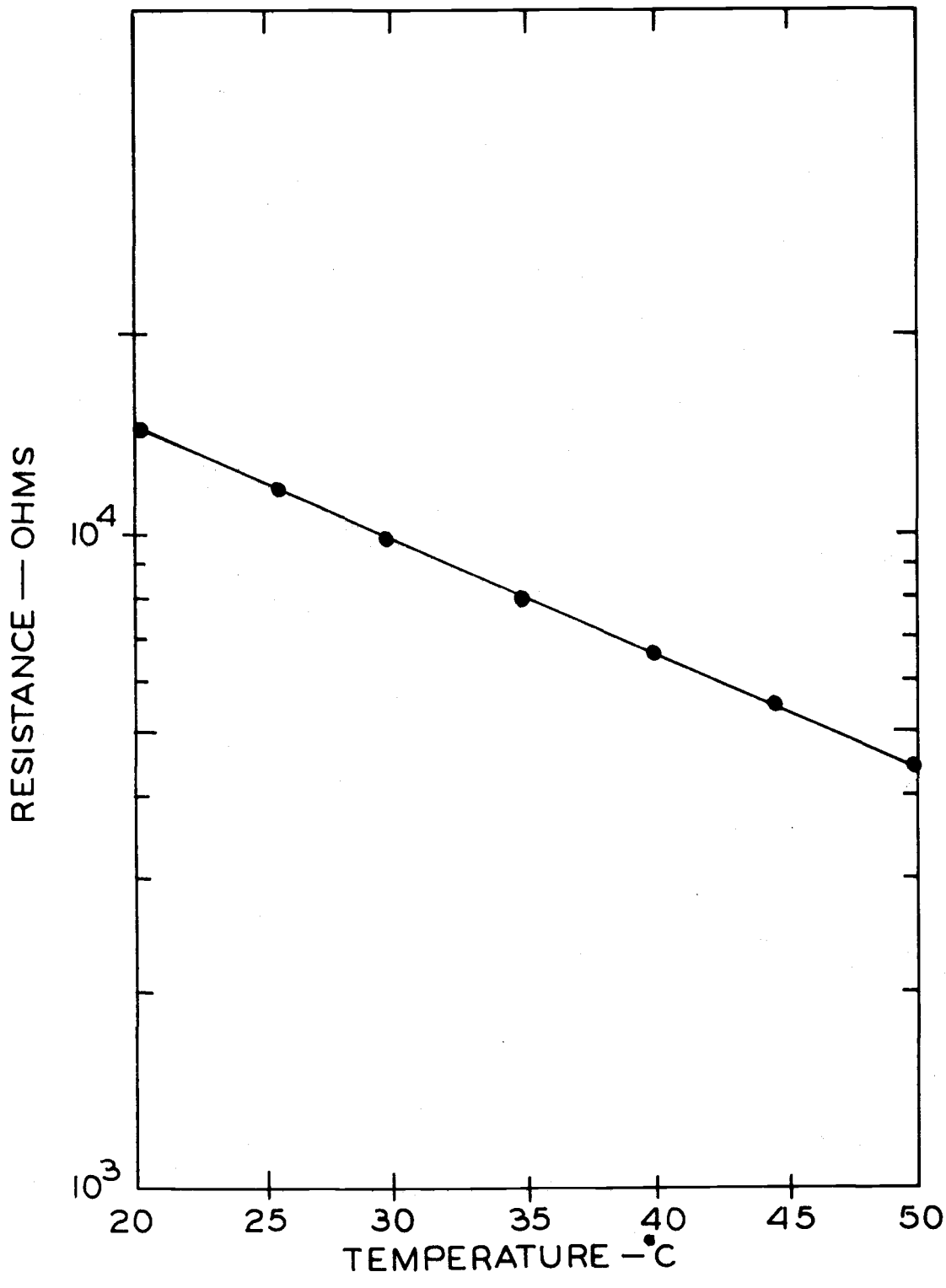

Figure 14. Thermistor resistance as a function of temperature.

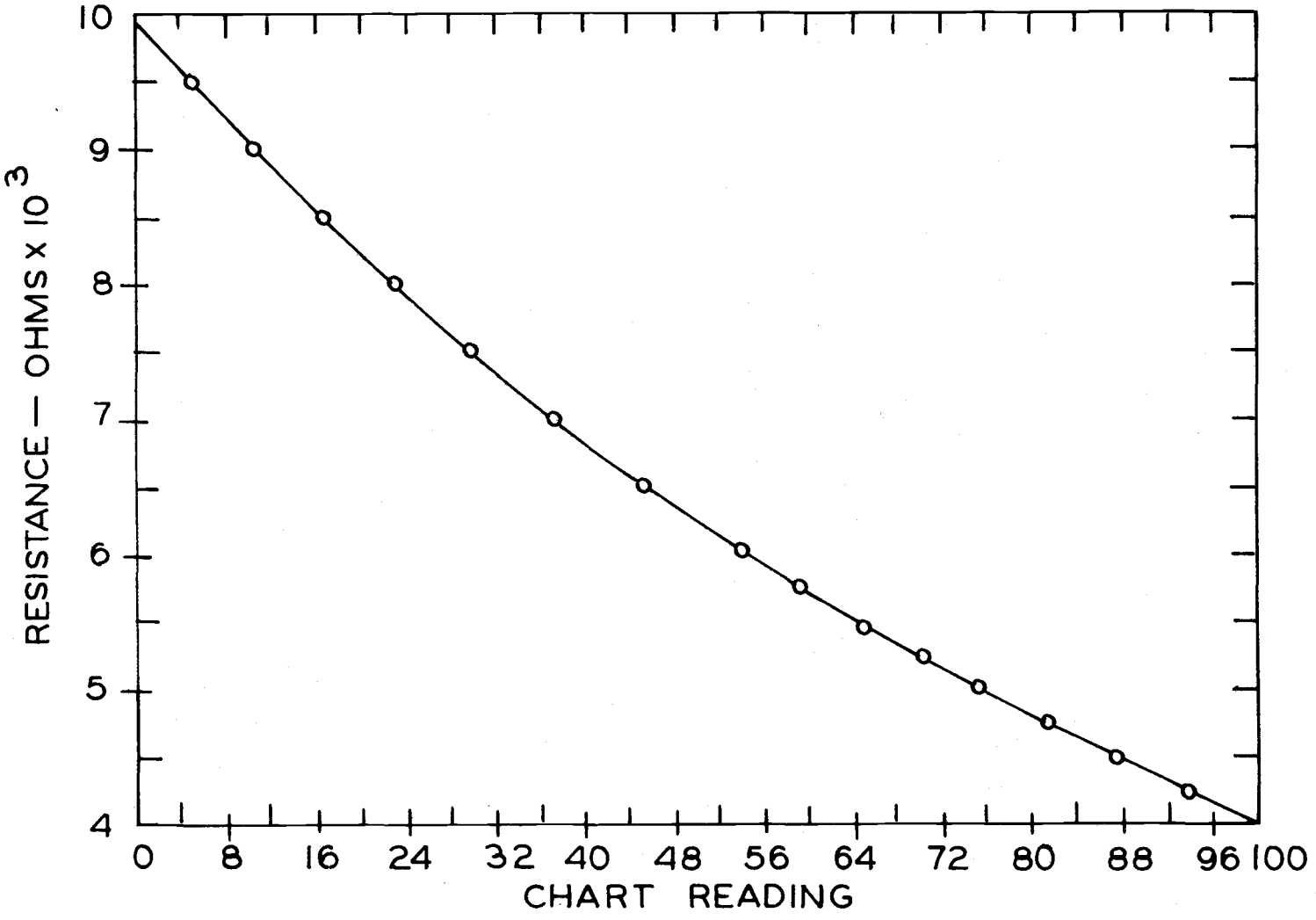

Figure 15. Calibration curve for the temperature recorder, showing the relation between chart reading and resistance.

system was activated with a time clock.

Water Application

An irrigation water source was placed 30 cm deep and 1.5 cm from the right hand wall of the soil column immediately above the heat source. It consisted of a porous tube, 3.5 cm long with an I.D. = 0.9 cm and was made of ceramic material with pore sizes ranging from 60 to 70 microns. A graduated Mariotte bottle was connected to the porous tube. The water source configuration simulated a subsurface irrigation source, 30 cm deep with a 77 cm spacing. Different evaporation conditions were simulated by the sinusoidal surface heat loads. The water content at a point close to the heat source was monitored with a gamma-ray attenuation system. Water was applied by the irrigation tube at a rate sufficient to keep the water content at its initial value. This rate was obtained by trial and error. When the appropriate rate of water application was established, several readings of water content were taken with the gamma-ray attenuation system. The points in the soil column at which soil water content measurements were made are shown in Figure 16.

Water Content Determinations

A non-destructive method for the measurement of soil water content was required. Gamma ray attenuation was employed for this

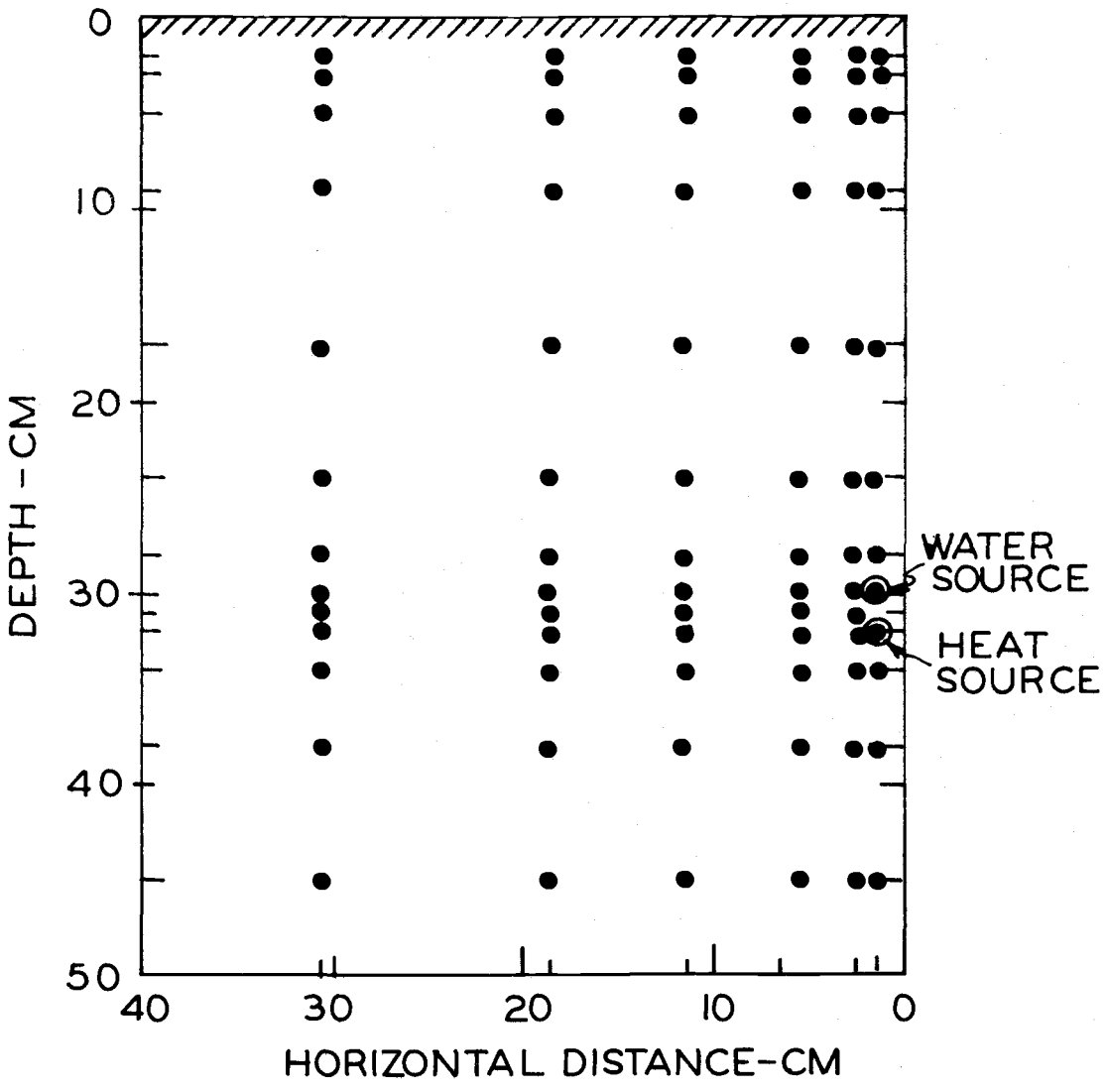

Figure 16. Positions at which water content measurements were made.

purpose by Gurr (1962), Ferguson and Gardner (1962), Rawlins and Gardner (1963), and Davidson et al. (1963). This method was used in these experiments.

The gamma-ray attenuation method is based on Beer-Lambert's Law which states that the probability that a gamma particle passing a substance is absorbed is proportional to the density of absorbing material, the distance travelled through the substance, and a characteristic coefficient. This law is obeyed when the particles are propagated in the form of monochromatic radiation. The density of the soil medium is described by the soil bulk density, ρ_s. The proportionality coefficient is defined as the mass absorption coefficient, μ, so that Beer-Lambert's Law can be written as

$$\frac{d\Lambda}{\Lambda} = -\mu\rho_s \, dz \, . \tag{15}$$

Integrating Equation (15) between the limits Λ_0 without an absorbing medium, and Λ with an absorbing medium of thickness z, yields

$$\Lambda = \Lambda_0 \exp(-\mu\rho_s z) \, , \tag{16}$$

where Λ and Λ_0 are the transmitted, and incident radiation intensities, μ is the mass absorption coefficient (cm^2/g), ρ_s is the bulk density of the medium (g/cm^3), and z is the thickness of the medium (cm). In the present experiments wet soil samples were

placed in containers. Under these conditions absorption by the container walls, the soil water, and the soil particles occurs. Hence Beer-Lambert's Law becomes

$$\Lambda = \Lambda_0 \exp[-(\mu_w\theta+\mu_s\rho_s)z - \mu_c\rho_c z_c] , \qquad (17)$$

where μ_w, μ_s, μ_c are the mass absorption coefficients of water, soil, and container material (cm^2/g), ρ_s, ρ_c are the bulk densities of soil and container material (g/cm^3), θ is the soil water content (cm^3/cm^3), and z, z_c are the sample and container wall thickness (cm). For the experimental conditions used here, the transmitted intensity, Λ, is a function of soil water content, since all other parts of the sample remained unchanged. The change in water content at any point in the soil column and at any time, t, can be obtained, using Equation (17). At time $t = t_1$

$$\Lambda_1 = \Lambda_0 \exp[-(\mu_s\rho_s+\mu_w\theta_1)z - \mu_c\rho_c z_c] , \qquad (18)$$

and at time $t = t_2$

$$\Lambda_2 = \Lambda_0 \exp[-(\mu_s\rho_s+\mu_w\theta_2)z - \mu_c\rho_c z_c] . \qquad (19)$$

Divisions of Equation (19) by Equation (18) yields

$$\frac{\Lambda_2}{\Lambda_1} = \exp[-(\theta_2-\theta_1)\mu_w z] , \qquad (20)$$

or

$$\ln \frac{\Lambda_2}{\Lambda_1} = -\mu_w z(\theta_2 - \theta_1) , \tag{21}$$

or

$$\Delta\theta = \theta_2 - \theta_1 = \frac{-1}{\mu_w z} \ln \frac{\Lambda_2}{\Lambda_1} , \tag{22}$$

where Λ_1 and Λ_2 are the transmitted radiation intensities at time t_1 and time t_2, respectively and $\Delta\theta$ is the change in water content (cm^3/cm^3). Substituting the value of μ_w for Americium 241, which was determined by Klock (1968) to be 0.1947 cm^2/g, and $z = 4$ cm, the width of soil sample, Equation (22) becomes

$$\Delta\theta = 1.351 \ln \frac{\Lambda_1}{\Lambda_2} \tag{23}$$

Equation (23) was used to calculate changes in the water content from the recorded measurements of Λ_1 and Λ_2.

The initial soil water content was determined gravimetrically at the start of the experiments. Soil water contents were also determined gravimetrically at several points when the experiments were terminated.

Gamma Ray Attenuation Equipment

The gamma-ray attenuation equipment consisted of a source of

monochromatic, low energy γ-radiation, gamma-ray-spectrometer, printer, and an automatic scanner. The gamma ray spectrometer was an assembly of a Hewlett-Packard 5201L scaler-timer, a 5551A high voltage power supply, and a 10602A scintillation detector.

The source of low energy gamma radiation employed was 229 mc Americium (Am^{241}), emitting nearly monochromatic gamma rays with approximately 60 percent of its radiation at an energy of 0.061 MeV. With this low energy output, a minimum of shielding is required. The two essential functions of a gamma-ray spectrometer, the detection of gamma rays and the measurement of their energies, are performed by the scintillation detector and the pulse height analyzer.

The scintillation detector has three parts: (i) the scintillation thallium activated sodium iodide crystal, (ii) the photomultiplier tube, and (iii) the amplifier. A gamma-particle entering the detector produces a voltage pulse suitable for measurement. The single channel pulse height analyzer sorts the pulses from the scintillation detector according to amplitude, passing those lying between two preselected limits to the scaler-timer and rejecting the others. The scaler-timer accumulates and stores pulses in digital form. The scaler also adds the pulses during a precisely defined time period. The pulse height analyzer was set to detect transmitted gamma radiation with energies 0.061 ± 0.015 MeV. The output from

the scaler was digitized and routed directly to a printer (Model HP562 AR). A digital to analog converter (Model HP580 A) was included which allowed recording the count rate with a Heathkit (Model EUW-20A) recorder when desired.

An automatic scanner was designed to move the source-detector assembly in a programmed geometric pattern with relation to the sample box. Measurements were initiated at four hour intervals by a time clock.

Sample Positioning

The source and the detector were assembled in a rigid frame to maintain the correct orientation of the collimated beam of gamma rays when moved. The assembly was mounted on a movable plate supported by split-bearings and two parallel shafts. This plate could be moved horizontally in either direction by a motor driven lead screw. Movement was controlled by a helical path pin programmer. By proper placement of program pins, the scanner could be commanded to stop the source-detector assembly at points in one cm increments along the horizontal axis of the sample box.

The sample box was mounted on a platform suspended by two vertical lead screws and two shaft and bearing assemblies. This platform could be raised or lowered by a second motor and chain drive connected to the lead screws. The platform position was

controlled by a programmer similar to that described above.

The horizontal and vertical motions were interconnected by limit switches and relays to automatically scan according to a preset program. A gating circuit was connected to the scaler-timer starting a preset count at each desired position. A second timer circuit allowed repetition of the scanning pattern at predetermined intervals.

The experimental equipment arrangement, with some modifications, is similar to the one employed by Nagpal (1971) as shown in Figure 17.

1. Stepping switch selector
2. Strip-chart recorder for thermistor
3. Stepping switch logic and power supply
4. Gamma attentuation system control box
5. Vertical motion program cam
6. Horizontal motion program cam
7. Am-241 source
8. Heater assembly
9. Sample cell
10. Pulse height analyzer, scaler-timer
11. High voltage power supply
12. Digital printer
13. Heater power supply
14. Heater sinusoidal programmer
15. Scintillation detector

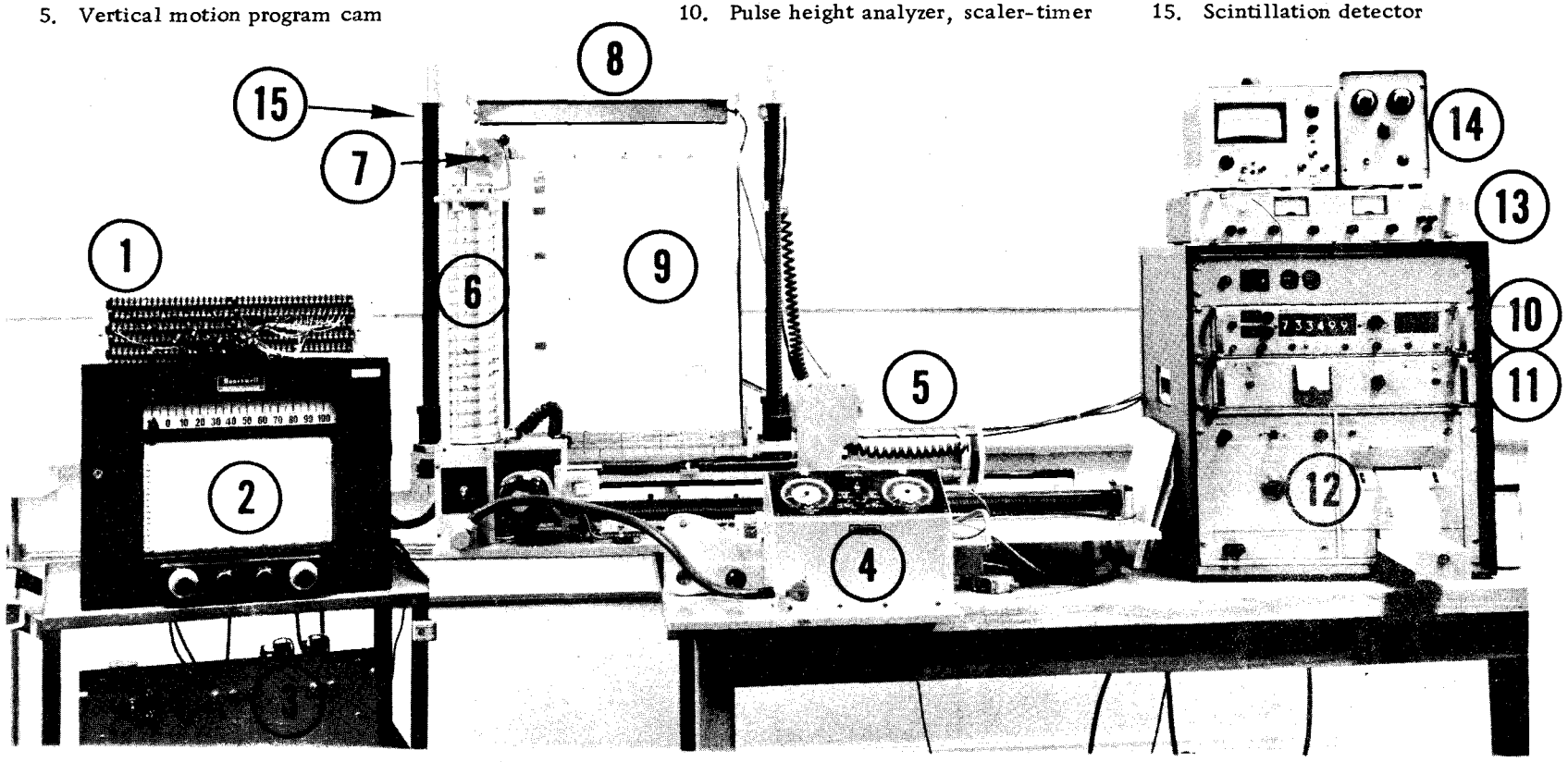

Figure 17. Experimental equipment arrangement used for the study of the soil warming and subsurface irrigation system. The sample holder (9) consists of a box with inside dimensions of 48 x 40 x 4 cm. Insulation provided around the box prevented all heat exchange except at the soil surface.

TEMPERATURE DISTRIBUTIONS

Experimental Results

Temperature readings obtained at preselected points in time during three days while equilibrium conditions existed were averaged. Figure 18 shows the temperature as a function of depth at 0:00, 4:00, 8:00, 12:00, 16:00, and 20:00 o'clock in the heated Quincy loamy sand at heat source temperatures of 29, 36, and 44 C and a sinusoidal surface heat load with a maximum of 117 watts. The measurements were made in a vertical profile centered over the heat source. Subsurface heating raised the soil temperature throughout the profile. The temperature rise was highest near the heat source. The effect of heating on the temperature of the soil was small near the soil surface. The soil surface temperatures were below the air temperature at all heat source temperatures during the cooling period.

The soil surface temperatures at 8:00 o'clock were 19.6 and 22.4 C for heat source temperatures of 29 and 44 C, respectively. They were less than the room temperature of 23 C near the soil surface during the cooling period starting at 20:00 o'clock and terminating at 8:00 o'clock. The room temperature of 23 C was the upper limit of the daily room temperature variation. The depths of the shallow surface layers with temperatures below 23 C at 8:00 o'clock were 19, 12, and 7 cm at heat source temperatures of 29, 36, and

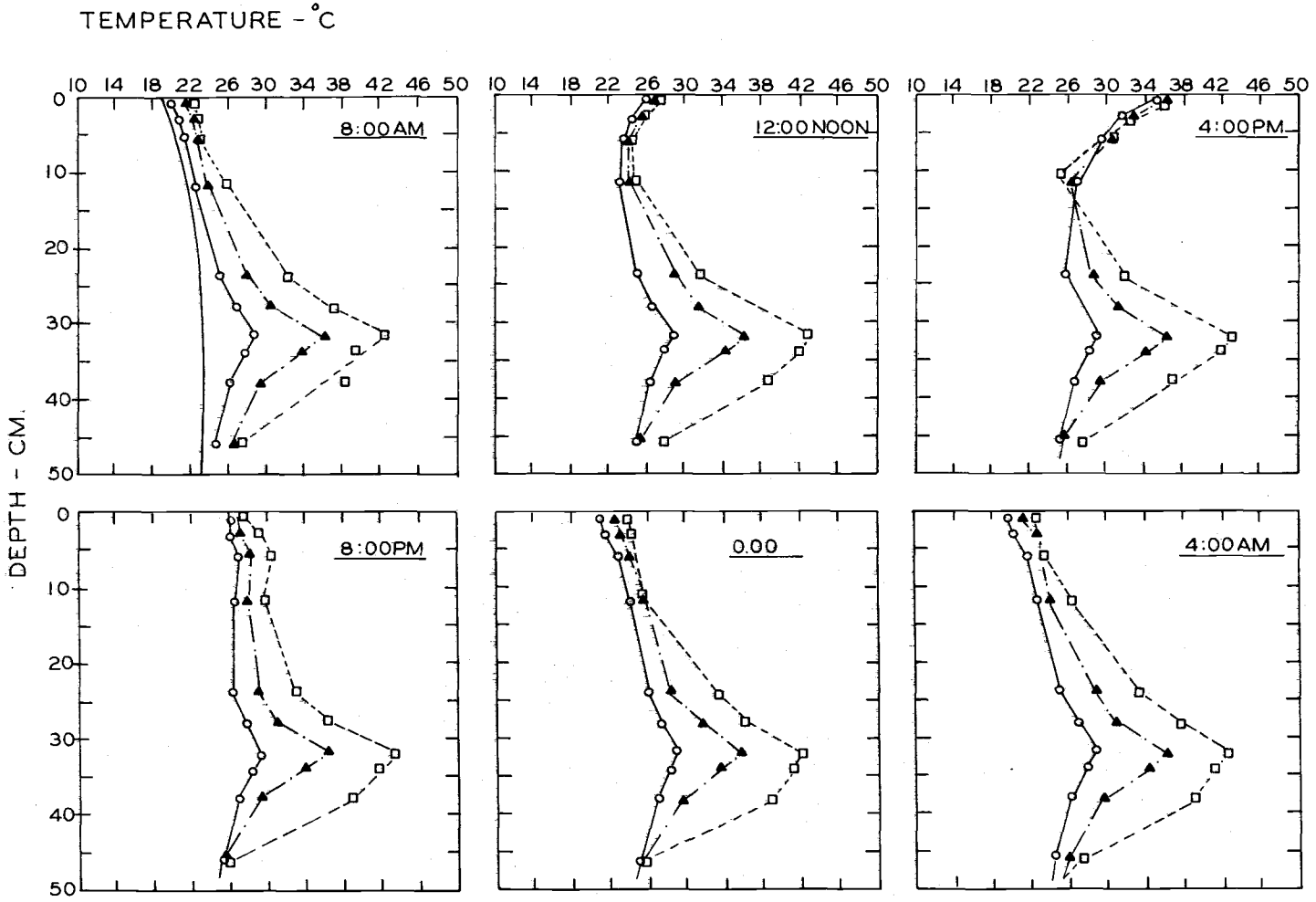

Figure 18. Soil temperature as a function of depth measured at four-hour intervals at heat source temperatures of 29 C (o), 36 C (x), and 44 C (Δ) in Quincy soil. Measurements were made in a vertical profile centered over the heat source.

44 C, respectively. The temperature of the surface layer increased during the heating period (12:00 to 16:00 o'clock) due to the surface heating.

Equilibrium temperature isotherms are shown in Figures 19, 20, and 21. No heat was applied at the soil surface in the experiments shown in these diagrams. The heat source temperature influenced the temperature of the area near the heat source greatly. Its effect decreased rapidly at points away from the heat source. The horizontal distance from the heat source to the point at which the temperature was 5 C above room temperature is shown in Table 7 as a function of the temperature difference between heat source and the unheated soil surface. The relationship was dependent on the soil texture. The distance was greatest in the loamy sand and smallest in the silt loam.

The isotherms shown indicate that a wide range of temperatures occurs in a profile heated with line heat sources. This can be important if the crop grown in the field has a narrow temperature range for optimum growth. Soil temperatures higher than the optimum root temperature may have an adverse effect on crop production. The optimum root temperature for many crops grown in temperate climates is about 25 C. Temperatures higher than 25 C were observed near the heat source. The distance over which temperatures higher than 25 C occurred was a function of the heat source temperature. The soil volume with temperatures higher than 25 C was small

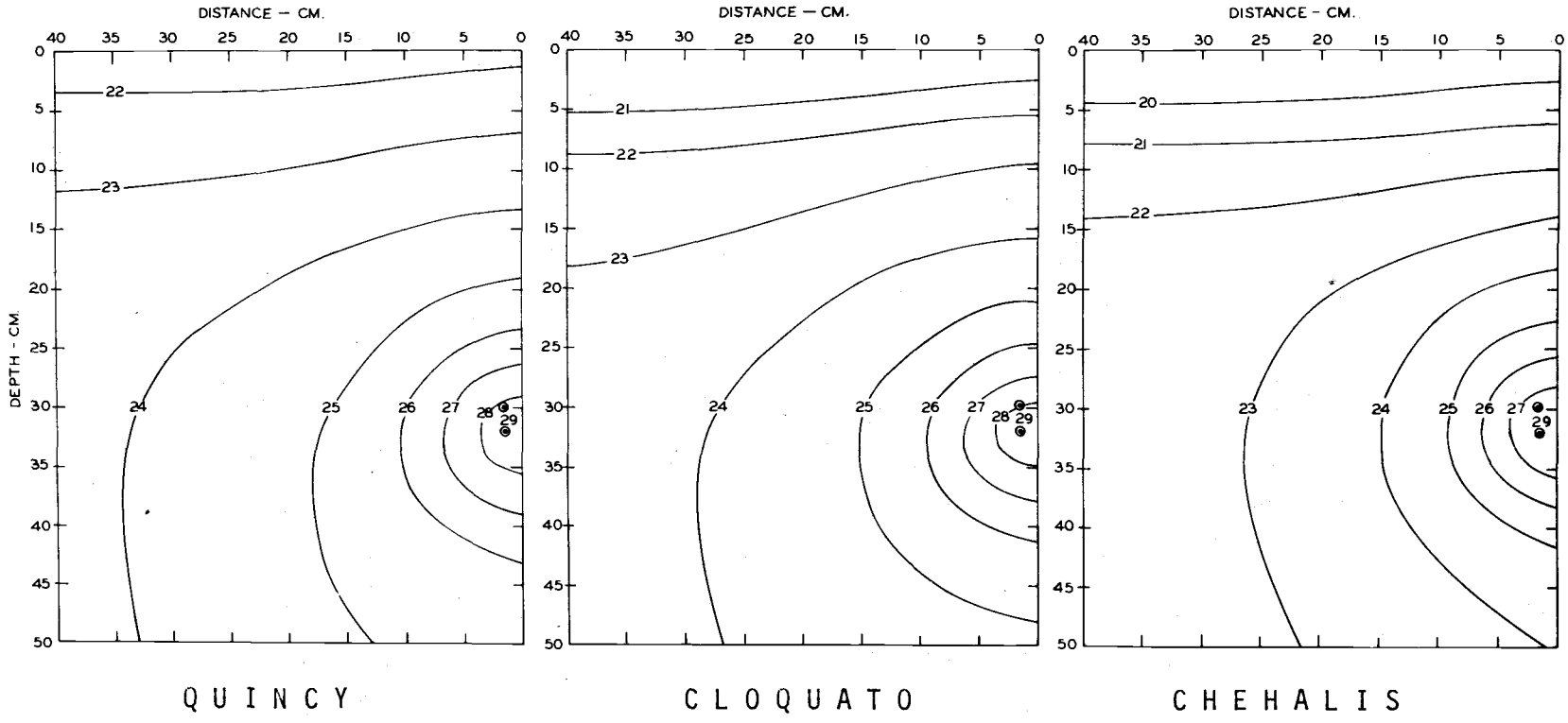

Figure 19. Measured equilibrium temperature isotherms for the Quincy, Cloquato, and Chehalis soils at a heat source temperature of 29 C. No heat was applied at the soil surface.

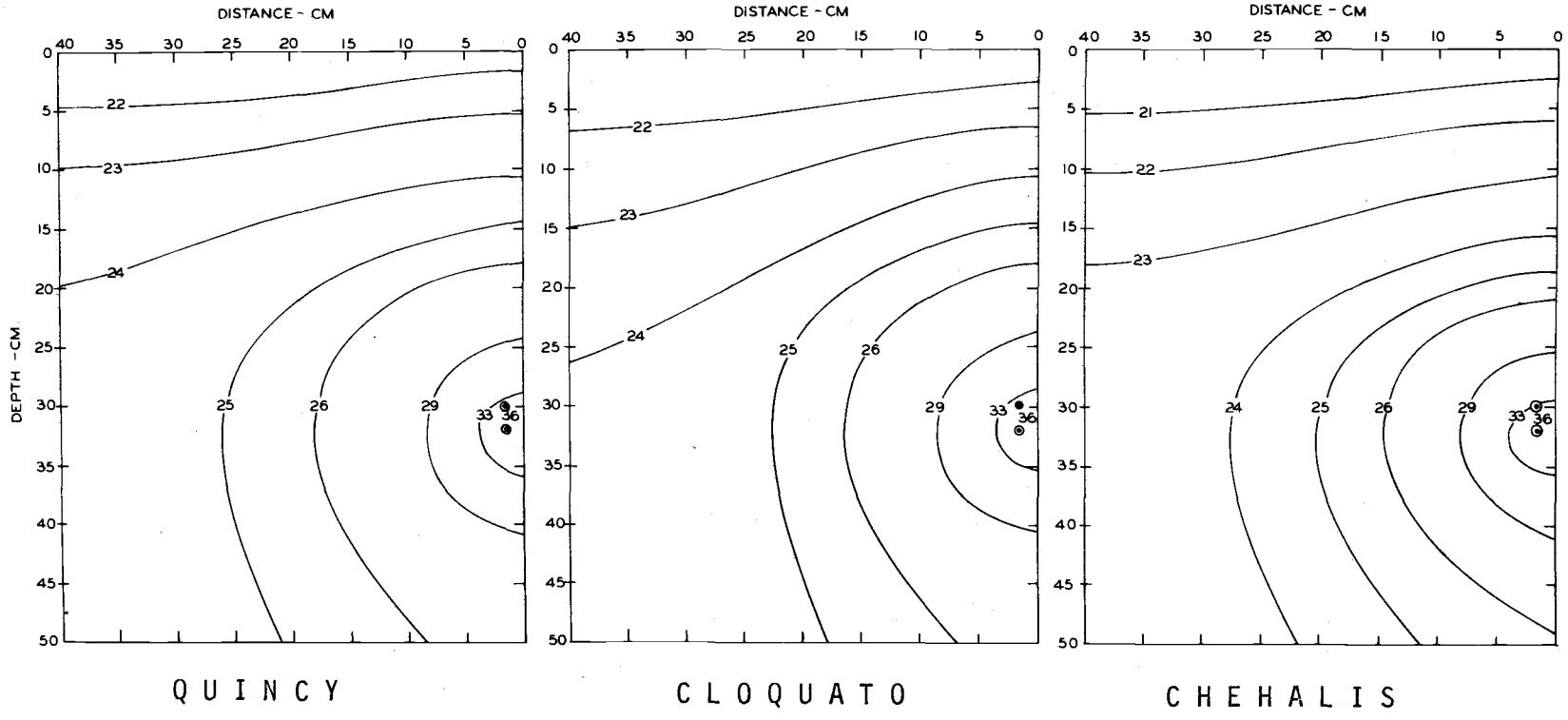

Figure 20. Measured equilibrium temperature isotherms for the Quincy, Cloquato, and Chehalis soils at a heat source temperature of 36 C. No heat was applied at the soil surface.

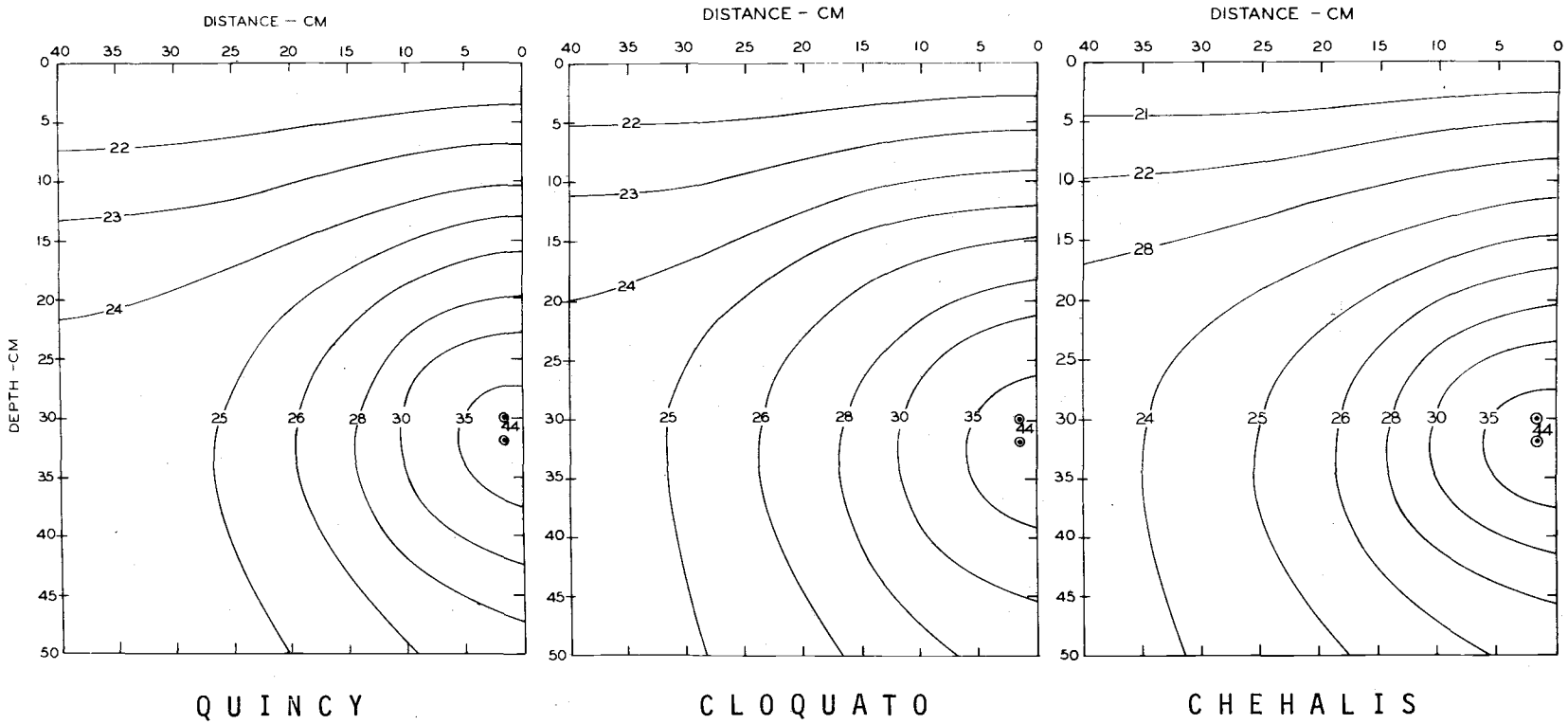

Figure 21. Measured equilibrium temperature isotherms for the Quincy, Cloquato, and Chehalis soils at a heat source temperature of 44 C. No heat was applied at the soil surface.

at a heat source temperature of 29 C, but much larger at a heat source temperature of 44 C. The adverse effect of soil temperatures above 25 C can be prevented by planting the crop seedlings some distance away from the heat sources. Soil warming had little effect on the temperature of the upper 10 cm of the soil. The thickness of this layer increased as the unheated soil temperature decreased. This is the layer at which seed germination usually occurs. Optimum temperatures for germination of most seeds ranges from 15-40 C (Mayer and Poljakoff-Mayber, 1963). When the unheated soil temperature is lower than the optimum temperature for seed germination, soil warming will not help to improve the seed germination.

Table 7. Relationship between the horizontal distance (d) from the heat source, at which a 5 C temperature rise occurred and the difference in temperature between heat source and unheated soil surface (ΔT).

Soil	Source Temperature	ΔT	d
	C	C	cm
Quincy loamy sand	29	6	4.0
Quincy loamy sand	36	13	10.0
Quincy loamy sand	44	21	15.0
Cloquato loam	29	8	3.5
Cloquato loam	36	13	9.5
Cloquato loam	44	23	12.5
Chehalis silt loam	29	6	2.5
Chehalis silt loam	36	13	9.0
Chehalis silt loam	44	23	12.5

Theoretical Considerations

Kendrich and Havens (1973) presented analytical solutions to the problem of describing temperature fields for systems of buried parallel line heat sources. Using an imaging method the following equation was obtained

$$T_{(x,y)} - T_{su} = \frac{q}{2\pi\lambda}\left[\ln\sqrt{\frac{x^2+(h-y)^2}{x^2+(h+y)^2}} + \sum_{n=1}^{N}\ln\sqrt{\frac{(ns-x)^2+(h-y)^2}{(ns-x)^2+(h+y)^2}} + \sum_{n=1}^{N}\ln\sqrt{\frac{(ns+x)^2+(h-y)^2}{(ns+x)^2+(h+y)^2}}\right], \quad (24)$$

where x is the horizontal distance from the heat source (cm), h is the distance from soil surface to the heat source (cm), y is the vertical distance from the soil surface (cm), $(ns\pm x)$ is the horizontal distance from the source to any point in the system from the center heat source, s is the lateral distance between heat sources, q is the heat flow rate per unit length of heat source (cal/cm sec), λ is the thermal conductivity of the soil (cal/cm sec C), $T_{(x,y)}$ is the temperature of the medium at any point in the system (C), T_{su} is the soil surface temperature (C), and N is the number of heat sources.

The rate of energy dissipation from the system of buried heat sources is given by

$$q = \frac{2\pi\lambda\,(T_s - T_{su})}{\ln\left(\frac{2h-r}{r}\right) + \sum_{n=1}^{N} \ln\left(\frac{(ns)^2+(2h-r)^2}{(ns)^2+r^2}\right)}, \qquad (25)$$

where T_s is the temperature of the heat source (C), and r is the radius of the heat source (cm). Equation (25) follows from Equation (24) when used to estimate the temperature at the heat source. It shows that the rate of energy dissipation is proportional to the soil thermal conductivity, the difference between heat source temperature and soil surface temperature, and inversely proportional to a sum of terms which might be called the "shape factor" since it depends on the depth, spacing, and radius of the heat sources in the soil warming system.

The development of Equations (24) and (25) was based on the following assumptions: (i) constant, uniform soil apparent thermal conductivity, (ii) no radial temperature variation in the cross-section of the heat source, (iii) constant, uniform soil surface temperature, (iv) steady-state operation, (v) heat is transferred in the soil in the radial direction only, and (vi) all sources have the same temperature and dissipate heat at the same rate.

It was deemed desirable to test the validity of this equation for the conditions of the experiments.

The soil surface temperature varied during the day according to

the applied surface heat load in several of the experiments. A daily average of the soil surface temperature was used in the calculations. The measured rates of energy dissipation per unit length of the heat source, q, are shown in Table 8. An average apparent thermal conductivity for the soil column was used, although the conductivity was not uniform throughout the soil column because of variations in the soil water content and temperature. The soil column had a reflecting boundary at the lower end. Thus it did not present a semi-infinite medium as was assumed in the derivation of Equation (24).

Table 8. Measured energy dissipation rates in Quincy, Cloquato, and Chehalis soils with different heat source temperatures and surface heat loads.

Heat Source Temperature	Max. Surface Heat Load	Energy Dissipation Rate Per Unit Length of Heat Source		
		Quincy	Cloquato	Chehalis
C	Watts	---------- cal/cm sec ----------		
29	0	0.0257	0.0275	0.0246
	13	0.0269	0.0213	0.0199
	52	0.0221	0.0203	0.0162
	117	0.0223	0.0210	--
36	0	0.0514	0.0454	0.0536
	13	0.0526	0.0444	0.0437
	52	0.0545	0.0466	0.0425
	117	0.0537	0.0456	0.0511
44	0	0.0784	0.0713	0.0588
	13	0.0787	0.0651	0.0558
	52	0.0734	0.0664	0.0481
	117	0.0682	0.0571	--

The equation was used to calculate the temperatures at the grid points identified in Table 9. Then the difference between calculated and measured temperature was obtained. Results are shown in Table 9. A negative number means that the measured temperature was higher than the calculated temperature. The heat source was close to the point at the depth of 35 cm (actual depth was 32 cm) and horizontal spacing of 5 cm (actual spacing was 1.5 cm). The difference is also shown as a percentage of the measured values. Equation (24) underestimates temperatures near the heat source and overestimates temperatures near the soil surface. The heat source was placed 1.5 cm from the right hand side of the box. It heated a portion of the wall of the box near the heat source. Back radiation may have increased the temperatures of the soil around the heat source so that higher measured temperatures were obtained. Temperatures were overestimated near the lower end of the soil column. The measured temperatures converged to the air temperature at this boundary.

The soil column terminated a distance of 16 cm below the heat source. This boundary consisted of a 4 cm thick acrylic sheet. Thermistors were inserted in holes bored in this sheet. Upper and lower thermistors were placed at the interfaces of the wet soil and acrylic sheet, and air and acrylic sheet, respectively. Thermistors were also placed 2.4 cm below the soil and acrylic sheet interface. Thermistors were located at 2.5, 7.5, 17.5, and 32.5 cm away from

Table 9. Difference between measured temperatures and temperatures calculated according to the Kendrick and Havens (1973) model (calculated-measured) at the indicated grid points in C (top) and in percent of the measured value (bottom).

Depth	29 C				36 C				44 C			
	5	15	25	35	5	15	25	35	5	15	25	35
cm	C											
Quincy												
5	-0.1	-0.1	-0.2	-0.3	-0.8	-0.5	0.6	-0.6	0.9	0.9	0.9	0.7
15	-0.2	-0.2	-0.3	-0.5	-0.3	-0.4	-0.8	-1.0	1.2	1.4	1.1	0.7
25	0.0	0.0	-0.2	-0.4	-0.3	-0.3	-0.	-0.8	0.5	2.0	1.6	1.1
35	0.1	0.0	-0.1	-0.3	-0.9	0.2	0.1	-0.5	0.0	2.1	2.5	1.5
45	-0.8	-0.3	-0.3	-0.5	-0.3	0.7	0.2	-0.4	2.5	2.3	2.5	2.0
Cloquato												
5	-0.9	-0.5	-0.6	-0.8	0.7	1.0	1.1	1.2	0.4	0.4	0.2	0.1
15	-0.4	-1.0	-1.2	-1.6	1.8	1.6	1.4	0.9	1.2	1.0	0.6	0.4
25	0.4	-0.3	-0.9	-1.4	2.2	2.7	0.9	1.1	1.7	1.6	1.6	0.8
35	0.6	0.0	-0.6	-1.0	2.5	3.3	2.4	1.3	2.0	2.7	1.9	1.2
45	0.4	-0.3	-0.6	-0.9	2.3	2.9	2.2	1.4	3.6	2.8	2.0	1.2
Chehalis												
5	1.2	1.2	1.0	0.8	1.5	1.8	1.8	1.7	0.8	1.0	0.8	0.6
15	0.7	0.7	0.5	0.2	2.3	2.7	1.9	1.1	1.8	1.0	1.1	0.5
25	1.4	1.0	0.9	0.5	2.7	2.6	2.6	1.5	2.0	2.4	1.8	1.1
35	0.2	1.4	1.1	0.7	1.7	3.1	2.7	1.9	0.9	2.5	2.6	1.7
45	1.8	1.2	1.1	0.9	3.6	3.1	3.0	1.9	3.5	3.2	2.9	1.9

Table 9. Continued.

Depth	29 C				36 C				44 C			
	5	15	25	35	5	15	25	35	5	15	25	35
cm	%											
Quincy												
5	0.4	0.4	0.9	0.9	3.5	2.2	2.7	2.7	3.9	4.0	4.1	3.2
15	0.8	0.8	1.3	2.1	1.2	1.6	3.3	4.2	4.6	5.6	4.6	3.0
25	0.0	0.0	0.8	1.7	1.0	1.1	0.4	3.3	1.6	7.3	6.3	4.5
35	0.4	0.0	0.4	1.3	2.9	0.7	0.4	2.0	0.0	7.4	9.7	6.1
45	3.0	1.2	1.2	2.0	1.1	2.7	0.8	1.6	8.5	8.5	9.8	8.1
Cloquato												
5	4.1	2.3	2.8	3.8	3.1	4.5	5.0	5.6	2.0	2.1	0.7	0.4
15	1.7	4.3	5.2	7.0	7.0	6.6	6.0	3.9	4.9	4.3	2.7	1.7
25	1.6	1.2	3.8	6.0	7.6	10.5	3.7	4.6	5.6	5.9	6.4	3.1
35	2.2	0.0	2.5	4.2	8.1	12.6	9.7	5.3	5.7	10.0	7.5	5.1
45	1.6	1.2	2.5	3.8	8.4	11.3	8.9	5.7	13.2	10.8	8.0	4.9
Chehalis												
5	5.8	5.9	5.0	4.0	6.9	8.5	8.6	8.2	3.6	4.7	3.8	2.8
15	3.0	3.1	2.3	0.9	9.7	11.6	8.3	4.8	7.2	4.2	4.7	2.2
25	5.6	4.2	3.9	2.2	9.6	10.3	10.9	6.4	6.6	9.2	7.3	4.6
35	0.8	5.8	4.8	3.1	5.4	12.0	11.1	8.1	2.6	9.1	10.4	7.1
45	7.4	5.1	4.8	4.0	13.7	12.4	12.5	8.1	12.7	12.4	11.7	7.9

the wall of the box where the heat source was located. Table 10 shows measured and calculated temperatures in the 4 cm thick lower wall of the soil container filled with Chehalis soil and a source temperature of 44 C.

Table 10. Measured and calculated temperatures in the lower wall of the container, filled with Chehalis soil, with a heat source temperature of 44 C.

Distance From Side		Soil-Wall Interface	Center of Wall	Air-Wall Interface
cm		---------- C ----------		
2.5	meas.	27.8	25.2	24.2
	calc.	30.2	29.6	29.3
7.5	meas.	27.6	24.9	24.2
	calc.	29.9	29.3	29.0
17.5	meas.	25.7	24.7	24.4
	calc.	28.3	28.1	27.9
32.5	meas.	24.7	24.3	24.5
	calc.	26.1	26.1	26.1

Temperature gradients were calculated from these measurements. Temperature gradients which caused heat leakage occurred over areas near the side of the box below the heat source. Total rate of energy leakage was obtained by multiplying the temperature gradients, energy leakage area, and thermal conductivity of the acrylic material. The rate of energy loss was found to be about 8 percent of the total heat input at the heat source at a 44 C heat source temperature. This percentage would be less for lower heat source

temperatures. The rate of energy loss at the lower end of the column was low because of the low thermal conductivity of the acrylic material. This material has a thermal conductivity of about 0.45 mcal/cm sec C which is less than that of air dry soil. The thermal conductivity of moist soil is more than 5 times that of the acrylic plastic.

The calculated temperatures were obtained with Equation (24), using the heat dissipation rate measured for the Chehalis soil at 44 C. The temperatures calculated at the indicated points thus apply to a semi-infinite soil medium, a condition quite different from those of the experiments. The results do however indicate reasons for the deviations from the Kendrick and Havens equations. A very large temperature difference (27.8 minus 24.2 C) existed across the acrylic wall below the heat source. This difference became progressively smaller at greater distance from the heat source. These measurements indicate that the deviations between measured and calculated temperatures can, at least in part, be attributed to the experimental conditions. Part of the energy was transferred from the box to the wall and supporting plate, particularly at the highest heat source temperatures. It is concluded then that Equation (24) can be properly used to calculate temperature distributions in soil warming systems. Field conditions would more closely correspond to the conditions assumed in the derivation of this equation.

The apparent soil thermal conductivity is temperature dependent and water content dependent. It was shown in an earlier chapter that large changes in soil apparent thermal conductivity occur as a result of changes in soil temperature and soil water content. These changes should be taken into account in any scheme for calculating temperature profiles. This can only properly be done by solving appropriate equations by a computer based scheme. However Equation (24) using average values for soil apparent thermal conductivity and a daily average soil surface temperature produces a good approximation.

Temperature Variations at the Soil Surface

Temperatures measured as a function of time and depth are shown in Tables 11, 12, and 13. Maximum and minimum temperatures estimated from the measured data as a function of depth are summarized in Table 14 for the three levels of radiation.

The largest amplitudes were obtained for the Cloquato and Chehalis soils. The amplitudes increased with higher surface radiation loads for all soils.

The temperature variation as a function of time and depth is given by van Wijk and de Vries (1963) as follows:

$$T_{(y,t)} = T_{ay} + A_0 \exp(-y/D) \sin(\omega t + \phi_0 - y/D), \qquad (26)$$

Table 11. Measured and calculated soil temperatures at the indicated depths and times for Quincy soil with a source temperature of 29 C at three radiation loads.

Time	1.0 cm		3.0 cm		6.0 cm		12.0 cm	
	Meas.	Calc.	Meas.	Calc.	Meas.	Calc.	Meas.	Calc.
	- - - - - - - - - - - - - - - - - - C - - - - - - - - - - - - - - - - - -							
25 Volt								
2:00	21.5	21.5	21.5	21.8	22.6	22.1	23.2	22.9
4:00	21.5	21.5	21.0	21.7	22.6	22.0	23.3	22.7
6:00	21.7	21.5	21.5	21.8	22.6	22.0	23.4	22.6
8:00	21.6	21.7	21.5	21.9	22.7	22.1	23.3	22.7
10:00	21.7	22.0	21.5	22.2	22.6	22.3	23.1	22.8
12:00	21.9	22.3	22.0	22.4	22.8	22.5	23.4	22.9
14:00	22.6	22.4	22.3	22.6	23 0	22.6	23.4	23.0
16:00	22.6	22.5	22.5	22.6	23.1	22.7	23.6	23.1
18:00	22.5	22.4	22.3	22.6	23.1	22.7	23.5	23.1
20:00	21.8	22.3	21.7	22.4	22.9	22.6	23.6	23.4
22:00	--	22.0	--	22.2	--	22.5	--	23.0
24:00	--	21.7	--	21.9	--	22.3	--	22.9
50 Volt								
2:00	21.4	21.8	21.3	22.2	21.6	22.7	23.1	23.5
4:00	20.9	21.5	21.1	21.7	22.0	22.2	23.4	23.0
6:00	20.4	21.9	20.6	21.9	21.7	22.0	22.9	22.7
8:00	20.8	22.9	20.5	22.5	21.9	22.4	22.8	22.7
10:00	21.2	24.3	21.0	23.6	22.1	23.1	22.8	22.9
12:00	23.6	25.6	22.8	24.8	22.9	24.0	23.0	23.3
14:00	25.0	26.5	24.8	25.7	24.3	24.8	23.7	23.8
16:00	25.2	26.8	25.4	26.2	24.9	25.3	24.3	24.3
18:00	25.2	26.3	25.3	26.1	25.4	25.5	24.7	24.6
20:00	23.3	25.3	23.6	25.4	24.5	25.1	24.8	24.7
22:00	21.9	24.0	22.0	24.3	23.2	24.4	24.3	24.5
24:00	21.6	22.7	21.7	23.2	22.8	23.5	23.7	24.1

Table 11. Continued.

Time	1.0 cm Meas.	1.0 cm Calc.	3.0 cm Meas.	3.0 cm Calc.	6.0 cm Meas.	6.0 cm Calc.	12.0 cm Meas.	12.0 cm Calc.
	- - - - - - - - - - - - - - - - - C - - - - - - - - - - - - - - - - -							
75 Volt								
2:00	20.5	21.4	20.8	22.1	22.2	22.8	23.3	23.1
4:00	20.4	20.5	20.4	20.8	21.9	21.7	22.8	22.2
6:00	20.5	21.3	20.5	20.9	21.8	21.6	22.7	21.7
8:00	20.9	23.5	20.8	22.4	21.7	22.5	22.8	21.8
10:00	21.2	26.7	21.0	24.7	21.9	23.3	22.8	22.4
12:00	26.7	29.8	25.9	27.4	23.8	26.3	23.1	23.4
14:00	31.1	31.1	30.2	29.7	27.0	28.1	24.8	24.6
16:00	32.6	33.0	31.4	30.9	29.1	29.2	26.4	25.5
18:00	31.1	32.2	31.2	30.8	29.2	29.3	27.2	26.0
20:00	24.8	29.9	26.0	29.4	26.4	28.3	26.8	25.9
22:00	22.2	26.8	22.8	27.0	24.3	26.6	25.4	25.3
24:00	21.3	23.7	21.6	24.3	23.0	24.6	24.3	24.2

Table 12. Measured and calculated soil temperatures at the indicated depths and times for Cloquato soil with a source temperature of 29 C at three radiation loads.

Time	1.0 cm		3.0 cm		6.0 cm		12.0 cm	
	Meas.	Calc.	Meas.	Calc.	Meas.	Calc.	Meas.	Calc.
	- - - - - - - - - - - - - - - - - C - - - - - - - - - - - - - - - - -							
25 Volt								
2:00	19.4	19.0	19.8	19.4	21.6	20.2	22.6	21.0
4:00	19.0	18.6	19.1	19.1	21.1	19.8	22.2	21.0
6:00	18.6	18.6	18.5	19.0	20.6	19.5	21.4	20.7
8:00	19.6	19.0	19.4	19.3	21.0	19.5	21.9	20.5
10:00	19.6	19.5	19.9	19.8	21.2	19.8	22.0	20.5
12:00	19.7	20.1	19.8	20.3	21.2	20.2	22.1	20.7
14:00	20.2	20.7	20.3	20.8	21.6	20.7	22.5	21.0
16:00	21.0	21.0	21.0	21.2	22.0	21.1	22.6	21.4
18:00	21.0	21.0	21.1	21.2	22.1	21.4	22.8	21.7
20:00	20.4	20.7	20.7	21.0	22.1	21.4	22.9	21.9
22:00	20.1	20.1	20.4	20.5	21.9	21.1	22.9	21.9
24:00	20.0	19.5	20.3	19.9	21.8	20.7	22.7	21.7
50 Volt								
2:00	20.3	20.6	20.7	20.9	22.5	21.6	23.6	22.3
4:00	19.6	19.8	20.0	20.2	22.1	20.9	23.0	22.0
6:00	19.6	19.6	19.6	20.0	21.6	20.5	22.5	21.7
8:00	19.9	20.2	20.2	20.4	21.8	20.6	22.7	21.5
10:00	20.2	21.3	20.5	21.3	22.0	21.1	22.8	21.6
12:00	20.1	22.7	20.4	22.5	22.0	21.8	22.8	21.9
14:00	21.7	24.0	21.4	23.5	22.3	22.7	23.1	22.3
16:00	24.3	24.8	23.9	24.2	23.4	23.4	23.4	22.8
18:00	24.8	24.9	24.6	24.4	24.4	23.8	24.0	23.1
20:00	22.6	24.4	23.0	24.0	24.1	23.7	24.3	23.3
22:00	21.3	23.3	21.8	23.1	23.4	23.2	24.1	22.2
24:00	21.1	21.9	21.3	22.0	23.0	22.4	23.9	22.9

Table 12. Continued.

Time	1.0 cm Meas.	1.0 cm Calc.	3.0 cm Meas.	3.0 cm Calc.	6.0 cm Meas.	6.0 cm Calc.	12.0 cm Meas.	12.0 cm Calc.
	- - - - - - - - - - - - - - - - - C - - - - - - - - - - - - - - - - -							
75 Volt								
2:00	23.1	23.7	22.9	23.5	24.8	24.1	25.1	23.8
4:00	22.0	21.2	22.0	21.5	23.9	22.5	24.4	23.3
6:00	21.7	20.7	21.4	21.0	23.3	21.6	23.7	22.8
8:00	22.1	22.4	21.7	22.1	23.3	21.7	23.6	22.5
10:00	23.1	25.8	22.3	24.4	23.5	22.7	23.7	22.6
12:00	23.0	30.0	22.7	27.4	23.9	24.4	24.0	23.1
14:00	27.0	23.9	25.1	30.3	24.4	26.3	24.2	23.8
16:00	35.5	36.4	32.5	32.3	27.8	27.9	25.1	24.5
18:00	37.3	36.9	34.4	32.8	30.3	28.8	26.5	25.1
20:00	29.7	35.2	30.0	31.7	30.0	28.6	26.4	25.3
22:00	25.6	31.7	25.8	29.4	27.5	27.7	27.1	25.2
24:00	24.2	27.6	24.1	26.4	26.0	26.0	26.1	24.8

Table 13. Measured and calculated soil temperatures at the indicated depths and times for Chehalis soil with a source temperature of 29 C at three radiation loads.

Time	1.0 cm		3.0 cm		6.0 cm		12.0 cm	
	Meas.	Calc.	Meas.	Calc.	Meas.	Calc.	Meas.	Calc.
	- - - - - - - - - - - - - - - - - - C - - - - - - - - - - - - - - - - - -							
25 Volt								
2:00	20.3	19.9	20.6	20.1	22.0	20.6	22.8	21.5
4:00	18.7	19.7	19.2	20.0	21.4	20.3	22.2	21.3
6:00	19.7	20.0	19.8	20.3	21.1	20.3	22.0	21.3
8:00	20.4	20.7	20.8	21.0	21.6	20.6	22.4	21.3
10:00	20.6	21.6	20.8	21.9	21.6	21.0	22.2	21.5
12:00	21.2	22.4	21.4	22.7	21.8	21.5	22.7	21.7
14:00	21.9	23.0	22.1	23.3	22.4	21.9	22.8	22.0
16:00	21.7	23.1	22.6	23.4	22.6	22.2	22.9	22.1
18:00	22.2	22.8	21.8	23.1	22.6	22.2	22.9	22.2
20:00	20.9	22.1	21.4	22.4	22.4	21.9	22.9	22.2
22:00	21.0	21.2	20.8	21.5	22.6	21.5	22.7	22.0
24:00	20.6	20.4	20.7	20.7	22.3	21.0	22.5	21.7
50 Volt								
2:00	22.6	21.6	23.1	21.9	24.2	22.6	24.8	23.6
4:00	22.3	21.1	22.7	21.4	23.8	21.9	24.4	23.1
6:00	22.1	21.6	22.4	21.6	23.5	21.7	24.0	22.8
8:00	22.5	22.8	22.7	22.5	23.6	21.9	24.1	22.7
10:00	22.7	24.6	22.8	23.8	23.7	22.7	24.1	22.8
12:00	24.5	26.3	24.0	25.2	24.0	23.6	24.1	23.2
14:00	27.6	27.6	26.9	26.2	25.4	24.5	24.6	23.6
16:00	29.0	28.0	28.4	26.8	26.4	25.2	25.4	24.1
18:00	28.0	27.6	28.0	26.6	26.8	25.4	25.7	24.3
20:00	25.1	26.3	26.1	25.9	26.4	25.2	25.9	24.5
22:00	23.8	24.6	24.4	24.4	25.5	24.5	25.8	24.4
24:00	22.8	22.8	23.0	23.0	24.6	23.6	24.8	24.1

Table 13. Continued.

Time	1.0 cm		3.0 cm		6.0 cm		12.0 cm	
	Meas.	Calc.	Meas.	Calc.	Meas.	Calc.	Meas.	Calc.
	- - - - - - - - - - - - - - - - - C - - - - - - - - - - - - - - - - -							
75 Volt								
2:00	24.3	24.4	24.6	24.4	25.9	25.0	26.2	25.9
4:00	23.9	22.6	24.5	23.0	25.5	23.6	26.1	25.0
6:00	23.4	22.8	23.7	23.0	24.8	23.1	25.3	24.3
8:00	23.3	24.7	23.6	24.4	24.7	23.6	25.2	24.1
10:00	23.5	27.9	--	26.8	24.6	25.0	24.9	24.3
12:00	27.2	31.5	25.6	29.5	24.9	26.8	24.8	25.0
14:00	35.1	24.4	31.5	31.9	27.9	28.7	25.6	25.9
16:00	36.7	36.1	--	33.3	30.1	30.0	--	26.8
18:00	36.7	36.0	35.1	33.3	31.6	30.5	27.9	27.4
20:00	30.7	34.1	31.1	31.9	30.7	30.1	28.4	27.7
22:00	25.9	30.9	--	29.5	27.7	28.7	27.9	27.4
24:00	24.9	27.3	25.4	26.8	26.7	26.8	27.0	26.8

Table 14. Maximum and minimum temperatures, amplitudes, and time lags as a function of depth for Quincy, Cloquato, and Chehalis soils with a heat source temperature of 29 C at three surface heat loads.

Soil	Maximum Surface Heat Load	Depth	Temperature		Amplitude
			Maximum	Minimum	
	Watts	cm	- - - - - - - - - C - - - - - - - - -		
Quincy	13	1	22.6	21.5	0.55
		3	22.5	21.0	0.75
		6	23.1	22.6	0.25
		12	23.6	23.2	0.20
	52	1	25.2	20.4	2.40
		3	25.4	20.5	2.45
		6	25.4	21.7	1.85
		12	24.8	22.8	1.00
	117	1	32.6	20.4	6.10
		3	31.4	20.4	5.50
		6	29.2	21.7	3.75
		12	27.2	22.7	2.25
Cloquato	13	1	21.0	18.6	1.20
		3	21.1	18.5	1.30
		6	22.1	20.6	0.75
		12	22.9	21.4	0.75
	52	1	24.8	19.6	2.60
		3	24.6	19.6	2.50
		6	24.4	21.6	1.40
		12	24.3	22.5	0.90
	117	1	37.3	21.7	7.80
		3	34.4	21.4	6.50
		6	30.3	23.3	3.50
		12	27.1	23.6	1.75
Chehalis	13	1	22.2	18.7	1.75
		3	22.6	19.2	1.70
		6	22.6	21.1	0.75
		12	22.9	22.0	0.45
	52	1	29.0	22.1	3.45
		3	28.4	22.4	3.00
		6	26.8	23.5	1.65
		12	25.9	24.0	0.95
	117	1	36.7	23.3	6.70
		3	35.1	23.6	5.75
		6	31.6	24.6	3.50
		12	28.4	24.8	1.80

where $T_{(y,t)}$ is the temperature (C) at any depth y (cm) at time t (sec), T_{ay} is the average temperature at any depth in the soil column during a period (C), A_0 is the surface amplitude (C), D is the damping depth (cm), ω is the angular frequency ($2\pi\nu$ where ν is the frequency of temperature variation) equal to 7.27×10^{-5} sec^{-1} for a diurnal variation, and ϕ_0 is the phase constant.

The phase constant, ϕ_0, can be calculated from

$$\omega t_1 + \phi_0 - \frac{y}{D} = \frac{\pi}{2} , \tag{27}$$

where t_1 is the time at which the maximum temperature at a depth y occurs. Equation (26) describes the temperature variation about an average temperature at any depth. The average temperature at any depth can be written as follows:

$$T_{ay} = T_y + A_0 \exp(-y/D). \tag{28}$$

Substitution of Equation (28) in the Equation (26) yields,

$$T_{(y,t)} = T_y + A_0[\exp(-y/D)]\{1+\sin(\omega t+\phi_0-y/D)\}, \tag{29}$$

where T_y is calculated with Equation (24).

Equations (27) and (28) were used to calculate the soil temperature variation as a function of time and depth. A period of 24 hours was used in these calculations. The damping depth, D, is related to

the thermal properties of the medium and the angular frequency,

$$D = \left(\frac{2\lambda}{C\omega}\right)^{1/2} . \qquad (30)$$

The surface amplitudes A_0 used in Equation (29) were calculated from the equation

$$A_z = A_0 e^{-z/D} , \qquad (31)$$

where A_z is the amplitude (C) at any depth. A_z values for each soil and radiation intensity are shown in Table 14. The plot of $\ln A_z$ versus depth in cm, gives a straight line with a negative slope, which is the reciprocal of the damping depth. The intercept of this straight line with the $\ln A_z$ axis is $\ln A_0$. The results of these operations are shown in Table 15. Results of the calculations of the soil temperatures as a function of time and depth in the three soils at a heat source temperature of 29 C and at different radiation intensities are shown in Tables 11, 12, and 13. Observed temperatures were lower than calculated near the soil surface for all samples. Differences at the 1 cm depth were time dependent in all samples. The differences were higher at the time of rising and falling temperature. This is due to the fact that the rate of energy supply at the surface did not follow a perfect sinusoidal fluctuation while a sinusoidal model was used.

Table 15. Surface amplitudes and damping depths as a function of surface heat load for Quincy, Cloquato, and Chehalis soils with a heat source temperature of 29 C.

Soil	Surface Heat Load	Surface Amplitude	Damping Depth
	Watts	C	cm
Quincy	13	0.6	14.1
	52	2.9	11.8
	117	6.9	10.6
Cloquato	13	1.3	9.2
	52	3.0	9.9
	117	9.5	6.4
Chehalis	13	1.9	8.3
	52	3.9	8.2
	117	7.7	8.2

Conclusions

The effect of heat source temperature on soil surface temperature is small in moist soils. Heat source temperatures of 29 and 44 C increased the surface temperatures only 2 and 4 C respectively. The surface temperature is mainly influenced by air temperature and not by heat source temperature. The proposed system of soil warming can not be expected to raise soil surface temperatures much to improve conditions for seed germination in the spring. Other means for increasing the temperature of the soil surface, like petroleum mulching (Kowsar et al., 1969) must be used.

A portion of the soil column with heat source temperatures of 36 and 44 C had higher temperatures than the optimum range for plant growth. High soil temperatures in the root zone can be prevented by placing the heat sources deeper and farther apart.

RATE OF ENERGY DISSIPATION

Results

The duration of the time periods during which the heat source was energized were recorded with a Rustrak event recorder. Lengths of the traces were measured with a ruler and summed. The sum was divided by the total length of time to obtain the fraction of time τ shown in Equation (15). Energy input at the heat source was then calculated. Measurements were made from the time the maximum soil surface temperature occurred until the minimum soil surface temperature occurred. The rate of energy input was lowest when high surface temperatures prevailed and highest during the cooling periods. An average rate of energy input at the heat source was calculated for the experiments with a variable surface heat load.

Results of energy input measurements are shown in Table 16. The energy dissipation rate increased with heat source temperature for all three soils. The energy dissipation rate was highest in the Quincy soil and lowest in the Chehalis soil for each temperature treatment. The energy dissipation rates were much higher than those reported in a parallel soil warming study conducted in the open field (Rykbost, 1973). The highest energy dissipation rate measured in the open field was 0.0302 cal/cm^{2}min. It occurred on a fine textured soil (Woodburn) with no vegetation in the middle of February at a

Table 16. Heat source temperatures, soil surface temperatures, and energy dissipation rates for Quincy, Cloquato, and Chehalis soils for the indicated surface radiation loads.

Surface Heat Load	Heat Source Temperature			Average Temperature at Depth of 1 cm			Energy Dissipation Rate		
	Quincy	Cloquato	Chehalis	Quincy	Cloquato	Chehalis	Quincy	Cloquato	Chehalis
Watts	C			C			cal/cm^{2}min		
0	29.3	28.2	29.0	21.5	18.8	19.8	0.0385	0.0412	0.0368
13	29.3	28.0	28.4	21.9	19.8	20.8	0.0404	0.0320	0.0299
52	29.0	28.2	28.9	22.5	21.3	24.4	0.0332	0.0305	0.0243
117	29.1	28.3	29.1	24.4	26.2	27.8	0.0335	0.0318	--
0	37.2	35.2	36.4	20.5	20.7	20.2	0.0770	0.0681	0.0804
13	36.7	35.1	35.8	20.0	20.9	21.0	0.0789	0.0666	0.0655
52	36.8	34.8	35.5	22.7	22.0	21.8	0.0818	0.0702	0.0637
117	36.4	34.7	35.2	27.0	23.8	24.2	0.0810	0.0684	0.0768
0	43.3	46.9	46.9	21.2	21.1	20.1	0.1176	0.1070	0.0881
13	43.5	46.1	46.3	21.5	21.4	20.7	0.1180	0.0976	0.0837
52	42.8	45.6	42.7	23.4	21.8	22.3	0.1101	0.0996	0.0722
117	42.9	45.9	--	27.1	24.3	--	0.1023	0.0856	--

source temperature of 34 C and a soil temperature of 10 C at 2.5 cm below the surface. The heat sources were at a depth of 92 cm with a spacing of 182 cm. Comparison of this result with Table 16 indicates that the energy dissipation rate in the open field was about 30 percent of that measured in the laboratory. Higher rates of energy dissipation in the laboratory experiment were due to the lesser depth and closer spacing. Equation (25) gives the rate of energy dissipation as a function of depth, spacing, radius of heat source, soil thermal conductivity, and temperature difference between heat source and soil surface. The equation indicates that the rate of energy dissipation would be lower if the heat sources were placed deeper and farther apart. Soil thermal conductivity also influences the rate of energy dissipation. It depends on the soil texture, water content, and temperature (Figures 4, 5, and 6). Its value is higher for coarse textured soils and higher water content. Hence, higher energy dissipation rates were obtained in Quincy soil than Chehalis soil (Table 16).

The energy dissipation rate depends on the temperature gradient. Equation (25) also indicates that the temperature gradient is needed to calculate energy dissipation rates in soil warming systems. Temperature gradients were obtained from the difference in temperature at the heat source and at a depth of 1 cm below the soil surface. The temperature at the 1 cm depth varied during the day in the experiments with a variable surface heat load. An average

temperature was calculated by averaging the measurements obtained at two hour intervals at the five thermistor positions at the 1 cm depth. The variation in heat source temperature was less than 0.2 C. An average heat source temperature was calculated for each experiment. A summary of heat source temperatures and soil temperatures at the 1 cm depth are shown in Table 16.

Equation (25) was developed for steady state conditions. These conditions were not achieved in the experiments with changing surface heat loads. For the purpose of the present analysis the daily average temperature at the 1 cm depth was used. Energy dissipation rates were plotted as a function of the difference in the average temperature of the heat source and the average temperature at 1 cm. The correlation between the energy dissipation rates and the temperature differences was determined by using a least square method to fit the equation:

$$F = A + B(T_s - T_{su}) , \qquad (32)$$

where F is the rate of energy loss (cal/cm^{2}min), T_s is the heat source temperature (C), T_{su} is the average soil temperature at 1 cm (C), and A and B are constants. The solid lines shown in Figure 22 were calculated using Equation (32) and values of A and B shown in Table 17.

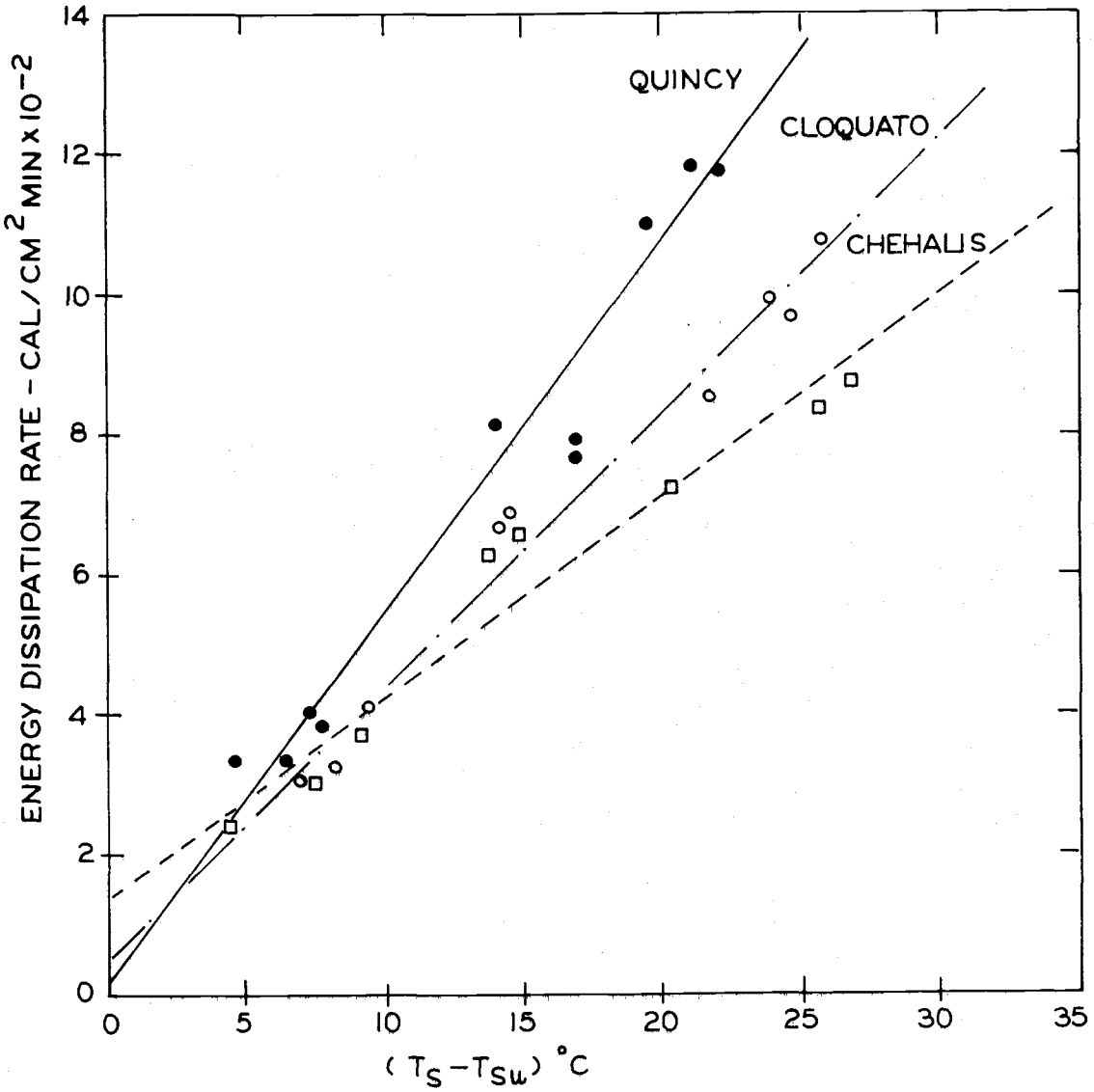

Figure 22. Mean daily energy dissipation rates as a function of the difference between mean daily heat source temperature and mean daily soil temperature at a depth of 1 cm.

Table 17. Parameters of regression models obtained from data in Table 16, correlation coefficients, and calculated thermal conductivities for Quincy, Cloquato, and Chehalis soils.

Parameter	Soil		
	Quincy	Cloquato	Chehalis
Intercept A ($cal/cm^2 min$)	0.00204[a]	0.00499[b]	0.01395[b]
Slope B ($cal/cm^2 min\ C$)	0.00531	0.00390	0.00287
Correlation coefficient R	0.97**	0.99**	0.97**
Slope B^1 ($cal/cm^2 min\ C$)	0.00543	0.00417	0.00360
Calculated thermal conductivities (cal/cm min C)	0.17	0.13	0.11

**Statistically significant at the 1 percent level.

[a]Statistically negligible at the 1 and 5 percent level.

[b]Statistically negligible at the 1 percent level only.

The value of B (slope of lines) is determined in part by the thermal conductivity of the soil. It was highest for Quincy soil and lowest for Chehalis soil. The regression lines should pass through the origin. This result was not obtained. The regression lines intercept the ordinate at 0.00204, 0.00499, and 0.01395 for Quincy, Cloquato, and Chehalis soils, respectively. This deviation may have been caused by several factors which include: (i) experimental error, (ii) non-steady-state conditions, (iii) leakage of energy from the heat source or from the lower end of the soil column, (iv) thermal inertia due to poor contact between electrical elements and the cover of the heat source, so that additional energy was required to raise the

temperature of the electrical element to overcome this contact resistance, (v) underestimation of the difference between heat source and soil surface temperatures resulting from the use of the temperature at a depth of 1 cm. Furthermore, data points in Figure 22 were obtained from different experimental soil columns with small differences in the water content and hence thermal conductivity.

A statistical analysis showed that the value of the intercept of Equation (32) with the ordinate, did not differ significantly from zero. Hence, using regression analysis, straight lines were fit to the data in Figure 22 which went through the origin according to the equation

$$F = B^1 \Delta T , \tag{33}$$

stating that the rate of energy loss, F, is proportional to the difference in temperature at the heat source and soil surface, ΔT. The values of B^1 are shown in Table 17.

Shape Factor

Equation (33) can be used to describe the rate of energy loss in soil warming systems. According to Kendrick and Havens (1973),

$$B^1 = \frac{2\pi\lambda}{\ln\left(\frac{2h-r}{r}\right) + \sum_{n=1}^{N} \ln \frac{(ns)^2+(2h-r)^2}{(ns)^2+r^2}} \tag{34}$$

Using the design parameters, $s = 77$ cm, $h = 32$ cm, $r = 0.5$ cm and $N = 1$ (for the laboratory column), the value $B^1 = 0.033\lambda$ was obtained.

Thermal conductivities were calculated by substituting values of B^1 from Table 17. Calculated values of λ are shown in Table 17. Results are in agreement with the measured values at the same water content.

Equation (33) can be written as

$$F = G\lambda\Delta T \,, \tag{35}$$

where

$$G = \frac{2\pi}{\ln\left(\frac{2h-r}{r}\right) + \sum_{n=1}^{N} \ln\left(\frac{(ns)^2+(2h-r)^2}{(ns)^2+r^2}\right)} \tag{36}$$

The parameter G can be called the "shape factor" since it depends only on the depth, spacing, and the radius of the heat source. Plots of G as a function of spacing, depth, and heat source radius are shown in Figure 23. The solution of Equation (36) is independent of N for values greater than 6. Depth and spacing influence the "shape factor", G, more than the radius of the heat source. The G value increases 43 percent by a ten-fold increase in the heat source radius at a depth and spacing of 30 and 30 cm, respectively. A five-fold increase in spacing (from 30 to 150 cm) with a heat source radius of

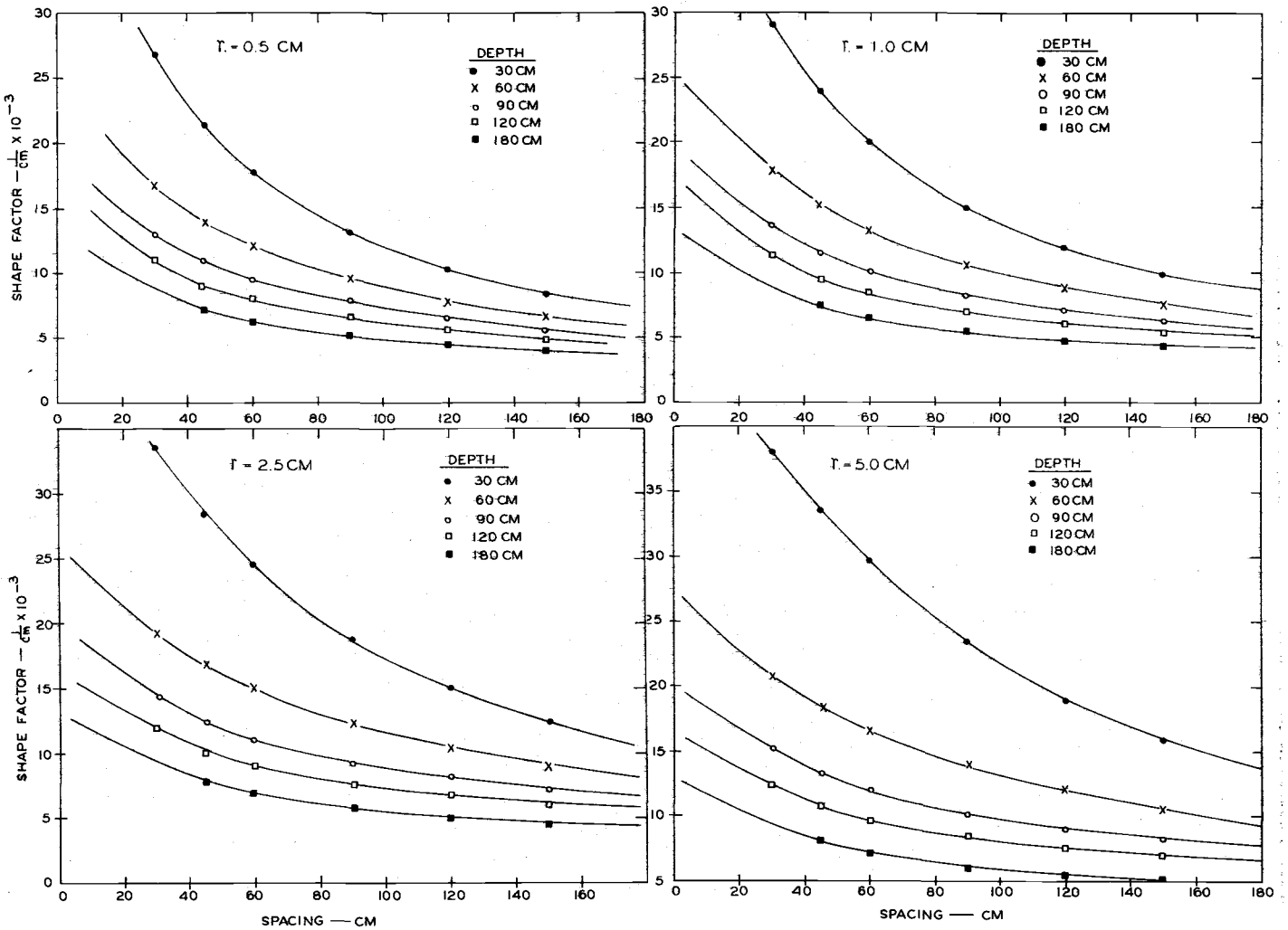

Figure 23. The shape factor, G, as a function of spacing for several depths and heat source radii of 0.5, 1.0, 2.5, and 5.0 cm.

0.5 cm increased G values only 31 percent. The G value increases 29.5 percent by increasing the depth six-fold (from 30 cm to 180 cm) at a spacing of 30 cm and heat source radius of 0.5 cm. At a given heat source radius, spacing has the greatest influence on the "shape factor" at the shallow depths. At a heat source radius of 1.0 cm an increase in spacing from 60 cm to 120 cm decreases G values 67 and 37 percent at 30 and 150 cm depths.

Effect of Surface Irradiation

Energy dissipation rates as a function of ΔT at different surface heat loads are shown in Figure 24. The slopes of the straight lines shown in these figures (cal/cm^{2}min C) are reported in Table 18. Increasing the surface heat load from 0 to 13 watts changed the slope very little. The biggest changes occurred in the Quincy soil with the slope increasing from 0.00495 to 0.00720 by increasing the surface radiation cycle from a peak rate of 0 to 117 watts. Changes for the Cloquato and Chehalis soils were small, with small increases occurring by increasing the surface heat load.

The combined results were shown above in Figure 22. The slopes B^1 shown in Table 16 are nearly the same as the average values shown in Table 18.

The increase in the slopes with increasing surface irradiation may appear contradictory. Higher rates of surface irradiation

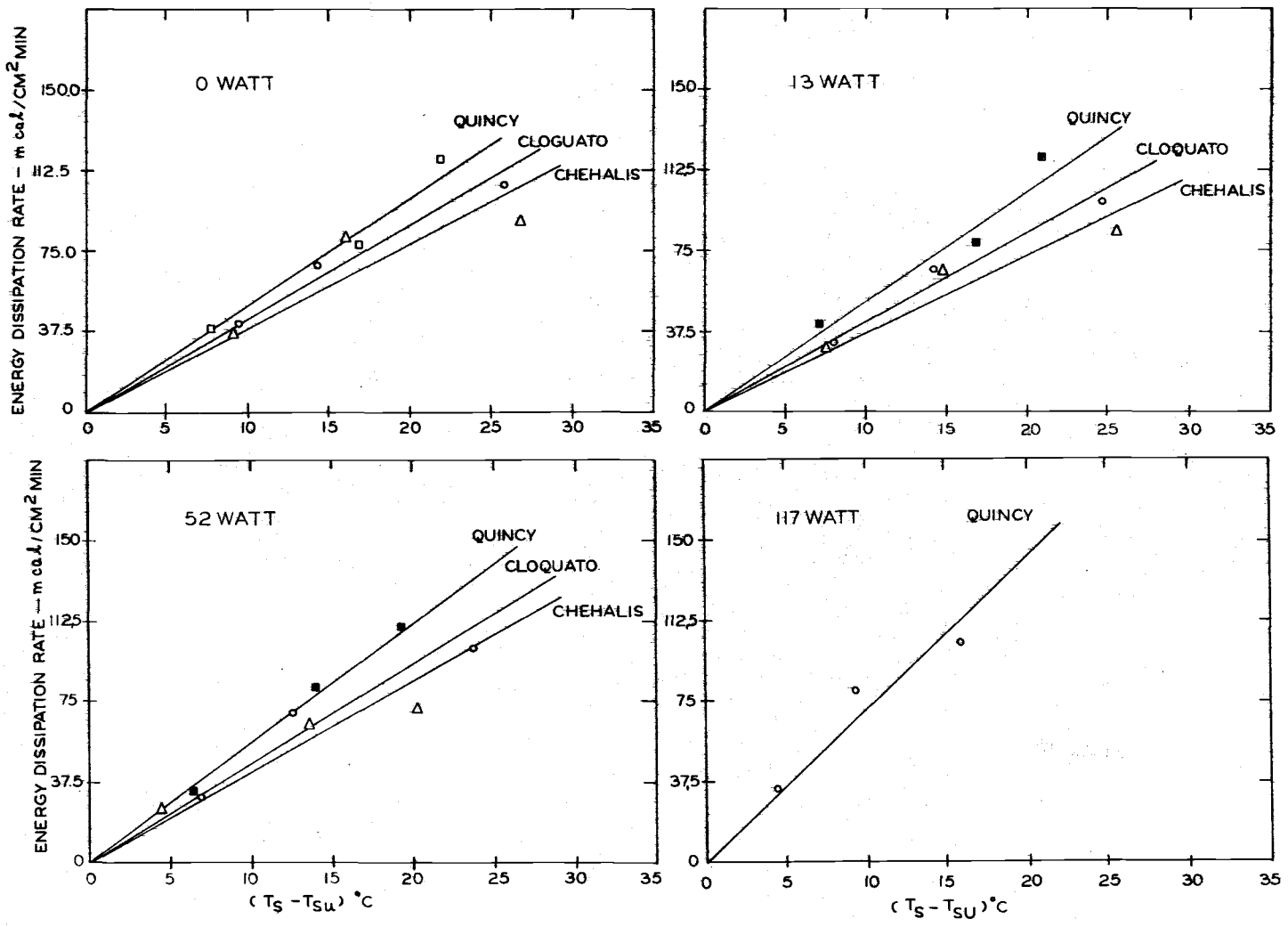

Figure 24. Energy dissipation rates at the heat source as a function of the temperature difference between heat source and soil surface for four rates of surface irradiation.

produce higher surface temperatures and therefore lower temperature gradients at a given heat source temperature.

Table 18. The ratio energy loss to temperature difference for Quincy, Cloquato and Chehalis soils with different surface heat load.

Surface Heat Load	F/ΔT		
	Quincy	Cloquato	Chehalis
Watts	- - - - - - cal/cm^{2}min C - - - - - - -		
0	0.00495	0.00435	0.00390
13	0.00514	0.00420	0.00368
52	0.00559	0.00458	0.00428
117	0.00720	---	---
Average	0.00572	0.00438	0.00395

The soil temperature profiles changed with the rate of surface heat supply. This change was most pronounced at the highest rate of surface heat input. Figure 25 shows a plot of daily average temperatures as a function of depth. The heat source temperature was 29 C.

Increasing the surface heat load from 0 to 13 watts changed the temperature profile little. The corresponding change in the value of the slope B^1 shown in Table 18 was also small. As the heat load at the soil surface increased, the temperature profile changed considerably. The depth below which the temperature was not affected by the surface heat load increased with increasing surface irradiation. Yet the results shown in Table 18 indicate that per unit temperature difference between the average soil surface temperature and the heat

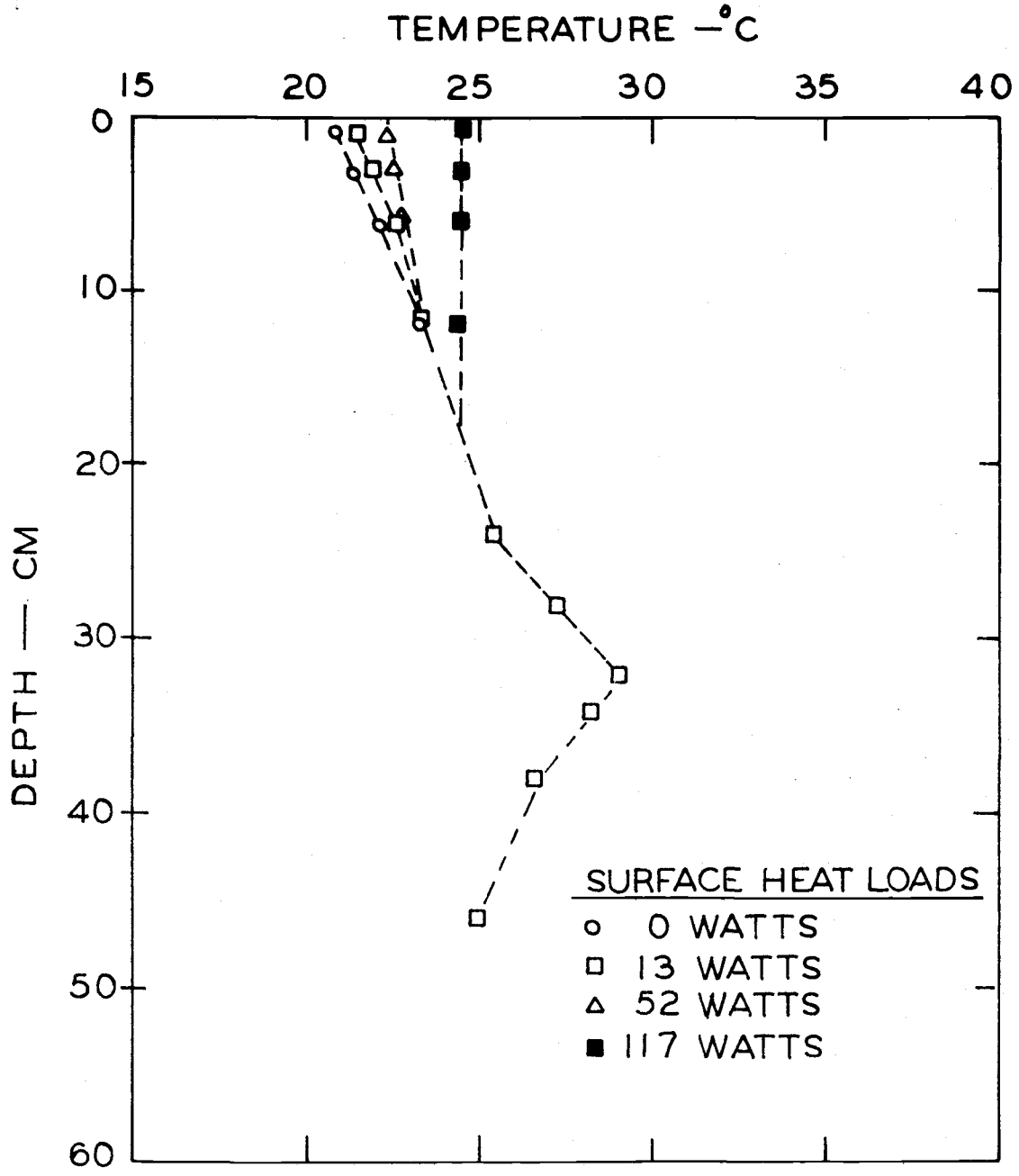

Figure 25. Daily average temperature as a function of depth for four levels of surface irradiation in a Quincy soil column.

source temperature more heat is dissipated through the Quincy soil than through the Cloquato and Chehalis soils and this difference becomes more pronounced at higher temperatures.

Land Area Requirements

Thermal conductivity values shown in Table 16 and a ΔT value of 20 C were used to calculate the total land area required to dissipate the waste energy generated by a 1000 MWe power plant with an efficiency of 34 percent. It was found that 2841, 3714, and 4390 hectares would be required for Quincy, Cloquato and Chehalis soils, respectively, with the heat sources buried 32 cm deep and 77 cm apart. A temperature change along the pipes was not taken into account in these calculations.

The shape factor is constant for a given installation, but values, of ΔT and λ depend on the physical properties of the soil, source temperature, and climatological factors. Energy dissipation rates may therefore be expected to vary seasonally. Irrigation and precipitation also cause seasonal changes. The rate of energy loss is more sensitive to the thermal conductivity and ΔT than to the depth, spacing, and radius of the heat source. In the Willamette Valley, Oregon high rates of energy loss occur during the cold season when the air temperature is low and the soil water content is high due to high precipitation and low evaporation rates. High soil water content

corresponds to high soil thermal conductivity. Temperature differences between the soil surface and the heat source are low during the warm season and the soil water content at that time is also low due to lack of rainfall. These conditions result in low rates of energy loss during the summer. Raising the heat source temperature increases ΔT and hence the rate of heat dissipation for a given climatological condition. The value of ΔT increases 78, and 167 percent by increasing the heat source temperature from 29 to 36 and 44 C respectively with a soil surface temperature of 20 C. Such an increase in ΔT increases the heat dissipation rate or decreases the total land area required to dissipate a given amount of waste heat. Results obtained by Rykbost (1973) indicate that a three-fold seasonal variation in energy dissipation rate occurred in the Willamette Valley, Oregon with a minimum in the late summer and a maximum in the late winter.

Daily Sensible Heat Flux Cycle at the Soil Surface

Heat flux at the soil surface of the columns with sinusoidal radiation loads can be analyzed using a model formulated by Gardner and Hanks (1966). The heat absorbed by a layer of thickness, Δy, is used to evaporate water and raise the temperature of the material in this layer. The total heat flux ($cal/cm^2 min$), ΔH, into a layer of thickness, Δy, can be writted as

$$\Delta H = \frac{EL + C\Delta T\Delta y}{\Delta t} \tag{37}$$

or

$$\Delta H = L \frac{\Delta\theta}{\Delta t} \Delta y + C \frac{\Delta T}{\Delta t} \Delta y , \tag{38}$$

where E is the evaporation ($cm = \Delta\theta \cdot \Delta y$), L is the heat of vaporization of water (580 cal/cm^3), C is the heat capacity of layer Δy, including water ($cal/cm^3 C$), ΔT is the change in temperature in time interval t (C), Δy is the thickness of the layer (cm), Δt is the time interval (min), and $\Delta\theta$ is the change in water content (cm^3/cm^3).

The first member of the right side of Equation (38) represents the heat used for evaporation and the second member the heat used for increasing the temperature of the material. The sensible heat flux can therefore be calculated with

$$\Delta H = C \frac{\Delta T}{\Delta t} \Delta y . \tag{39}$$

The calculations were made by dividing the column into layers varying in thickness, Δy. The temperatures of the layer $T_{\Delta y}$, is given by:

$$T_{\Delta y} = T_{(y_1+y_2)/2} \tag{40}$$

For selected times t, the sensible heat flux was calculated using Equations (39) and (40). The heat capacity values needed in

Equation (29) are given by

$$C = x_s C_s + x_w C_w + x_a C_a \quad (cal/cm^3 C), \tag{41}$$

where x is the volume fraction, C is the heat capacity, and the subscripts s, w, and a denote the solid, liquid, and gas phases. Since C_a is very small, the term $x_a C_a$ is usually neglected. The heat capacities of the soils were calculated using heat capacity values of 0.68, 0.56, 0.56, and 1.0 $cal/cm^3 C$ for the soil particles of the Quincy, Cloquato, and Chehalis soils, and water, respectively.

Results of the calculations are shown in Figures 26, 27, and 28. These figures show the sensible heat flux for Quincy, Cloquato and Chehalis soils as a function of time for the 13, 52, and 117 watts surface heat loads. The daily total of energy exchanged at the soil surface can be obtained by integrating the area under curves. The results are shown in Table 19. The quantities of sensible heat into and out of the soil columns were not exactly the same. The small discrepancies were caused by errors in estimating the temperatures and heat capacities.

The amount of sensible heat flux increased with increasing surface heat load. The quantity of sensible heat exchanged was the same for the three soils at low heating rates. When the surface heat load was highest, soil water content at the soil surface decreased in

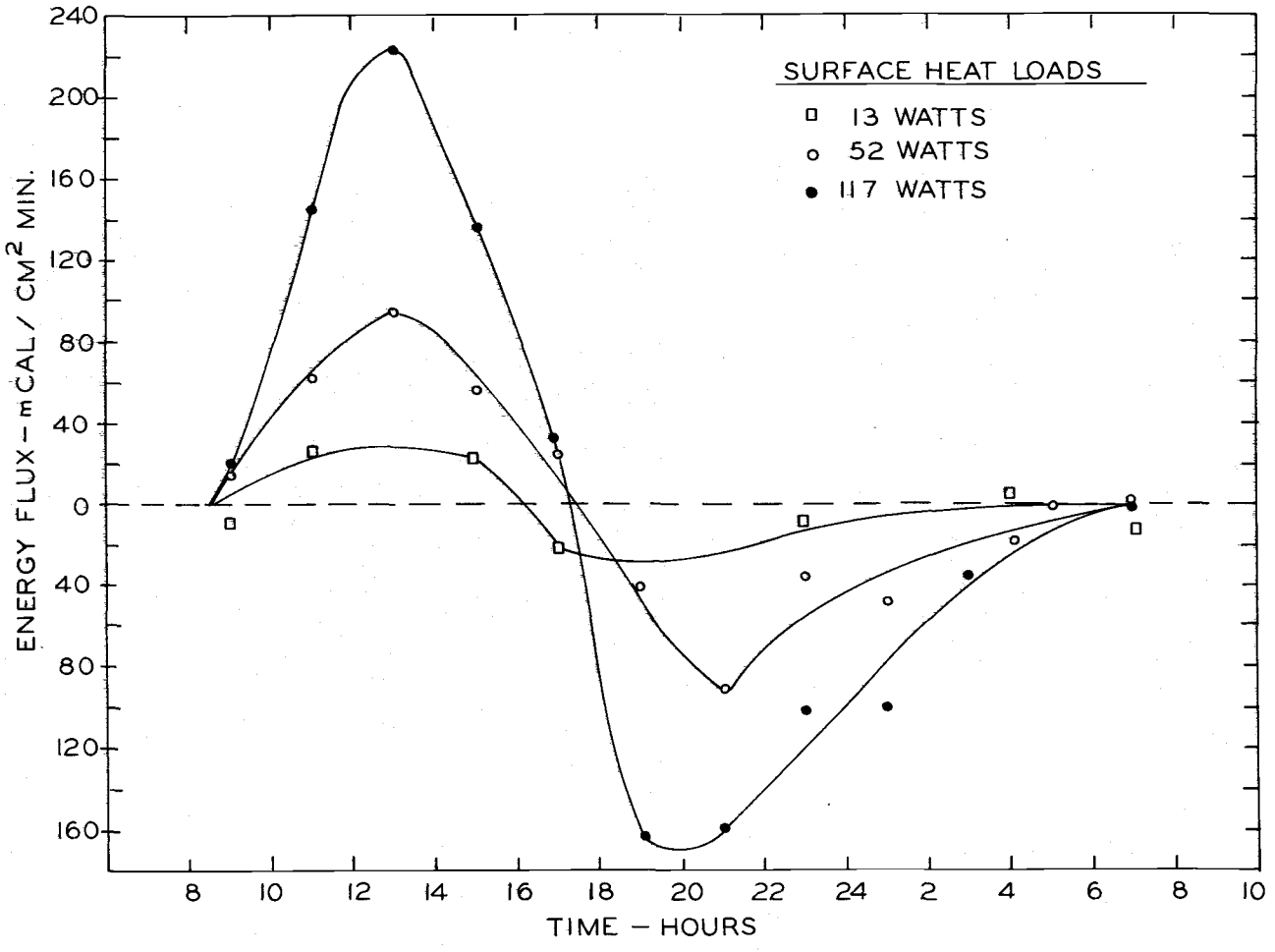

Figure 26. Sensible heat flux variations in the unsaturated Quincy soil column with different surface heat loads and a heat source temperature of 29 C.

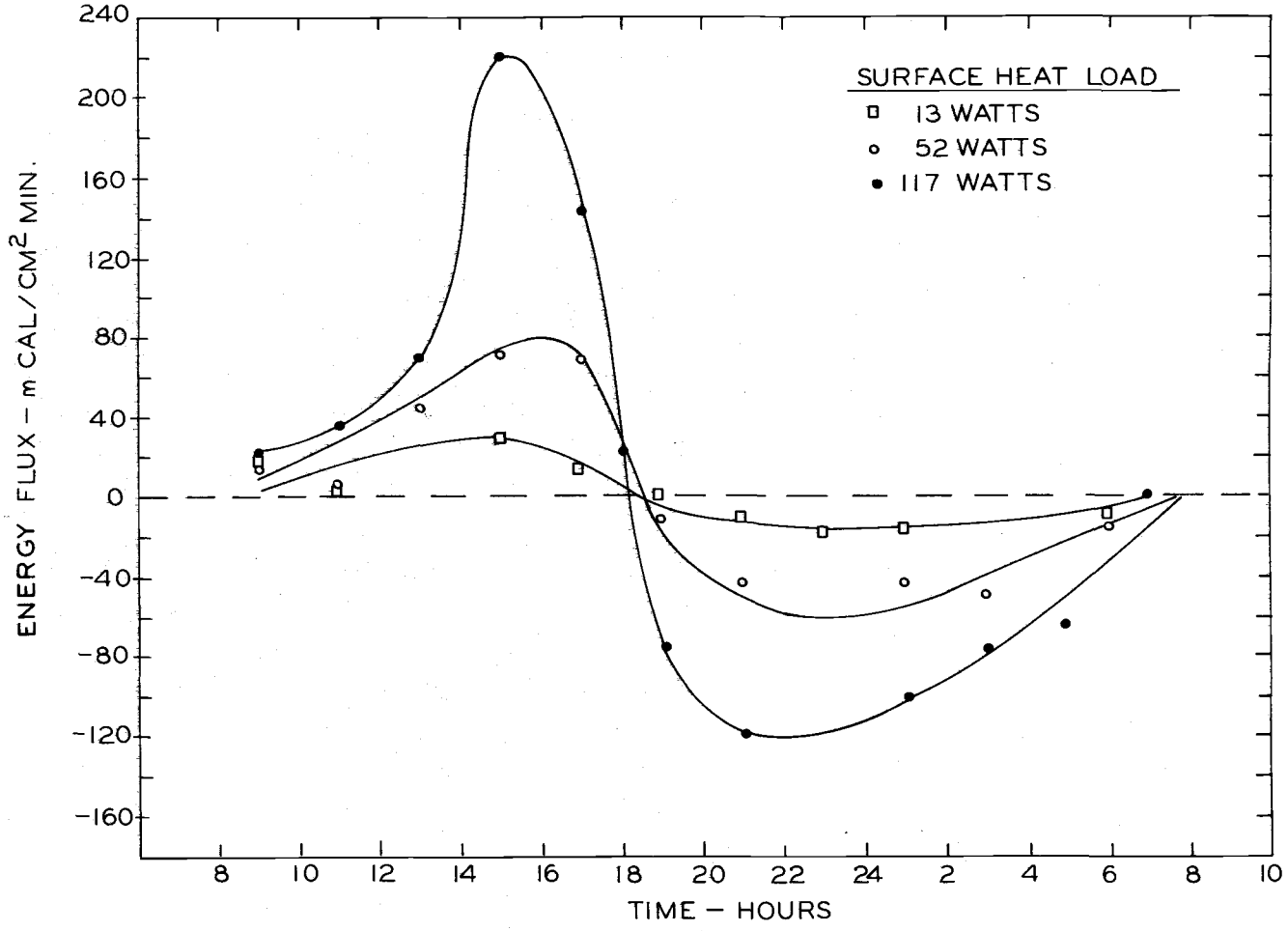

Figure 27. Sensible heat flux variations in the unsaturated Chehalis soil column with different surface heat loads and a heat source temperature of 29 C.

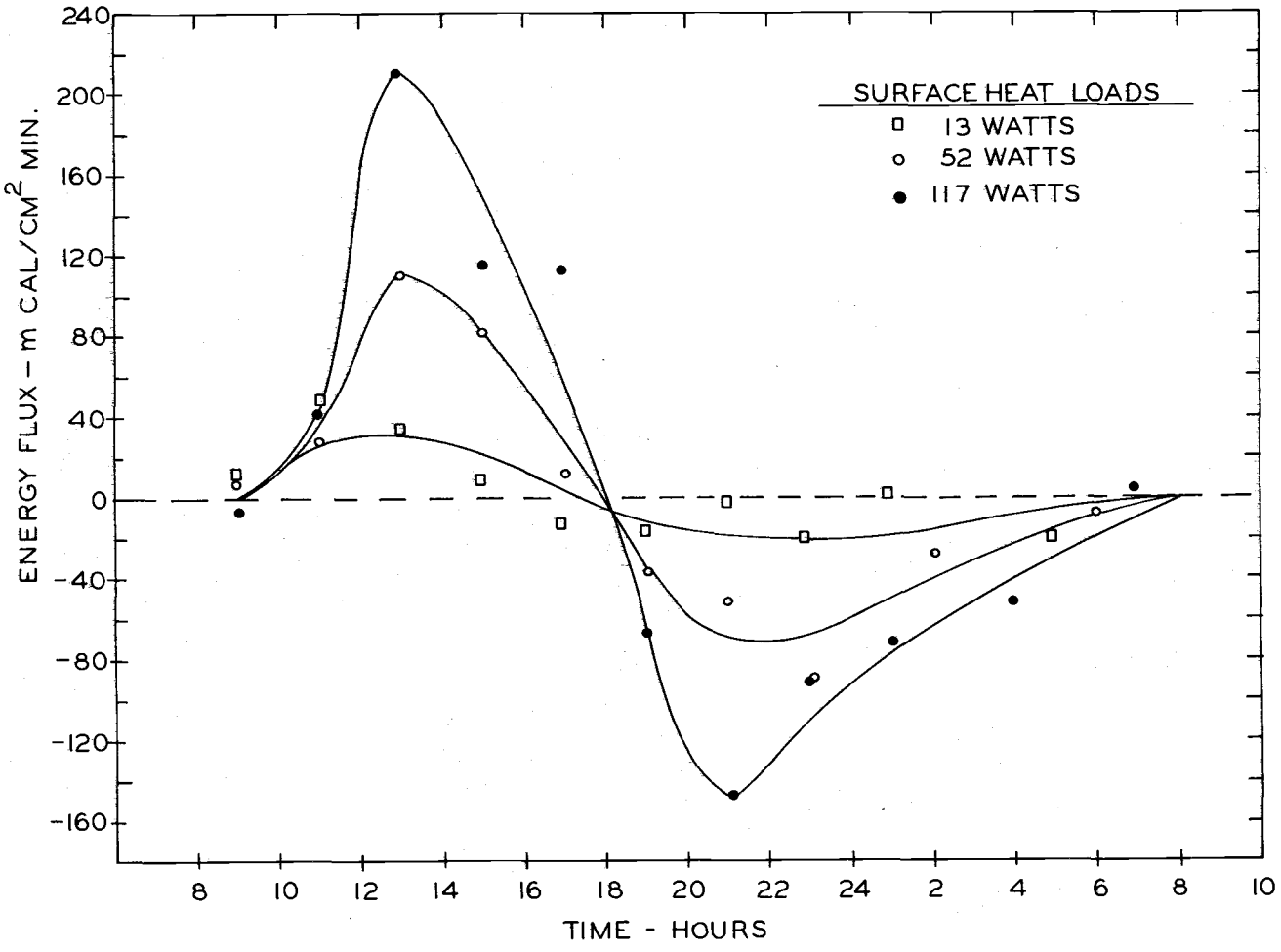

Figure 28. Sensible heat flux variations in the unsaturated Cloquato soil column with different surface heat loads and a heat source temperature of 29 C.

Cloquato and Chehalis soils and thereby lowered the heat capacities and soil thermal conductivities. The thermal conductivity of the Quincy soil was higher than for the Cloquato and Chehalis soils so that the amount of sensible heat entering into this soil was higher at the highest surface heat load.

Table 19. Energy exchanged at the surface of soil columns of Quincy, Cloquato, and Chehalis soils with different surface heat loads and a heat source temperature of 29 C.

Soil	Surface Heat Load	Sensible Heat Flux	
		In	Out
	Watts	cal/cm^2	cal/cm^2
Quincy	13	9.7	9.6
	52	27.9	29.4
	117	63.4	64.7
Cloquato	13	9.3	8.7
	52	27.7	28.5
	117	53.4	61.0
Chehalis	13	9.0	9.2
	52	28.5	29.3
	117	52.3	53.6

The energy dissipation rates from the heat sources maintained at 29 C and the maximum sensible heat fluxes are shown in Table 20 for all three soils as a function of the maximum rate of surface irradiation. The maximum sensible heat flux rate was about 0.030 $cal/cm^2 min$ for all three soils when the maximum rate of surface irradiation was 13 watts. This was nearly equal to the rate of

energy dissipation from the heat source. At higher rates of surface irradiation the maximum heat flux rate far exceeded the rate of heat dissipation from the heat sources.

Table 20. Maximum sensible heat fluxes and energy dissipation rates from the heat sources with a temperature of 29 C as a function of surface heat load for Quincy, Cloquato and Chehalis soils.

Surface Heat Load	Maximum Sensible Heat Flux			Energy Dissipation Rate From the Heat Source		
	Quincy	Cloquato	Chehalis	Quincy	Cloquato	Chehalis
Watts	- - - - - - - - - - - - cal/cm^{2}min - - - - - - - - - - - -					
0	0.000	0.000	0.000	0.0385	0.0412	0.0368
13	0.030	0.030	0.032	0.0404	0.0320	0.0299
52	0.093	0.080	0.110	0.0332	0.0305	0.0243
117	0.224	0.220	0.210	0.0335	0.0318	--

It was shown above that the sensible heat flux did not decrease the rate of energy dissipation very much.

Conclusions

The energy dissipation rate was highest in Quincy soil and lowest in Chehalis soil at a given temperature difference between heat source and soil surface. When the surface temperature remains constant, the energy dissipation rate increases with heat source temperature. The results obtained showed good agreement with predictions from the theoretical model presented by Kendrick and Havens (1973).

This model was developed for steady state conditions with a constant soil surface temperature. Analysis of this study showed that it can be used to predict the energy dissipation rate for non-steady state conditions with a varying soil surface temperatures, by using an average surface temperature. The model appears to be adequate for predicting land area requirements for the dissipation of given amounts of waste energy.

The total land area required to dissipate the waste energy from a 1000 MWe power plant is higher in Chehalis soil than in Quincy soil. The land area required depends more on the thermal conductivity and the difference between heat source and soil surface temperature than on the depth and spacing.

WATER MOVEMENT

Soil Water Distribution Without Subsurface Irrigation

Quincy soil was subjected to a daily surface irradiation cycle with a maximum rate of heat application of 117 watts for seven consecutive days with the heat source temperature at 29 C. The initial soil water content was 0.30 cm^3/cm^3. Changes in the initial soil water content were measured with a gamma ray attenuation system at four hour intervals at 78 positions in the soil column. The water content distribution existing on the seventh day is shown in Figure 29. The soil water content was lowest in the region near the heat source and increased gradually at points away from it. The water content was 0.04 cm^3/cm^3 near the heat source and 0.14 cm^3/cm^3 at the 5 cm depth. Plants cannot survive in Quincy soil when the water content decreases below 0.10 cm^3/cm^3. The soil water content was less than this critical value over most of the soil column. Soil water depletion also decreased the apparent thermal conductivity of the soil, making the system less efficient as a heat dissipation mechanism.

In a drying soil column with no subsurface heating, the water content is usually highest in the lower region of the column and decreases gradually toward the evaporating sites at the soil surface. The soil water content distribution in the column with soil warming was quite different. It was lowest near the heat source and increased

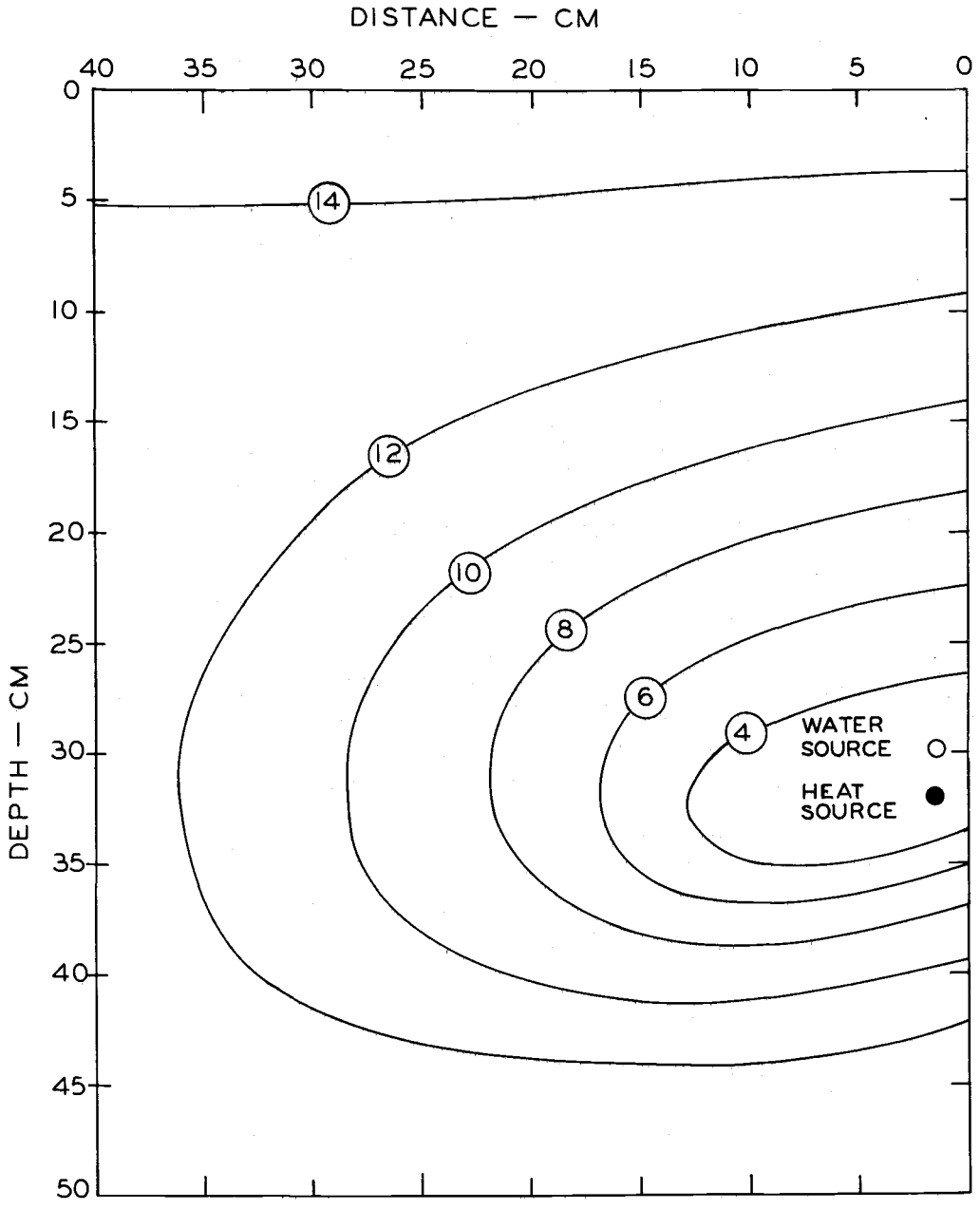

Figure 29. Distribution of water in a Quincy soil exposed to a heat source temperature of 29 C for seven days at a room temperature of 22 C. Heat was applied at the soil surface as described in the text. The solid lines connect points of the same water content. They are labelled in percent of total volume. The initial water content was .30 cm^3/cm^3. No water was added to the soil surface or near the heat source.

toward the soil surface.

Water depletion near the heat source occurs as a result of mass flow and vapor flow. Surface tension of water decreases with increasing temperature, thus weakening the forces retaining water in the warm regions and causing mass flow toward the cool regions to occur. This mechanism continues until all the capillary water has been removed and the capillary channels are broken. At this water content the hydraulic conductivity of the soil is very low. As the soil water content decreases, large interconnecting air filled pores become available for vapor diffusion. The water vapor pressure in the pore spaces in the high temperature regions exceeds that in the lower temperature regions. Hence water vapor movement is initiated. The vapor pressure gradients are maintained by evaporation in the high temperature regions and condensation in the low temperature regions. The vapor movement and subsequent condensation creates a hydraulic gradient opposite to the temperature gradient. The evaporation may be compensated for by a return flow of water resulting from these hydraulic gradients. If the ratio of hydraulic conductivity to vapor diffusivity is very low, the vapor diffusion process ceases only when all capillary water has been removed from the high temperature region. The water content of the soil next to the heat source at which an equilibrium between evaporation and return mass flow is established depends on the heat source

temperature, soil type, and rate of liquid and vapor transfer.

Once most of the capillary water has been removed, the hydraulic conductivity is very low. Consequently, even by ceasing energy input at the heat source, a zone once dried out may take a long time to regain its normal water content (Milne and Mochlinski, 1964; Boersma and Rykbost, 1973). Milne and Mochlinski observed the recovery of water in soil around power transmission lines when water was available to wet the soil profile. They reported that the water content in the wet zone of a sandy soil recovered from about 2.7 percent to about 5.0 percent, but in the dry zone only from about 0.4 percent to 0.6 percent. They also found that the recovery of water in clay soil was negligible.

Soil Water Distribution With Subsurface Irrigation

Soil columns packed with Quincy, Cloquato, and Chehalis soils were subjected to heat source temperatures of 29, 36, and 44 C and daily cycles of surface irradiation with maximum rates of heat application of 0, 13, 52, and 117 watts. The soil water content at a point close to the heat source was monitored continuously with the gamma-ray attenuation system. Water lost by evaporation at the soil surface was replaced from a porous cup located 2 cm above the heat source. Water was applied at 4 hour intervals until midnight. The next supply of water was made at 8:00 a.m. Water

was applied from the subsurface irrigation system at a rate such that the water content at the point close to the heat source did not decrease below its initial value. Water requirements to prevent drying near the heat source were determined by trial and error. Arbitrary rates of water were initially applied and the water content at a point near the heat source was monitored by the gamma-ray attenuation system at short time intervals between consecutive water application periods. The accepted water application rate was the one which resulted in a water content variation of less than 0.005 cm^3/cm^3 at this point during the water application intervals.

When a constant rate of water application was obtained for a particular treatment, application was continued at this rate for three days. During this period, several readings of soil water content were taken with the gamma-ray attenuation system at predetermined points in the soil columns. Averages of these readings were calculated and used to plot the soil water distribution in the soil columns. An example is shown in Figure 30. The soil water content decreased toward the soil surface with the steepest gradients immediately above the heat source. Average values of soil water content as a function of depth were calculated for two regions. The region identified as "over" in Tables 21, 22, and 23 was a 5 cm wide column against the right hand wall of the container and included the water source and heat source. The region identified as "away" was the

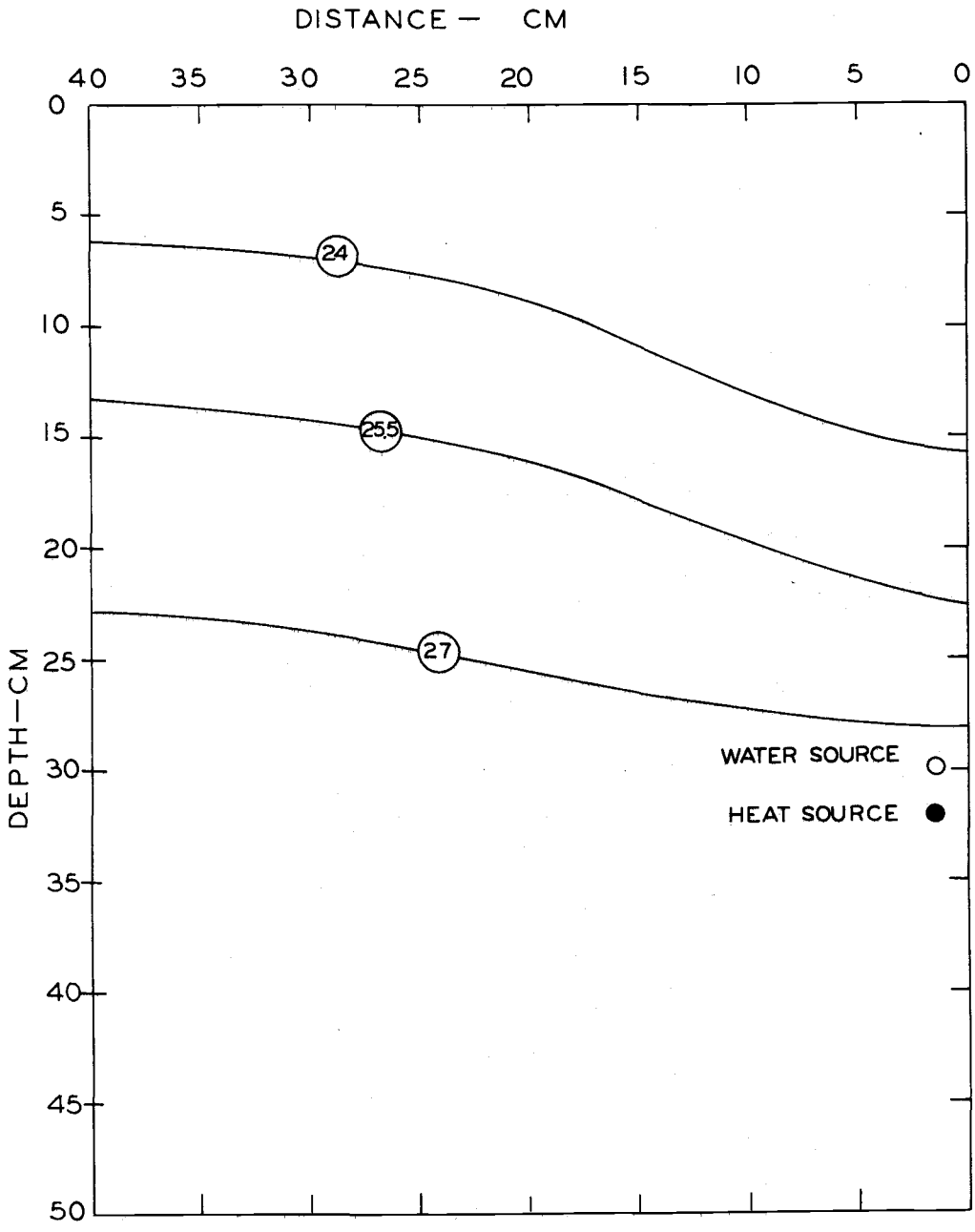

Figure 30. Distribution of water in the Quincy soil exposed to a heat source temperature of 36 C with water being added near the heat source at the rate required to maintain a constant water content. The solid lines connect points of the same water content and are labeled in percent of total volume.

Table 21. Average soil water content "over" and "away from" the heat source as a function of depth in the Quincy soil column at the indicated surface heat loads and heat source temperatures.

Heat Source Temperature	Depth	0 Watts		13 Watts		52 Watts		117 Watts	
		Over	Away	Over	Away	Over	Away	Over	Away
C	cm	cm^3/cm^3							
29	1	0.123	0.202	0.128	0.195	0.120	0.194	0.109	0.184
	4	0.190	0.205	0.192	0.195	0.179	0.189	0.161	0.177
	8	0.170	0.174	0.175	0.214	0.177	0.202	0.155	0.180
	15	0.248	0.214	0.245	0.209	0.233	0.227	0.217	0.219
	25	0.280	0.299	0.278	0.300	0.266	0.288	0.248	0.281
	29	0.271	0.300	0.272	0.296	0.257	0.296	0.226	0.288
	33	0.296	0.319	0.295	0.334	0.297	0.324	0.287	0.316
	46	---	---	---	---	---	---	0.289	0.323
36	1	0.170	0.178	0.148	0.166	0.149	0.156	0.122	0.114
	4	0.178	0.180	0.169	0.175	0.160	0.167	0.153	0.152
	8	0.169	0.214	0.158	0.204	0.155	0.193	0.153	0.188
	15	0.206	0.187	0.180	0.232	0.168	0.222	0.165	0.222
	25	0.235	0.236	0.230	0.230	0.233	0.239	0.228	0.237
	29	0.217	0.238	0.225	0.227	0.230	0.240	0.247	0.248
	33	0.241	0.227	0.253	0.234	0.252	0.235	0.253	0.249
	46	0.243	0.252	0.246	0.250	0.243	0.252	0.242	0.252
44	1	0.156	0.156	0.133	0.143	0.107	0.120	0.096	0.113
	4	0.193	0.197	0.186	0.178	0.174	0.182	0.174	0.184
	8	0.229	0.222	0.222	0.212	0.206	0.198	0.206	0.192
	15	0.241	0.282	0.237	0.275	0.217	0.251	0.211	0.241
	25	0.269	0.275	0.285	0.282	0.291	0.278	0.286	0.290
	29	0.253	0.282	0.260	0.295	0.268	0.284	0.271	0.279
	33	0.295	0.286	0.303	0.286	0.300	0.276	0.202	0.282
	46	0.297	0.323	0.297	0.323	0.289	0.305	0.295	0.318

Table 22. Average soil water content "over" and "away from" the heat source as a function of depth in the Cloquato soil column at the indicated surface heat loads and heat source temperatures.

Heat Source Temperature	Depth	0 Watts		13 Watts		52 Watts		117 Watts	
		Over	Away	Over	Away	Over	Away	Over	Away
C	cm	cm^3/cm^3							
29	1	0.279	0.248	0.195	0.231	0.153	0.180	0.103	0.133
	4	0.319	0.331	0.275	0.307	0.226	0.254	0.234	0.230
	8	0.463	0.429	0.426	0.398	0.417	0.394	0.397	0.396
	15	0.446	0.433	0.411	0.390	0.390	0.371	0.413	0.411
	25	0.502	0.535	0.485	0.531	0.475	0.527	0.477	0.497
	29	0.501	0.476	0.498	0.459	0.497	0.449	0.485	0.510
	33	0.505	0.535	0.496	0.527	0.501	0.528	0.517	0.541
	46	0.552	0.574	0.565	0.566	0.559	0.557	0.569	0.576
36	1	0.474	0.525	0.470	0.518	0.469	0.501	0.458	0.458
	4	0.462	0.531	0.468	0.527	0.460	0.494	0.457	0.460
	8	0.495	0.474	0.498	0.476	0.485	0.481	0.476	0.473
	15	0.512	0.466	0.508	0.471	0.495	0.466	0.495	0.466
	25	0.448	0.499	0.447	0.502	0.426	0.493	0.446	0.488
	29	0.478	---	0.479	---	0.469	---	0.466	---
	33	0.468	0.485	0.473	0.487	0.470	0.476	0.468	0.474
	46	0.501	0.471	0.500	0.464	0.481	0.451	0.492	0.485
44	1	0.441	0.451	0.442	0.452	0.441	0.453	0.454	0.454
	4	0.455	0.461	0.467	0.455	0.452	0.450	0.441	0.441
	8	0.453	0.472	0.450	0.477	0.444	0.468	0.438	0.452
	15	0.480	0.491	0.469	0.481	0.474	0.475	0.471	0.471
	25	0.485	0.507	0.490	0.507	0.485	0.503	0.483	0.504
	29	0.485	0.517	0.486	0.515	0.489	0.513	0.495	0.511
	33	0.504	0.516	0.508	0.514	0.511	0.514	0.513	0.515
	46	0.592	0.583	0.534	0.575	0.532	0.570	0.530	0.570

Table 23. Average soil water content "over" and "away from" the heat source as a function of depth in the Chehalis soil column at the indicated surface heat loads and heat source temperatures.

Heat Source Temperature	Depth	0 Watts		13 Watts		52 Watts		117 Watts	
		Over	Away	Over	Away	Over	Away	Over	Away
C	cm	cm^3/cm^3							
29	1	0.279	0.283	0.241	0.249	0.243	0.254	0.219	0.222
	4	0.321	0.342	0.307	0.316	0.314	0.327	0.301	0.303
	8	0.366	0.357	0.348	0.339	0.350	0.351	0.339	0.335
	15	0.397	0.352	0.371	0.381	0.384	0.427	0.367	0.411
	25	0.475	0.446	0.449	0.421	0.466	0.435	0.457	0.429
	29	0.467	0.462	0.424	0.432	0.447	0.446	0.430	0.438
	33	0.466	0.455	0.451	0.432	0.462	0.449	0.450	0.435
	46	0.506	0.555	0.504	0.523	0.514	0.543	0.497	0.527
36	1	0.466	0.411	0.432	0.401	0.421	0.401	0.404	0.371
	4	0.431	0.400	0.412	0.396	0.411	0.392	0.395	0.364
	8	0.455	0.416	0.440	0.408	0.433	0.401	0.431	0.390
	15	0.484	0.482	0.469	0.476	0.456	0.472	0.447	0.465
	25	0.496	0.484	0.486	0.475	0.475	0.469	0.461	0.458
	29	0.488	0.474	0.476	0.465	0.474	0.465	0.476	0.469
	33	0.474	0.502	0.468	0.487	0.472	0.480	0.472	0.479
	46	0.529	0.525	0.508	0.513	0.497	0.515	0.480	0.518

20 cm wide column against the left hand side of the container. The region labeled "over" was above the heat source, while the region labeled "away" was centered 30 cm from the heat source. The water contents of the regions are shown in Tables 21, 22, and 23 as a function of depth, heat source temperature, and rate of surface irradiation. Data for Chehalis soil with heat source temperatures of 44 C were not obtained due to a mechanical failure of the equipment. The soil water content was highest in the regions near the heat and water source and gradually decreased towards the soil surface. The water content near the heat and water sources was nearly the same at all heat source temperatures and surface heat loads. The soil water content of the surface layer was lowest at the highest rate of surface heat application.

Comparison of Figure 29 with Figure 30 shows that it was possible to supply water to the entire column and maintain a high water content with the subsurface irrigation system. The soil water content was near field capacity, which is generally the optimum water content for crop production, throughout the column. The subsurface water application rates that were attained appear adequate to meet the evaporation needs in subsurface heating and irrigation systems for climatic conditions, and placement of heat and water sources used in these experiments. Additional experiments are needed to optimize the proposed system with respect to its geometry and soil type.

Water Application Rates

Water application rates from the subsurface irrigation system, required to prevent drying around the heat sources for different soils at different heat source temperatures and surface heat loads, are shown in Table 24. Water requirements increased with surface heat load (potential evaporation) and heat source temperature. The water requirements were higher for the Quincy soil than for the Cloquato or Chehalis soils. This is so because the Quincy soil with its coarse texture has a higher hydraulic conductivity than the Cloquato and Chehalis soils.

Table 24. Water application rate as a function of heat source temperature, surface heat load, and soil type.

Heat Source Temperature	Surface Heat Load	Water Application Rate		
		Quincy	Cloquato	Chehalis
C	Watts	------mm/day------		
29	0	3.00	2.25	1.50
	13	3.75	3.00	2.63
	52	4.50	3.38	3.00
	117	4.88	3.38	3.19
36	0	3.75	3.00	1.88
	13	4.50	3.75	2.25
	52	4.88	4.13	3.00
	117	5.25	4.50	3.75
44	0	4.50	3.38	2.25
	13	4.88	4.13	3.00
	52	5.63	4.88	3.38
	117	6.00	5.63	3.75

Effect of Surface Irradiation

Water requirements increased with surface heat load (potential evaporation) and heat source temperature. Examination of water application rates in Table 24 shows a curvilinear relationship between water requirement and heat applied at the soil surface. The rate of increase of water required to meet the evaporation demand at higher soil surface heat loads was lowered by the limited rate of water transmittance to the evaporative sites at the soil surface. Soil water content profiles in Quincy, Cloquato and Chehalis soils with heat source temperatures of 29 C are shown in Figures 31, 32, and 33. The soil water content decreased towards the soil surface. The soil water content decreased drastically near the surface in the Cloquato and Chehalis soils columns. The decrease was smaller in the Quincy soil. Higher soil water content gradients occurred in fine textured soils (Cloquato and Chehalis) than in coarse textured soil (Quincy). However, the water requirement was higher for the Quincy soil than for the Cloquato or Chehalis soils. This is so because the Quincy soil with its coarse texture has a higher hydraulic conductivity than the Cloquato and Chehalis soils.

Formation of a dry layer of soil near the surface impeded water movement to the atmosphere (Milthrope, 1960; Gardner, 1958; Hadas and Hillel, 1972). Gardner and Hillel (1962) reported a salt crust

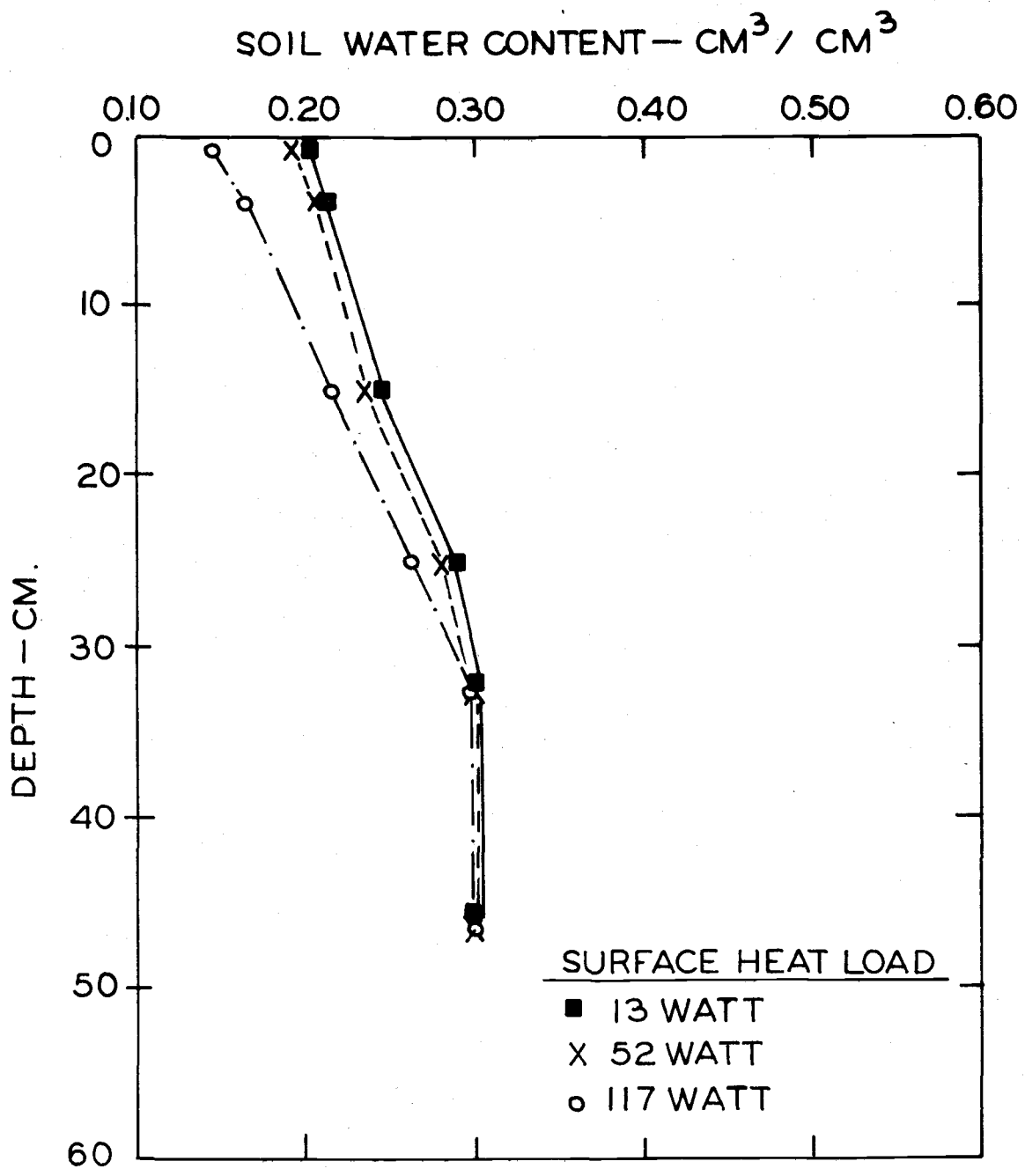

Figure 31. Soil water content as a function of depth for Quincy soil at three surface heat loads and a heat source temperature of 29 C. The results were obtained by averaging the water content of soil layers 2 cm thick.

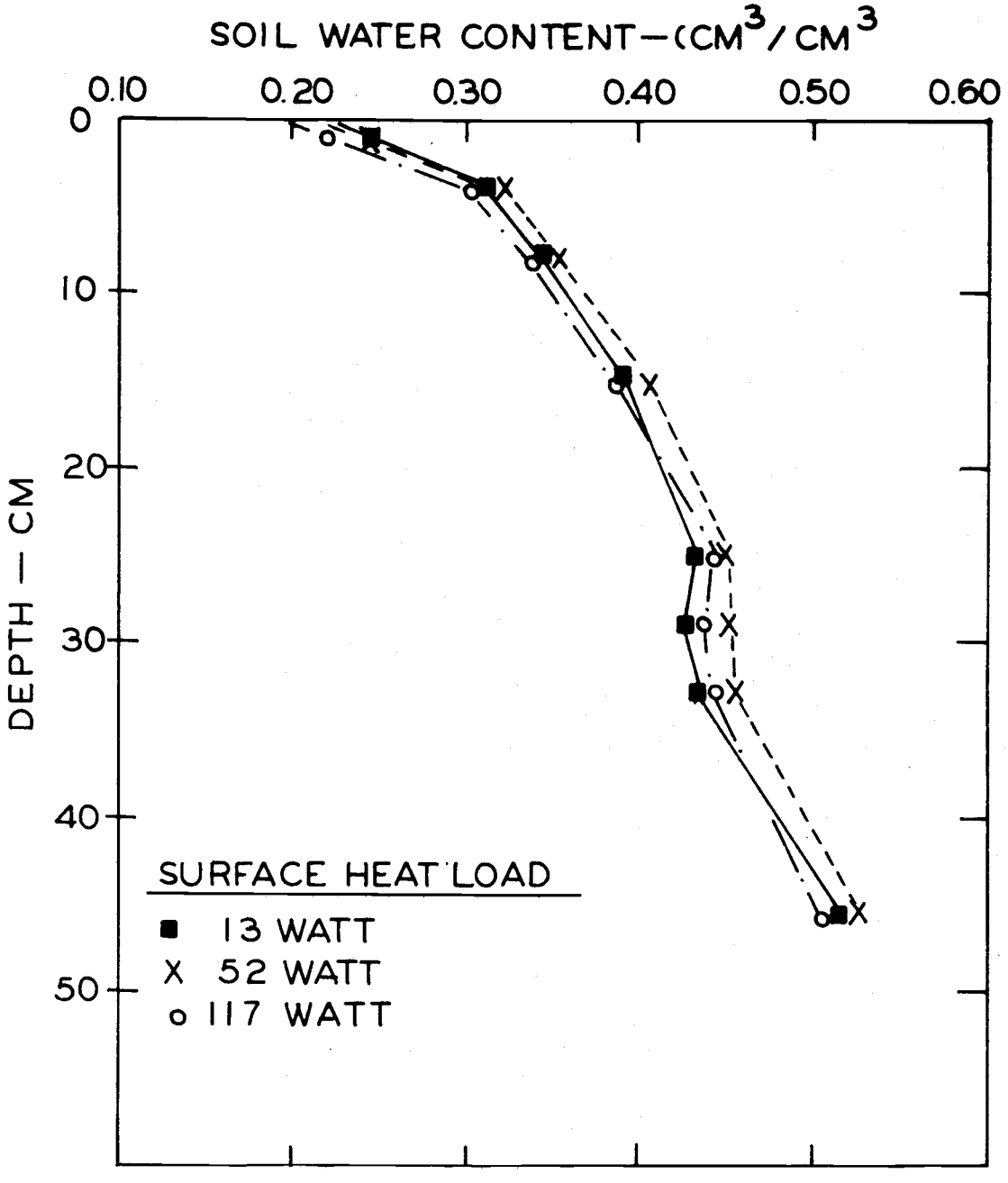

Figure 32. Soil water content as a function of depth for Cloquato soil at three surface heat loads and a heat source temperature of 29 C. The results were obtained by averaging the water content of soil layers 2 cm thick.

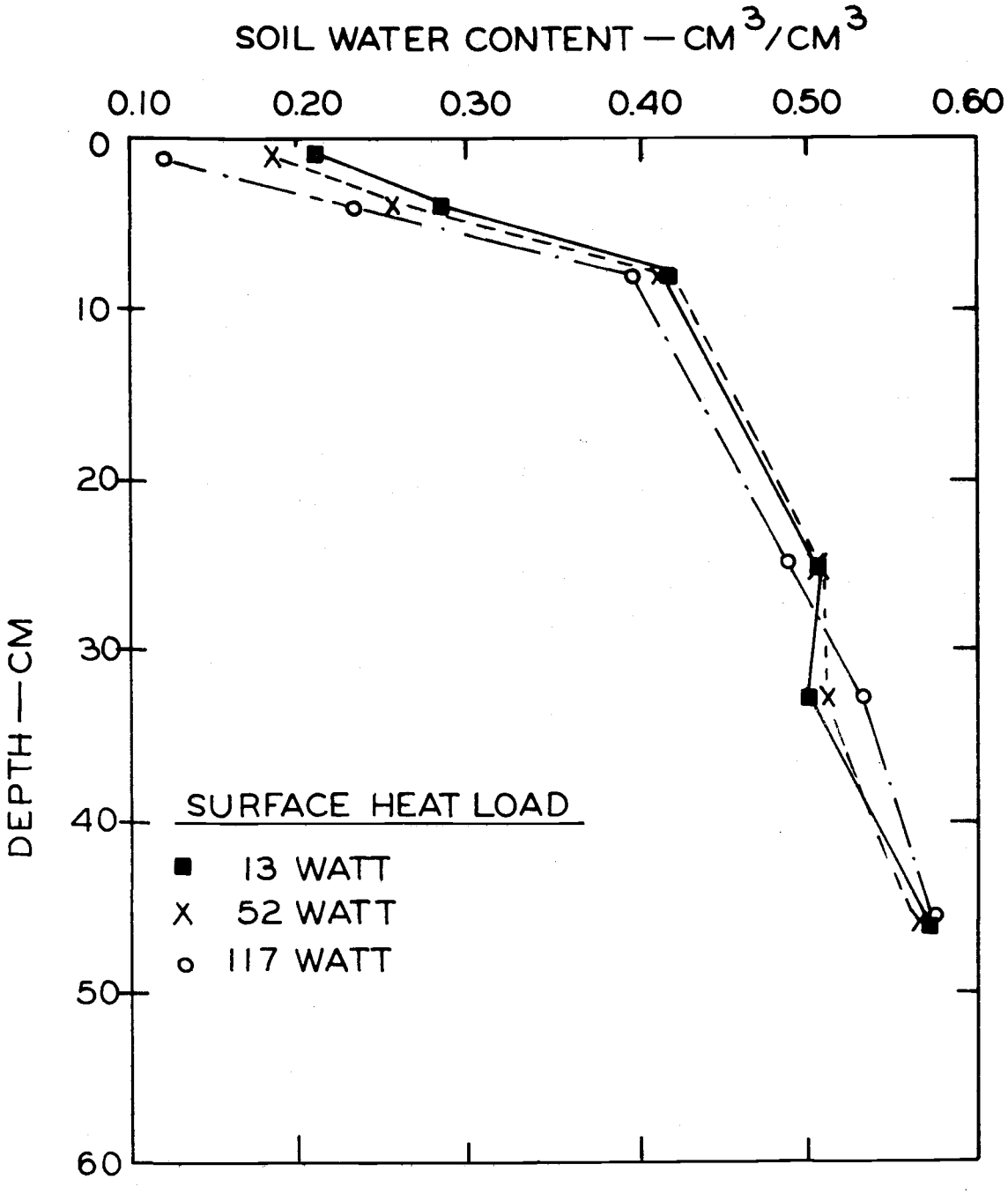

Figure 33. Soil water content as a function of depth for Chehalis soil at three surface heat loads and a heat source temperature of 29 C. The results were obtained by averaging the water content of soil layers 2 cm thick.

formation of relatively salt free soil surfaces as a result of the evaporation process. They suggested that this crust was the cause of a marked reduction in evaporation rate in their experiments. Slatyer (1958) also reported that as the evaporation process proceeded water moved to the surface while evaporation deposited salt on the surface. As a result the soil water potential decreased at the soil surface and evaporation decreased accordingly. Soil surface drying and salt accumulation was observed in the present experiments. The rate of increase in the water requirements at higher surface heat loads (Table 24) might have been decreased as a result. The sinusoidal surface heat load changed the surface layer temperature sinusoidally during the day. The temperature gradient near the soil surface changed accordingly. Higher surface heat loads reversed the temperature gradient at the soil surface during the time of maximum surface temperature variation (Tables 11, 12, and 13). Downward water movement induced by periodic surface temperature variations has been reported by Hadas (1968). Vapor flow contributes most to downward water flow because the water content at the surface is low. This mechanism might also have depressed the increase in evaporation rates from the soil column at higher applied surface heat loads. Similar results were reported by Gardner and Hillel (1962).

Effect of Soil Texture

Soil texture also affected the water application rates. It was highest for Quincy loamy sand. The rate at which water is supplied to the evaporative sites is controlled by soil water content gradients and the hydraulic conductivity of the soil. Figures 31, 32, and 33 show that the smallest water content gradients occurred in the Quincy soil. They were larger in the Cloquato and Chehalis soils. Higher values of the conductivity in the coarse textured soil (Quincy) compensated for the low water content gradient (Jackson, 1963). The soil water content at the surface of all three soils was about 0.30 cm^3/cm^3 except for the highest rate of irradiation, the peak rate of 117 watts. Equal water content in soils with different textures corresponds to different soil water potentials. The lower soil water potential in Chehalis soil lowered its evaporation rate. Similar results were reported by Makkink and van Heemst (1956). Their data showed that on wet soil the potential evapotranspiration was maintained for a certain period of time after which the actual evapotranspiration became lower than the potential evapotranspiration as the soil water potential decreased.

Water Application Rates as a Function of Heat Source Temperature

The water application rates were plotted as a function of the

temperature difference between the heat source and the soil surface at different surface heat loads (Figures 34, 35, 36, and 37). These rates were evaluated in terms of potential evaporation rates for the laboratory conditions as measured by a weighing procedure. The soil container was filled with water and subjected to the different radiation cycles used in the experiments. The decrease in weight of the column over a period of time was used to estimate the potential evaporation for the laboratory conditions. These rates were 2.5, 3.3, 5.2 and 10.3 mm/day at sinusoidal surface heat loads with peak rates of 0, 13, 52 and 117 watts, respectively.

The water application rates increased with increasing temperature differences between the heat source and soil surface for all three soils. Straight lines were drawn through the experimental points and the slopes of these lines (mm/day C) were obtained. No statistical procedure was used since adequate data points are not available for each line. The results are given in Table 25. The rates were highest for the Quincy soil and lowest for the Chehalis soil. The rates increased with increasing surface heat load because more energy for evaporating water was available at the soil surface.

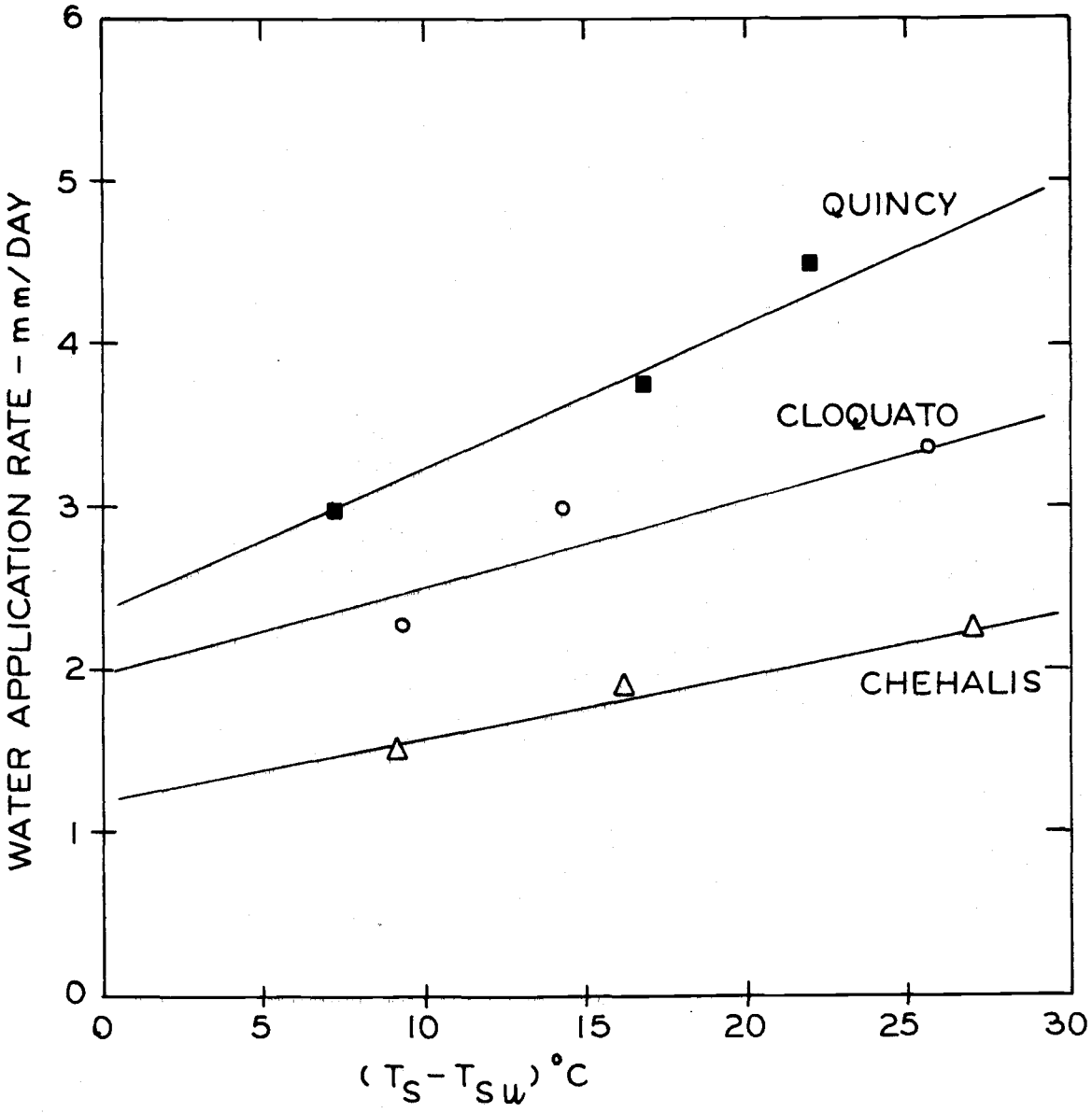

Figure 34. Water use rates as a function of the temperature difference between heat source and soil surface for Quincy, Cloquato, and Chehalis soils with no surface heat load.

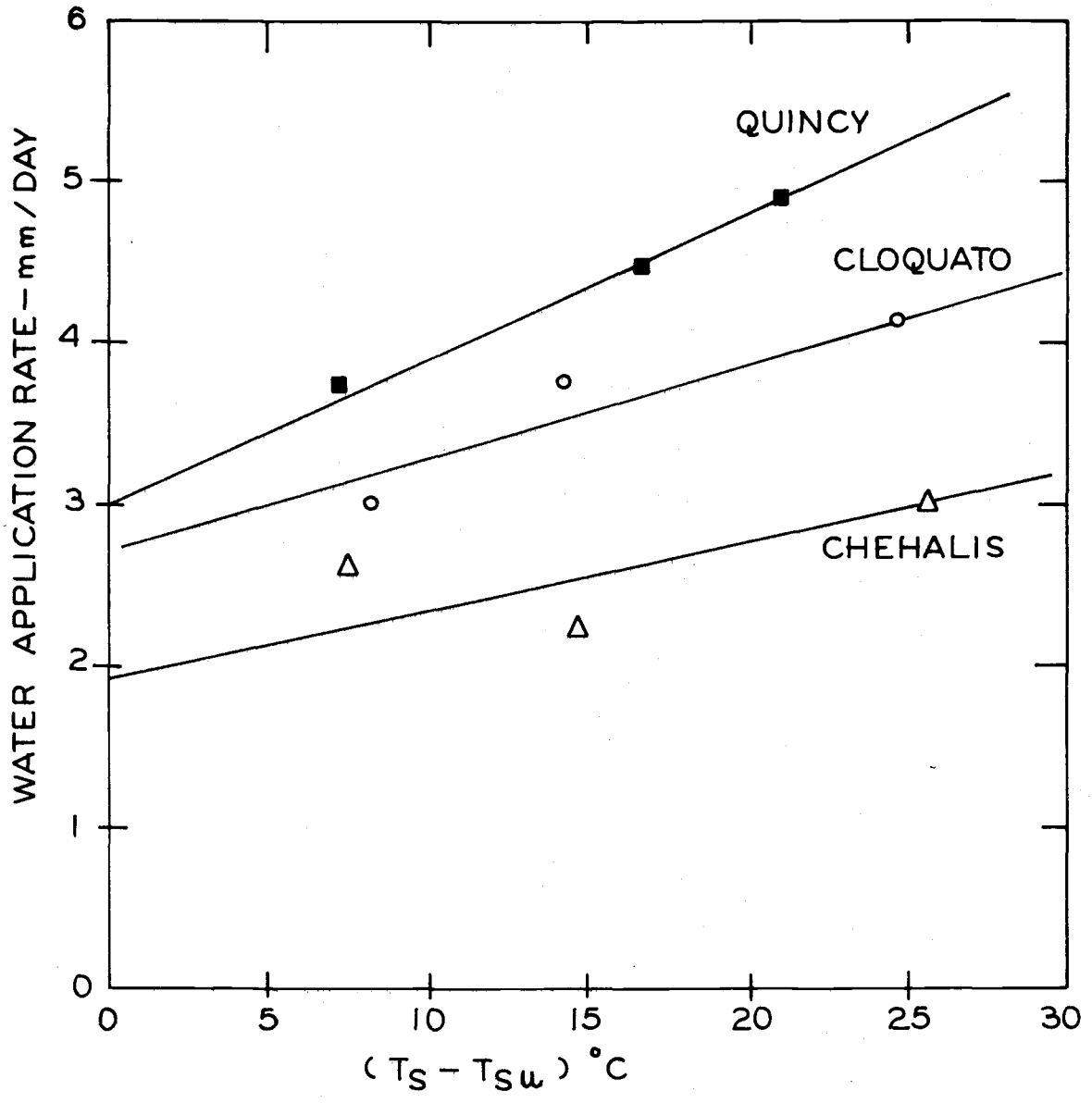

Figure 35. Water use rates as a function of the temperature difference between heat source and soil surface for Quincy, Cloquato and Chehalis soils with 13 watts surface heat load.

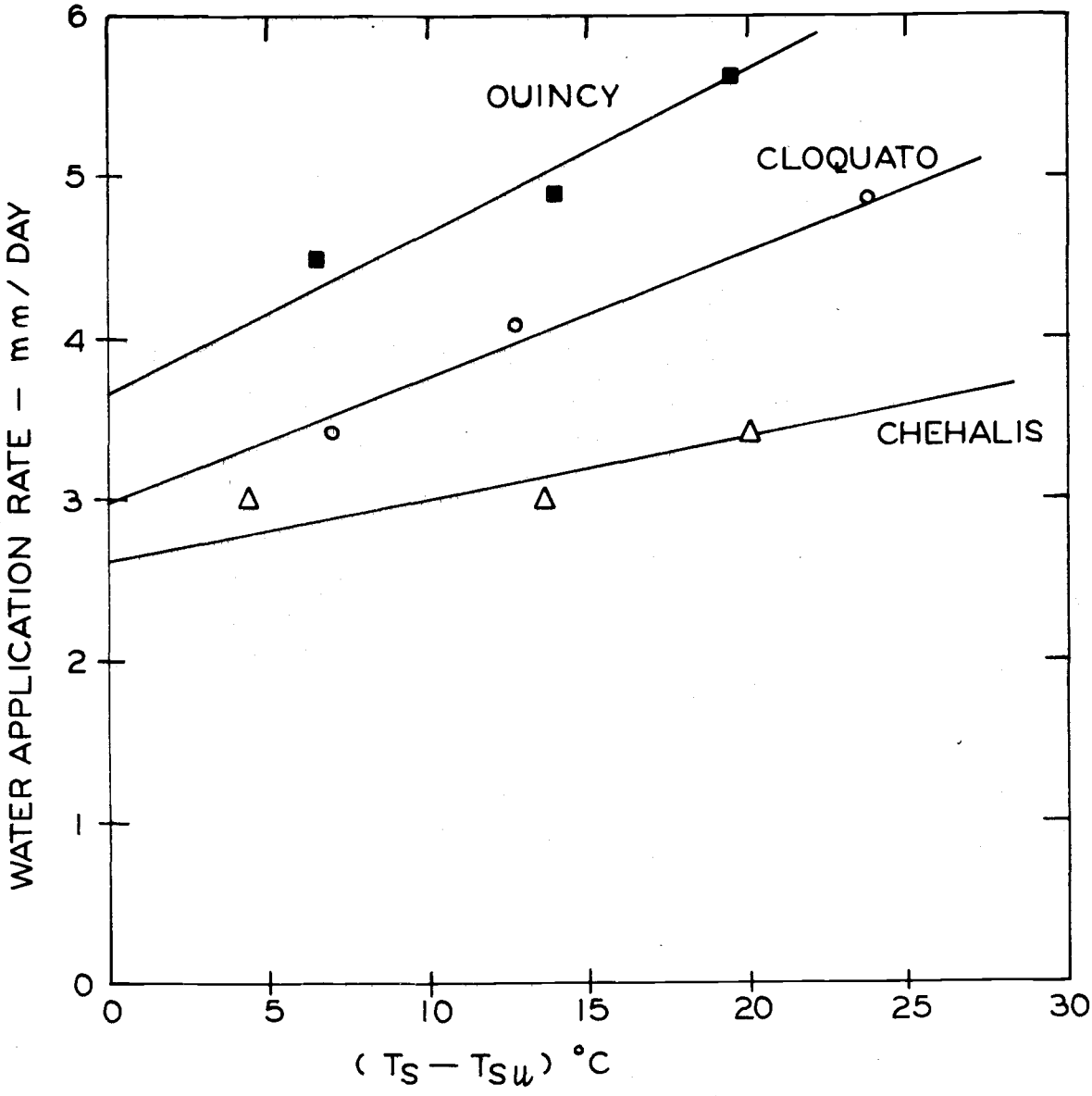

Figure 36. Water use rates as a function of the temperature difference between heat source and soil surface for Quincy, Cloquato and Chehalis soils with 52 watts surface heat load.

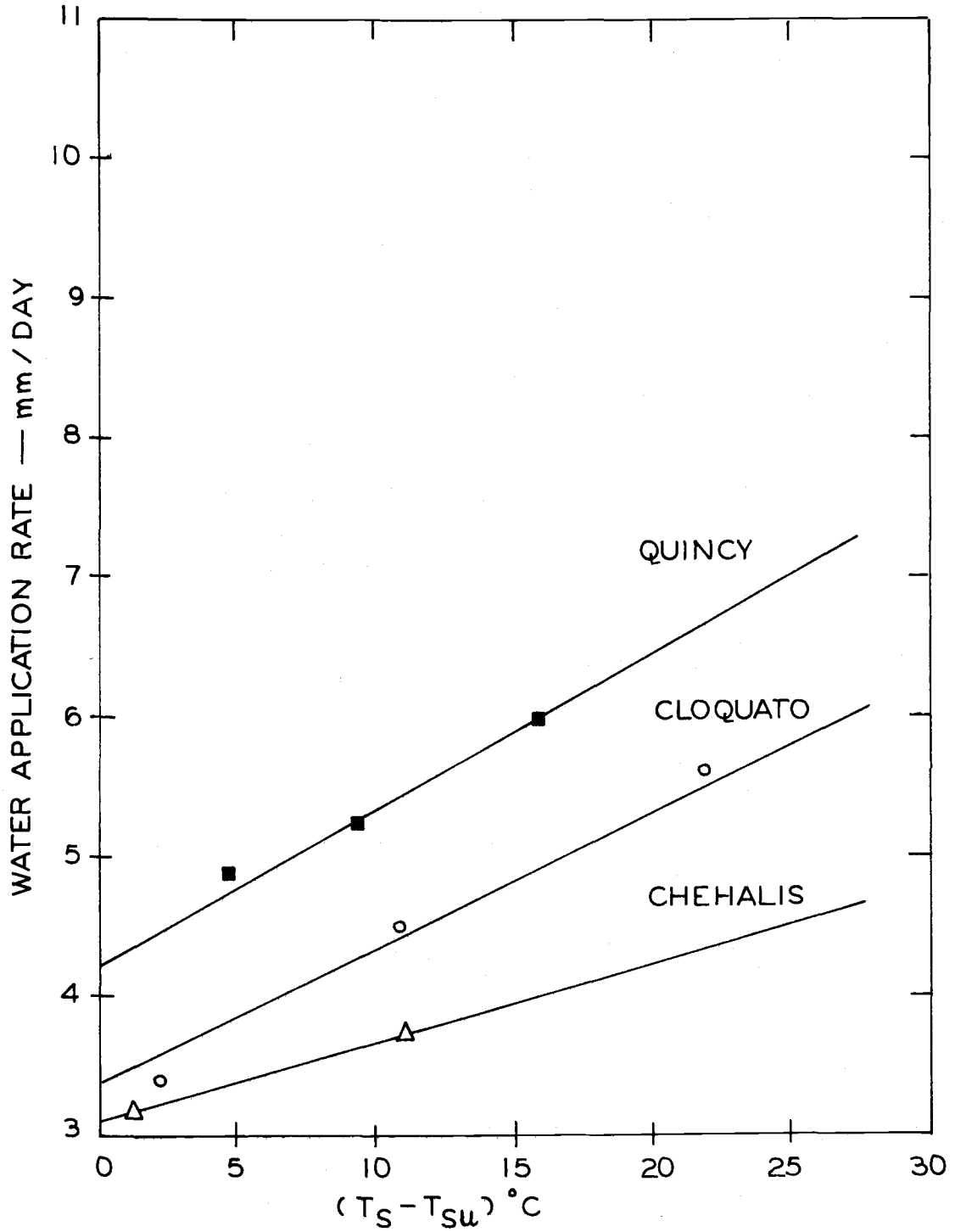

Figure 37. Water use rates as a function of the temperature difference between heat source and soil surface for Quincy, Cloquato and Chehalis soils with 117 watts surface heat load.

Table 25. Rate of increase of water application rate per unit temperature difference between heat source and soil surface at different surface heat loads for Quincy, Cloquato and Chehalis soils.

Surface Heat Load	Water Use Rate/(T_s-T_{su})		
	Quincy	Cloquato	Chehalis
Watts	- - - - - - - mm/day C - - - - - - -		
0	0.075	0.056	0.039
13	0.091	0.059	0.042
52	0.100	0.078	0.040
117	0.113	0.100	0.057

Rates of Water Loss With Subsurface Irrigation But No Subsurface Heating

The rates of water flow that would occur in the soil columns without subsurface heating but with subsurface water application, at the imposed surface heat loads were obtained. The assumption that these rates are proportional to the temperature differences as shown in Figures 34 through 37 was used for this analysis. Temperature differences for conditions without subsurface heating, but with subsurface irrigation were assumed to be the differences between the daily average temperatures at the soil surface and the average temperature of the column equilibrated at room temperature without subsurface heating. Using these temperature differences, water loss rates were obtained from Figures 34 through 37. Results are shown in Table 26.

Table 26. Estimated rates of water loss from Quincy, Cloquato, and Chehalis soils without subsurface heating, but with subsurface water application.

Surface Heat Load	Measured Evap. Rate	Rate of Water Loss		
		Quincy	Cloquato	Chehalis
Watts	mm/day	- - - - - - - - - mm/day - - - - - - - - -		
0	2.5	2.45	2.05	1.30
13	3.3	3.10	2.80	1.95
52	5.2	3.65	3.00	2.65
117	10.3	3.80	3.20	2.90

The rate of water application without subsurface heating was highest for the Quincy soil and lowest for the Chehalis soil. The Quincy soil with its higher hydraulic conductivity passes water more easily. The Quincy soil can meet the evaporative demand at surface heat loads of 0 and 13 watts, but not at the higher surface heat loads. The Cloquato and Chehalis soils can not meet these evaporative demands. The hydraulic conductivities of these soils are inadequate to sustain the required flow rates. The soil surface layers of Cloquato and Chehalis soils therefore dried at the higher surface heat loads (Tables 21, 22, and 23, and Figures 31, 32, and 33).

As the surface heat load increases a layer of soil near the surface dries out. This dry soil layer then becomes a barier to water movement. Hence, the rate of water loss increased little by increasing the heat load from 52 to 117 watts.

Water Application Rates in Relation to Crop Requirements

Potential evaporation rates and consumptive use values for the Willamette Valley growing season are shown in Table 27. Evaporation in the laboratory, measured by the weighing procedure varied from 7.50 cm/month to 30.90 cm/month. Table 28 shows the consumptive use rates for alfalfa and water application rates achieved with the subsurface irrigation system without subsurface heating and with a heat source temperature of 44 C. The laboratory conditions cover the range of potential evaporation occurring in the Willamette Valley. The water supplied by the subsurface irrigation system without subsurface heating was not sufficient to meet the highest crop requirements as indicated by the consumptive use for alfalfa. However, with a heat source temperature of 44 C sufficient water could be supplied to meet the crop requirements in Quincy and Cloquato soils, but not in Chehalis soils.

Subsurface Irrigation Near Power Transmission Lines

Drying of the soil near power transmission lines has been observed. Extremely high cable temperatures due to drying of the soil resulted, which caused power transmission failure. Cooling the cables was proposed to eliminate this problem. Maintaining a high

Table 27. Potential evaporation and consumptive use in the Willamette Valley.

Month	Field Potential Evaporation*	Consumptive Use For Alfalfa*
	cm/month	cm/month
April	6.90	4.03
May	14.27	10.43
June	16.30	13.35
July	24.18	16.23
August	20.19	14.03
September	12.29	9.70
October	6.06	3.68

*Data obtained from Watts et al. (1968).

Table 28. Rates of water loss from heated soil columns compared with consumptive use rates for alfalfa.

Month	Consumptive Use for Alfalfa	Heat Source Temp.	Surface Heat Load	Water Application Rate With No Subsurface Heating		
				Quincy	Cloquato	Chehalis
	cm/month	C	Watts	- - - - cm/month - - - - -		
May	10.43		0	7.35	6.21	3.81
June	13.35		13	9.24	8.34	5.85
July	16.23		52	10.24	9.00	7.74
August	14.03		117	11.25	9.21	8.61
				Water Application Rate With Subsurface Heating		
May	10.43	44	0	13.50	10.14	6.75
June	13.35		13	14.64	12.39	9.00
July	16.23		52	16.89	14.64	11.14
August	14.03		117	18.00	16.89	11.25

soil water content in the soil profile was also recommended by power transmission engineers. The practical value of water cooling for power transmission cables in the ground was examined by Milne and Mochlinski (1964) and Arman et al. (1964). Cooling was done by circulating water in pipes near the cables or by irrigating the soil with a perforated pipe from which water seeped into the soil near the cable right below. A huge volume of water was required for cooling with the piping system as compared with the irrigation method. The space between the circulating pipe and cables still dried out. This led to lower heat exchange rates between the circulating water and the cable. Subsurface irrigation was more efficient in cooling the cables. The function of the water was strictly to maintain a high apparent thermal conductivity in the soil. The amount of water required was small compared with that needed for the removal of heat by the circulation method. It was estimated that the irrigation method of cooling only used 10 percent of the water needed for the circulation method of cooling (Arman et al., 1964).

Conclusions

Surface evaporation and temperature gradient induced water flow depleted the soil water to below the wilting point in only a few days in soils heated with subsurface heat sources. Water depletion was most severe near the heat source.

Subsurface irrigation provides water to the soil to substitute for the water evaporated at the soil surface and migrated from the heat source region under temperature gradients. Subsurface irrigation makes it possible to maintain a soil water content near field capacity. As a result of the higher soil water content, the apparent thermal conductivity in soil with subsurface irrigation is 4 to 6 times greater than that in soil column with no subsurface irrigation for fine textured and coarse textured soils respectively. Hence the total land area required to dissipate a given amount of heat decreases 4 and 6 times in fine textured and coarse textured soils, respectively.

The subsurface irrigation system by itself is not sufficient to supply the consumptive use demand for crops in the Willamette Valley. However, when used in conjunction with the subsurface heating system, subsurface irrigation would be a feasible irrigation method.

BIBLIOGRAPHY

Adamson, A.W. 1960. The Physical Chemistry of Surfaces. Interscience Publishers: New York. 629 p.

Arman, A.N., D.M. Cherry, L. Gosland, and P.M. Hollingsworth. 1964. Influence of soil-moisture migration on power rating of cables in H.V. transmission systems. Proc. IEE, 3:1000-1016.

Boersma, L. 1970. Warm water utilization. p. 74-112. In: S.P. Mathur and R. Steward (ed.). Proceedings of the Conference on the Beneficial Uses of Thermal Discharges. New York State Department of Environmental Conservation. September 17-18.

Boersma, L. and K.A. Rykbost. 1973. Integrated system for utilizing waste heat from steam electric plants. Journal of Environmental Quality 2:179-187.

Bunting, A.H. and P.M. Cartwright. 1957. Agronomic aspects of environmental control. p. 96-110. In: J.P. Hudson (ed.). Control of the Plant Environment. Butterworths Scientific Publications: London.

Cary, J.W. 1963. Onsager's relations and non-isothermal diffusion of water vapor. Journal of Physical Chemistry 67:126-129.

Cary, J.W. 1964. An evaporation experiment and its irreversible thermodynamics. International Journal of Heat and Mass Transfer 7:531-538.

Cary, J.W. 1965. Water flux in moist soil: Thermal versus suction gradients. Soil Science 100:168-175.

Cary, J.W. 1966. Soil moisture transport due to thermal gradients: Practical aspects. Soil Science Society of America, Proceedings 30:428-433.

Clarkson, V.A. 1960. Effect of black polyethylene mulch on soil and microclimate temperature and nitrate level. Agronomy Journal 52:307-309.

Cochran, P.H., L. Boersma, and C.T. Youngberg. 1967. Thermal properties of a pumice soil. Soil Science Society of America, Proceedings 31:454-459.

Chudnovskii, A.F. 1962. Heat Transfer in the Soil. Published for the National Scientific Foundation, Washington, D.C., by the Israeli Program of Scientific Translations: Jerusalem, 164p.

Davidson, J.M., J.W. Biggar and D.R. Nielsen. 1963. Transient water flow in unsaturated soils measured by gamma radiation. Journal of Geophysical Research 68:4777-4783.

de Vries, D.A. 1952. Thermal Conductivity of Soil. Mededelingen van de Landbouwhogeschool te Wageningen 52:1-73.

de Vries, D.A. 1963. Thermal properties of soils. p. 210-235. In: W.R. van Wijk (ed.). Physics of Plant Environment. North-Holland Publishing Company: Amsterdam. 382 p.

Ferguson, H. and W.H. Gardner. 1962. Water content measurement in soil columns by gamma ray absorption. Soil Science Society of America, Proceedings 26:11-14.

Gardner, W.R. 1958. Some steady-state solutions of the unsaturated moisture flow equation with application to evaporation from a water table. Soil Science 85:228-232.

Gardner, H.R. and R.J. Hanks. 1966. Evaluation of the evaporation zone in soil by measurement of heat flux. Soil Science Society of America, Proceedings 30:425-428.

Gardner, H.R. and D.F. Hillel. 1962. The relations of external evaporative conditions to the drying of soils. Journal of Geophysical Research 67:4319-4325.

Gemant, A. 1950. The thermal conductivity of soil. Journal of Applied Physics 21:750-752.

Gurr, C.G. 1962. Use of gamma rays in measuring water content and permeability in unsaturated columns of soil. Soil Science 94:224-229.

Gurr, C.G., T.J. Marshall, and J.T. Hutton. 1952. Movement of water in soil due to a temperature gradient. Soil Science 74:335-345.

Hadas, A. 1968. Simultaneous flow of water and heat under periodic heat fluctuations. Soil Science Society of America, Proceedings 32:297-301.

Hadas, A. and D. Hillel. 1972. Steady-state evaporation through non-homogeneous soils from a shallow water table. Soil Science 113:65-73.

Hanson, E.G. and B.C. Williams. 1968. Subsurface irrigation of cotton. p. 281-292. In: Proceedings of National Irrigation Drainage Speciality Conference, Phoenix, Arizona. American Society of Civil Engineers.

Hanson, E.G., B.C. Williams, D.D. Fangmeier, and O.C. Wilke. 1970. Influence of subsurface irrigation on crop yields and water use. p. D1-D13. In: Proceedings of National Irrigation Symposium: University of Nebraska, Lincoln.

Hopper, F.C. and F.R. Lepper. 1950. Transient heat flow apparatus for the determination of thermal conductivities. Transaction of American Society of Heating Ventilating Engineers 56:309-324.

Jackson, R.D. 1963. Temperature and soil-water diffusivity relations. Soil Science Society of America, Proceedings 27:363-366.

Jones, H.E. and H. Kohnke. 1952. The influence of soil moisture tension on vapor movement of soil water. Soil Science Society of America, Proceedings 16:245-248.

Kendrick, J.H. and J.A. Havens. 1973. Heat transfer models for a subsurface, water pipe, soil-warming system. Journal of Environmental Quality 2:188-196.

Klock, G.O. 1968. Pore size distribution as measured by the mercury intrusion method and their use in predicting permeability. Ph.D. thesis, Oregon State University. 91 numbered leaves.

Kowsar, A., L. Boersma, and G.D. Jarman. 1969. Effects of petroleum mulch on soil water content and soil temperature. Soil Science Society of America, Proceedings 33:783-786.

Krischer, O. and H. Rohnalter. 1940. Warmeleitung und Dampfdiffusion in feuchte Gutern: V.D.I. Forschungsheft. 402 p.

Larson, W.E. and W.O. Willis. 1957. Light, soil temperature, soil moisture and alfalfa-red clover distribution between corn rows of various spacings and row directions. Agronomy Journal 49:422-426.

Lykov, A.V. 1966. Heat and Mass Transfer in Capillary-Porous Bodies. Pergamon Press: New York. 523 p.

Makkink, G.F. and H.D.J. van Heemst. 1956. The actual evapotranspiration as a function of the potential evapotranspiration and the soil moisture tension. Netherlands Journal of Agricultural Science 4:67-72.

Mayer, A.M. and A. Paljakoff-Mayber. 1963. The Germination of Seeds. Macmillan Co.: New York. 236 p.

Milne, A.G. and K. Mochlinski. 1964. Characteristics of soil affecting cable ratings. Proc. IEE, 3:1017-1039.

Milthrope, F.L. 1960. The income and loss of water in arid and semi-arid zones. p. 1-36. In: Plant-Water Relationships in Arid and Semi-Arid Conditions: Paris, UNESCO. 225 p.

Nagpal, N.K. 1971. Measurement and interpretation of physical properties of soils. Ph.D. thesis. Corvallis, Oregon State University. 159 numbered leaves.

Nakshabandi, G.A. and H. Kohnke. 1965. Thermal conductivity and diffusivity of soils as related to moisture tension and other physical properties. Agricultural Meteorology 2:271-279.

Nielsen, K.F. and E.C. Humphries. 1966. Effect of root temperature on plant growth. Soil and Fertilizers 29:1-7.

Nielsen, D.R., R.D. Jackson, J.W. Cary, and D.D. Evans. 1972. Soil Water. Am. Soc. Agron., Madison, Wisconsin. 176 p.

Newman, J.S. 1965. Evaluation of subirrigation for crop production. Proceedings of West Texas Water Conference 3:97-103.

Philip, J.R. and D.A. de Vries. 1957. Moisture movement in porous materials under temperature gradients. American Geophysics Union, Transactions 38:222-232.

Rawlins, S.L. and W.H. Gardner. 1963. A test of the validity of the diffusion equation for unsaturated flow of soil water. Soil Science Society of America, Proceedings 27:507-511.

Richards, S.J., R.M. Hagan, and T.M. McCalla. 1952. Soil temperature and plant growth. p. 303-480. In: Byron T. Shaw (ed.). Soil Physical Conditions and Plant Growth. Academic Press: New York. 491 p.

Rykbost, K.A. 1973. An evaluation of soil warming for increased crop production. Ph.D. thesis. Oregon State University, Corvallis. 275 numbered leaves.

Salisbury, F.B. and C. Ross. 1969. Plant Physiology. Wadsworth Publishing Company: Belmont, California. 747 p.

Schleirmacher, von A. 1888. Ueber die Warmeleitung der Gase. Annalen der Physik und Chemie 8:623-646.

Shaw, R.H. and W.F. Buchele. 1957. The effect of the shape of the soil surface profile on soil temperature and moisture. Iowa State College Journal of Science 32:95-104.

Skaggs, R.W. and E.M. Smith. 1967. Apparent thermal conductivity of soil as related to soil porosity. Paper No. 67-114 presented at the Annual Meeting of the ASAE at Saskatoon, Saskatchewan, June 27-30.

Slatyer, R.O. 1956. Evapotranspiration in relation to soil moisture. Netherlands Journal of Agricultural Science 4:73-76.

Smith, W.O. 1939. Thermal conductivities in moist soils. Soil Science Society of America, Proceedings 4:32-40.

Smith, W.O. and H.G. Byers. 1938. The thermal conductivity of dry soils of certain of the great soil groups. Soil Science Society of America, Proceedings 3:13-19.

Taylor, S.A. 1962. The influence of temperature upon the transfer of water in soil systems. Mededelingen Landbouwhogeschool Ghent 27:535-551.

Taylor, S.A. 1963. Simultaneous Flows in Soils and Plants. Utah State University Monographs, Logan, Utah. 101 p.

Taylor, S.A. and G.L. Ashcroft. 1972. Physical Edaphology. W.H. Freeman and Company: San Francisco. 533 p.

Taylor, S.A. and J.W. Cary. 1960. Analysis of the simultaneous flow of water and heat with the thermodynamics of irreversible processes. Seventh International Congress of Soil Science, Transactions, Madison, Wisconsin 1:80-90.

Taylor, S.A. and J.W. Cary. 1965. Soil water movement in vapor and liquid phases. In: Eckardt, F.E. (ed.). Methodology of Plant Eco-Physiology. Montpellier Symbosium, 1962. UNESCO Arid Zone Research 25:159-165.

U.S. Department of Commerce. 1972. Climatological data, Annual summary. 78:259-273.

van Wijk, W.R. and D.A. de Vries. 1963. Periodic temperature variation in a homogeneous soil. p. 102-143. In: W.R. van Wijk (ed.). Physics of Plant Environment. North-Holland Publishing Company: Amsterdam. 382 p.

Wadsworth, H.A. 1944. An interpretation of the moisture content-surface force curve for soils. Soil Science 58:225-242.

Watts, D.G., C.R. Dehlinger, J.W. Wolfe, and M.N. Shearer. 1968. Consumptive use and net irrigation requirements for Oregon. Agricultural Experiment Station, Oregon State University, Corvallis, Circular of Information No. 628.

Webb, J. 1956. The thermal conductivity of soil. Nature 177:989.

Weigand, C.L. and S.A. Taylor. 1962. Temperature depression and temperature distribution in drying soil columns. Soil Science 94:75-79.

Woodside, W. 1958. Calculation of the thermal conductivity of porous media. Canadian Journal of Physics 36:815-823.

Yankelev, L.F. 1954. The building industry (Stroitel'naya Promyshlennost') No. 4.

Yarosh, M.M., B.L. Nichols, E.A. Hirst, J.W. Michel, and W.C. Yee. 1972. Agricultural and aquacultural uses of waste heat. ORNL-4797; US-48-Biology and Medicine; UC-80-Reactor Technology, Oakridge National Laboratory, Oakridge, Tennessee, 54 numb. leaves.

Zetzsche, J.B., Jr. 1964. Evaluation of subirrigation with plastic pipe. American Society of Agricultural Engineers. Paper No. 64-731. St. Joseph, Michigan.